Development of an experimental test setup for evaluating the gas permeability of composites and polymer materials for liquid hydrogen storage

Robert Vincent de Koning

TU Delft

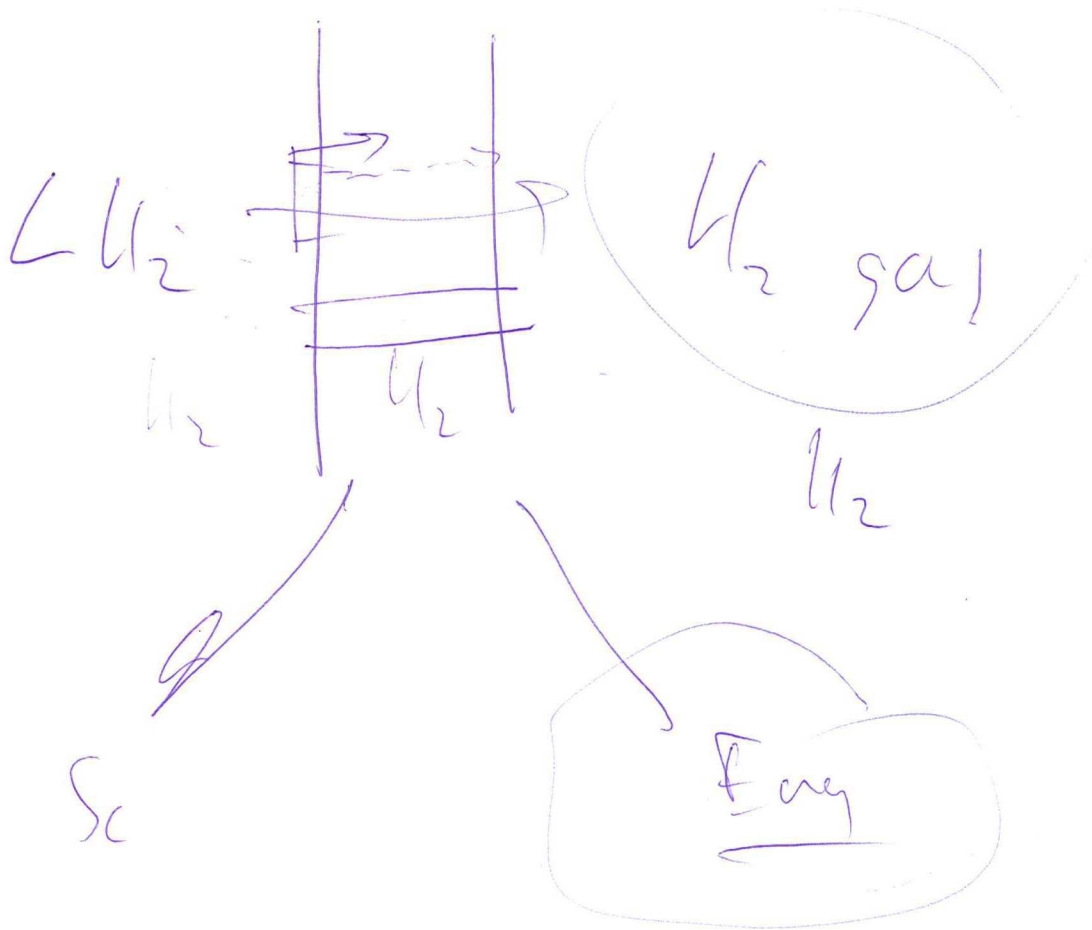
H_2
H_2
H_2
H_2 gas
H_2
Sc
Energy

10.05

10.50

Development of an experimental test setup for evaluating the gas permeability of composites and polymer materials for liquid hydrogen storage

by

Robert Vincent de Koning

to obtain the degree of Master of Science
at the Delft University of Technology.

CTE matrix → cracking → failure (gas escapes)
~ fibre

↳ liner = barrier

Student number: 1224042

Thesis committee:	Prof. dr. ir. R. Benedictus,	TU Delft, Chairman
	Ir. I.T. Tapeinos,	TU Delft, Supervisor
	Dr. ir. S. Koussios,	TU Delft, Supervisor
	Dr. R.M. Groves,	TU Delft, Supervisor
	Ir. J.A. Melkert,	TU Delft

TU Delft

10.7

2

10.24

3

10.41

4

10.57

Summary

Aerospace structures are always required to be as light as possible, in order to acquire a high cost efficiency. It is because of this that composites, such as carbon fiber reinforced plastics, having a high stiffness to density ratio are very interesting for aerospace structures. A structure that has received particular interest is the fuel tank to store liquid hydrogen in, which is usually made from aluminium. The desire is to make the tank lighter by using a composite, the anisotropic composite however poses some difficulties that need to be attended before it can be used safely: during a test by NASA a quarter scale tank failed due to unexpected permeation of hydrogen through microcracks, caused by repeated thermal and mechanical loading.
In this research it is proposed to cover the tank wall with a polymeric liner, with the aim of adding a barrier that is less prone to crack formation - and therefore leakage - than the composite tank wall. Because permeability values of materials are scarce, the objective in this research is to develop a gas permeability test apparatus and to use this to test multiple candidate liner materials. It is furthermore of interest to determine how the materials maintain their permeability characteristics while being strained, when exposed to a range of pressures and after undergoing multiple thermal cycles. It is furthermore investigated what the expected hydrogen volume loss will be of a hypothetical tank with a liner as a function of temperature, using the Arrhenius equation.
It was decided to design the apparatus and acquire data with the volumetric method as described in a permeability test standard of ASTM, based on cost, manufacturability and measurability. Also a permeant needed to be decided: although testing with hydrogen would provide the most accurate results, its high flammability is a large drawback. Based on molecule diameter and a study that compared permeability of hydrogen and helium, it was decided that helium, which is inert, would be a good alternative. Finally the materials needed to be decided upon. The fluoropolymers FEP, PTFE and PFA were selected as candidate liner materials based on their high flexibility and low glass temperature, the liquid crystal polymers Vectra A130 and A950 were selected based on their high stiffness, low coefficient of thermal expansion and suggested low permeability. Furthermore, a carbon fiber epoxy composite was selected as a candidate tank wall material, which is similar to composites used in literature. All materials were tested for permeability at the conditions specified in the previous paragraph and, in case of the fluoropolymers and liquid crystal polymers, compared to reference values as achieved by a third party, who was commissioned for this research. This approach resulted in a device with which the permeability of the materials under the predefined test conditions could be performed. With this device it was shown that the permeability of the anisotropic materials was greatly affected (i.e. large increase) by straining them, as opposed to the fluoropolymers which showed only a very small increase. The fluoropolymers on the other hand have 100 times higher permeability than the other material types. Thermal cycling showed a small increase for Vectra A950, while a small decrease for the fluoropolymers. With respect to the reference values, the measured values are all higher except for PTFE. Permeability as a function of pressure showed that Vectra A130 is influenced by the permeant, while the fluoropolymers remain largely unaffected. The expected volume loss of a hypothetical tank using the Arrhenius equation shows an exponential decrease in volume loss when decreasing the temperature. At 21 K, the temperature of liquid hydrogen, the leak rate is between 10^{-28} and 10^{-36} L/h for fluoropolymers and about 10^{-57} L/h for the liquid crystal polymers when using helium as permeant and applying a pressure between 3.8 and 5.7 bar of pressure.
The apparatus with the flat surface is essentially the correct device with which a permeability test should be performed. The data acquisition however can be improved as it lacks accuracy and precision, especially for low permeability materials. Regarding the test results it is concluded that straining the specimen by bending them by applying helium pressure results in a significant increase for the anisotropic materials. However, it cannot be quantified how strain affects the permeability, due to the nature of the test setup which allows for a heterogeneous strain field. In future this can be modified by designing a biaxial strain device around the apparatus. The isotropic materials are far less susceptible for the increase in permeability due to strain, nevertheless it has a 10 times higher permeability. Thermal cycling affected the permeability of Vectra A950 by a noticeable increase, while for the other materials the change was either not there or cannot be explained. Regarding the varying pressure test it can be concluded that the permeability of A130 is a function of pressure, while the fluoropolymers behave almost ideally. Based on the volume loss of a

hypothetical tank under the given assumptions it is concluded that volume flow out of the tank becomes negligible at 21 K, regardless of liner material used. From the observed influences of strain and thermal cycling on the liners and the notion that permeation goes to zero as temperature nears zero, it can be concluded that the mechanical stability of the liner under mechanical and thermal load is more important than the bulk material permeability.

Contents

Summary i

Contents ii

List of Figures v

List of Tables vii

Nomenclature ix

1 Introduction 1
- 1.1 Research motivation and objective . . . 1
- 1.2 Approach . . . 1
- 1.3 Structure . . . 2

2 Theoretical background 3
- 2.1 Gas permeability . . . 3
  - 2.1.1 Theory of gas permeability . . . 3
  - 2.1.2 Permeability test devices . . . 5
- 2.2 Load environment of cryogenic tanks . . . 8
  - 2.2.1 Mechanical loads . . . 9
  - 2.2.2 Thermo-mechanical loads . . . 10
  - 2.2.3 Preconditioning . . . 11
  - 2.2.4 Combination of loads and preconditioning . . . 12
- 2.3 Materials . . . 13

3 Apparatus and measurement method 15
- 3.1 Permeability apparatus . . . 15
  - 3.1.1 Apparatus design . . . 15
  - 3.1.2 Measurement method trade-off . . . 16
  - 3.1.3 Data acquisition . . . 17
  - 3.1.4 Apparatus calibration and error determination . . . 18
  - 3.1.5 Data analysis . . . 18
- 3.2 Materials . . . 25
  - 3.2.1 AS4/8552 . . . 26
  - 3.2.2 Fluoropolymers . . . 28
  - 3.2.3 Liquid crystal polymers . . . 28
- 3.3 Experiments . . . 29
  - 3.3.1 Introduction . . . 29
  - 3.3.2 Thermal cycling . . . 29
  - 3.3.3 Mechanical load . . . 30
  - 3.3.4 Varying pressure test . . . 31

4 Results 33
- 4.1 Introduction . . . 33
- 4.2 Composites . . . 33
- 4.3 Liquid Crystal Polymers . . . 35
- 4.4 Fluoropolymers . . . 36
- 4.5 Expected He and H_2 volume loss of pressure vessel . . . 38

5 Discussion 41
5.1 Introduction . . . 41
5.2 Apparatus . . . 41
5.3 Data acquisition . . . 41
5.4 Materials . . . 42
5.5 Test setup . . . 43
5.6 Test results . . . 43

6 Conclusions 45
6.1 Apparatus . . . 45
6.2 Data acquisition . . . 45
6.3 Materials . . . 45
6.4 Test setup . . . 45
6.5 Test results . . . 46

7 Recommendations 47
7.1 Introduction . . . 47
7.2 Apparatus . . . 47
7.3 Data acquisition . . . 47
7.4 Materials . . . 48
7.5 Test setup . . . 48

A Material properties 51
A.1 Fluoropolymers . . . 51
A.2 Liquid crystal polymers . . . 51
A.3 AS4/8552 . . . 52

B MATLAB Code 53
B.1 Excel to Matlab conversion tool . . . 53
B.2 Main program . . . 54
B.3 Correction functions . . . 55
B.4 Permeability function . . . 57
B.5 Deflected volume . . . 58
B.6 Classical Lamination Theory . . . 59
B.7 Strain of deflected sample . . . 60
B.8 Helium density calculation . . . 62

C Ideal gas law - Helium density 65

D Individual results 67

E Automation of measurements 73

F O-ring seal 75

Bibliography 77

List of Figures

2.1 Example of an Arrhenius plot for FEP, using reference values obtained from third party (see 3.2 for further details). . . . 5
2.2 Possible effects of pressure on the permeability [20] . . . 6
2.3 The volumetric gas permeability apparatus from the ASTM test standard. . . . 7
2.4 Volumetric gas permeability apparatus . . . 7
2.5 Sketch of the time-lag measurement method . . . 8
2.6 (a) Cryogenic pressure vessel; (b) Biaxial stress state of an element . . . 9
2.7 Cruciform test specimen with dimension and strain gauge locations . . . 10
2.8 Relation between biaxial load and permeability . . . 10
2.9 One thermal cycle of a specimen . . . 12
2.10 Measurement setup as used by Gates, Grenoble and Whitley . . . 13
2.11 Overview of the test setup at the Institute of Aerospace Technology in Osawa, Japan . . . 13
2.12 Helium permeability of epoxy resin and three fibre reinforced epoxies. . . . 14

3.1 Exploded view of the apparatus with a specimen . . . 15
3.2 Helium and hydrogen permeability of PVC, PE-HD and PA . . . 17
3.3 Program structure . . . 20
3.4 Deflection of a quasi-isotropic AS4/8552 sample at various pressures. Shown are the cross section of the sample when deflected, an overview of a deflected sample at 6 bar and the volume occupied by the deflected sample as a function of pressure. . . . 22
3.5 Flowchart of the Matlab program that analyzes the data. . . . 23
3.6 Flowchart of the Matlab program that calculates the permeability, the upper and lower limit, and the goodness of fit of the data. . . . 24
3.7 Flowchart of the entire setup. . . . 25
3.8 Arrhenius plot of FEP with hydrogen as the permeant . . . 26
3.9 Vacuum table build up. . . . 27
3.10 Cure cycle of the AS4/8552 composite as provided by Hexcel . . . 27
3.11 Arrhenius plot of reference data of fluoropolymers FEP, PFA and PTFE. . . . 28
3.12 Arrhenius plot of reference data of fluoropolymers FEP, PFA and PTFE. . . . 29
3.13 Temperature of a specimen during a cryogenic cycle measured with a K-type thermocouple, except for the cryogenic phase, where the temperature of the sample is assumed to have the temperature of the liquid nitrogen. . . . 30

4.1 Bar chart of the permeability measurement results for AS4/8552, including error margin. . . . 34
4.2 Example of the strain distributions in a ply of the Angleply layup at a pressure of 3.8 bar . . . 35
4.3 Bar chart of permeability measurement results (reference, base and cycled specimens) for the LCP's Vectra A130 and A950, including error margin. . . . 35
4.4 Same as figure 4.3, but now also including results for bended specimens. . . . 36
4.5 Graph of the permeability of Vectra A130 as a function of pressure. . . . 36
4.6 Graph of the GTR as a function of pressure of Vectra A130. . . . 37
4.7 Bar chart of permeability measurement results, including error margin, for the fluoropolymers PFA, FEP and PTFE. . . . 38
4.8 Graphs of the permeability as a function of pressure, including error margin, for the fluoropolymers PFA, FEP and PTFE. . . . 38
4.9 Permeability measurement results values as a function of pressure, including upper and lower limit error, for the fluoropolymers PFA, FEP and PTFE. . . . 38
4.10 The GTR as a function of pressure for the fluoropolymers PFA, FEP and PTFE. . . . 39
4.11 Helium loss per hour as a function of temperature for the fluoropolymers FEP, PFA and PTFE at pressure differences of 3.8 and 5.7 bar. . . . 39

4.12 Helium loss per hour as a function of temperature for the LCPs A130 and A950 at pressure differences of 3.8 and 5.7 bar. 40
4.13 Difference between hydrogen and helium loss per hour for FEP as a function of temperature for the LCPs A130 and A950 at pressure differences of 3.8 and 5.7 bar. 40

5.1 Graphic representation of the liner shrinkage and expansion due to the liquid hydrogen. 43

C.1 Difference given as percentage between the ideal gas law and the empirical relationship. 65

E.1 MCP9808 and BMP180 sensors connected on a breadboard. 74

F.1 First test with regular air. 75
F.2 Second test setup without helium balloon vacuum bag. 76
F.3 Second test result with helium. 76

List of Tables

3.1 Molecule diameters in picometer of helium and hydrogen 16
3.2 Tolerance of each element of the data acquisition setup. 18
3.3 Permeability values deduced from 3.8 for FEP with hydrogen as the permeant 26
3.4 Reference permeability values for the fluoropolymers 28
3.5 Activation energies and permeability constant of the fluoropolymers 28
3.6 Reference permeability values for the LCP's 29
3.7 Activation energies and permeability constant of the LCP's 29

4.1 Overview tests 33
4.2 Table of the permeability measurement results for AS4/8552, including error margin. 34
4.3 Maximum strains of the composite materials at a pressure of 3.8 bar. 34
4.4 Table of the permeability measurement results for the LCP's Vectra A130 and A950, including upper and lower limit of the error. 36
4.5 Table of the permeability measurement results as a function of pressure for the LCP Vectra A130. Upper and lower limit of the error are included. 37
4.6 Maximum strains of the LCP materials at a pressure of 3.8 bar. 37
4.7 Permeability measurement results values, including upper and lower limit error, for the fluoropolymers PFA, FEP and PTFE. 37
4.8 Maximum strains of the fluoropolymer materials 39

A.1 Mechanical and thermal properties of fluoropolymers PFA, FEP and PTFE 51
A.2 Mechanical and thermal properties of Vectra A130 and A950 51
A.3 Mechanical and thermal properties of UD AS4/8552 52

Nomenclature

Latin symbols

$\underline{P}$	Permeability coefficient	$mol/(m \cdot s \cdot Pa)$
A	Area	m^2
C	Permeant concentration	mol/m^3
D	Diffusion coefficient	m^2/s
ds	Arc length	m
G	Shear stiffness	N/m^2
H	Enthalpy	J
h	Slug height	mm
J	Diffusion flux	$mol/(m^2 \cdot s)$
M	Molar mass	kg/mol
P	Permeance	$mol/(m^2 \cdot s \cdot Pa)$
p	Pressure	Pa
Q	Stiffness matrix	N/m^2
q	Applied pressure	N/m^2
R	Universal gas constant	$J/(mol \cdot K)$
r	Radius	m
S	Solubility coefficient	m^3/kg
T	Temperature	K
t	Thickness	m
V	Volume	m^3
w	Deflection	m

Greek symbols

α	Coefficient of thermal expansion	m/K
ϵ	Strain	–
γ	Shear strain	–
κ	Curvature	$1/m$
ν	Poisson's ratio	–
ρ	Density	kg/m^3
σ	Stress	N/m^2
τ	Shear stress	Pa/m^2

Abbreviations

ADC	Analog to digital converter
Atm	Atmospheric
CF	Carbon fiber
CFRP	Carbon fiber reinforced plastic
CHATT	Cryogen Hypersonic Advanced Tank Technologies
CT	Cryogenic Temperature
CTE	Coefficient of Thermal Expansion
FEA	Finite Element Analysis

FEM	Finite Element Method
GTR	Gas Transmission Rate
IM	Intermediate Modulus
LCP	Liquid Crystal Polymer
LH2	Liquid Hydrogen
LHe	Liquid Helium
LN2	Liquid Nitrogen
RLV	Reusable Launch Vehicle
RT	Room Temperature
TLCP	Thermoset Liquid Crystal Polymer
UD	Unidirectional

1 Introduction

1.1. Research motivation and objective

Pressure vessels for liquid hydrogen storage were mostly made from metals in the past. The external tank of the Spaceshuttle for instance was made out of aluminium, and pressure vessels for long term storage on ground level are made of austenitic steels. For the aerospace sector the use of composites instead of metals would be interesting as the construction can be made more lightweight, hence more cost efficient in operational use. At present, the collaborative project CHATT (Cryogen Hypersonic Advanced Tank Technologies) has started to gain knowledge on cryogenic tanks for future aerospace applications. Interest is shown in the design and construction of a multi-lobe pressure vessel made out of the lightweight composite material, which is able to contain liquid hydrogen and with the intent to reuse for multiple launches into space.

NASA has the same intension, and already made and tested a quarter scale carbon fiber reinforced plastic (CFRP) sandwich pressure vessel in 1999, during which the tank failed. One of the most probable causes was that "microcracking of the inner facesheet allowed hydrogen infiltration into the core"[1]. This means that the hydrogen gas that has boiled off was able to permeate through a series of microcracks, probably caused by the repeated combination of a pressure load at cryogenic temperature. As the gaseous hydrogen leaked into the honeycomb structure, where the cracks did not propagate into the outer facesheet, the gaseous hydrogen was trapped in the honeycomb and could built up pressure, damaging the core and peeling of the inner and outer facesheets [1]. Since then, many experimental studies have been performed to quantify the gas permeation of various composite materials at various load environments and preloaded conditions, in order to find a composite material that is able to keep the liquid hydrogen in the vessel.

In this research it is proposed to cover the tank wall with a polymeric liner, with the aim of adding a barrier that is less prone to crack formation - and therefore leakage - than the composite tank wall. Because permeability values of materials are scarce, the objective in this research is to develop a gas permeability test apparatus and to use this to test multiple candidate liner materials. It is furthermore of interest to determine how the materials maintain their permeability characteristics while being strained, when exposed to a range of pressures and after undergoing multiple thermal cycles.

1.2. Approach

The project is started with a literature study on the subject of permeability of pressure vessels. Attention is paid to the load environment of the pressure vessel during its lifetime, cryogenic temperature effects, load effects and permeability test setups. Furthermore, the work performed at the TU Delft on this project before this research started was taken into consideration.

Because the CHATT project had already commenced before the start of this project, a part of the apparatus was already developed and was used as a base for further development. As the apparatus is key to the subsequent research, this development is completed as early as possible with the permeability test standard of ASTM [2] taken as the main reference for the development of the apparatus.

When the apparatus is ready, the permeability of the materials can be assessed. Tests are performed at room temperature to acquire the base permeability of each material. As the materials tested have also been sent to an external party, also possessing a permeability apparatus, reference values are obtained with which the

results can be compared with. The effect of temperature on the permeability in two separate ways: the permeability at cryogenic temperature is performed and the permeability after repeated exposure to cryogenic temperature is assessed.
Because the permeability can be a function of strain, it is desired to know the strain of the specimens in permeability tests with strained conditions, a model should made with the finite element analysis (FEA) tool ABAQUS. The same needs to be done for the cryogenic temperature condition, as the larger temperature drop also causes strains in the material.
The research shall be concluded with conclusions regarding the permeability of the materials and the effect of temperature and strain upon them. Furthermore the design choices made during the research shall be discussed and recommendations for possible follow-up research shall be given.

1.3. Structure

Chapter 2 will give the theoretical background of the project. First, it is explained what gas permeability is, what affects it and how it can be measured. Secondly, the load environment of the Reusable Launch Vehicle (RLV) is established and its components are discussed in relation to permeability. Results from literature are presented and explained. Thirdly, material properties in relation to permeability and pressure vessel design are discussed. This includes both composite tank wall and liner materials.
The third chapter will treat the methodology of the project. The first section will treat the gas permeability apparatus, in which the design of the apparatus is presented and explained. Furthermore, the data acquisition is established and a trade-off needs to be made between the methods available. After the construction of the apparatus, it needs to be calibrated and the data recorded has to be analyzed. As measurements seemed to be influenced by a number of factors, some calculations are considered to nullify these factors. This chapter will continue with the candidate materials for the permeability measurements, how these were made and some of their properties are discussed. As the candidate liner materials were also send to a third party with their own permeability apparatus, reference values for the permeability will also be listed in this section. The third section will treat how the experimental work is performed and discusses the variables that are incorporated into the experiments. The final section will detail how the Finite Element Model (FEM) was created with Abaqus.
The results are given in the fourth chapter, where first some of the raw data is presented and explained and how the various proposed corrections of Chapter 3 are able to improve the results. After this the resulting permeability values per material group are considered and statistics are given whenever possible. In the case of deflected specimen, also the strains are presented.
In the final chapters the results are discussed and conclusions drawn. Lastly, recommendations are given for future research on gas permeability and how to improve the gas permeability apparatus for that research.

2

Theoretical background

As explained in the introduction, since the failure of the CFRP pressure vessel for cryogenic applications in the X-33 of NASA, more research has been done on the gas permeability of CFRP and the effect of the load conditions on this. In this chapter it will be explained what permeability actually is and how it can be measured (Section 2.1). After that it will be explained what the load environment is and how it affects the pressure vessel and how that in turn influences the permeability (Section 2.2). Lastly, materials for the tank wall and liner are discussed in Section 2.3, together with their properties and how this may influence the permeability.

2.1. Gas permeability

This section will explain the theory behind gas permeability (Section 2.1.1) and includes some of the most important equations related to the subject as well as an empirical relation to determine permeability as a function of temperature. Also four measurement techniques to determine permeability are discussed in 2.1.2.

2.1.1. Theory of gas permeability

Permeation is the movement of molecules through a solid material and occurs in three stages according to the solution-diffusion model, based on Fick's law of permeation and Henry's law of solubilities: first the molecules, called the permeant, are adsorbed at the surface of the solid, next it diffuses through the solid and lastly it is desorbed at the opposite surface. The rate at which permeation occurs mostly dominated by the rate of diffusion, which is the slowest of the three stages, and depends on the microstructure, atomic bonding and density of the solid, and the size of permeant atom.
According to Fick's first law of diffusion, the rate of transfer of gas per unit area of the membrane is proportional to the diffusion coefficient times the gradient in permeant concentration normal to the surface:

$$J = -D\frac{\partial C}{\partial x} \tag{2.1}$$

With J being the diffusion flux $[mol/(m^2 \cdot s)]$, D the diffusion coefficient $[m^2/s]$ C the permeant concentration $[mol/(m^3)]$ and x the length coordinate measured normal to the surface $[m]$. Fick's first law assumes steady state condition, i.e. a linear gradient in concentration from the high concentration at the upstream side to a low concentration at the downstream side. This steady state is acquired after some time, and therefore Fick's second law of diffusion is needed to describe the change in concentration with time:

$$\frac{\partial C}{\partial t} = D\frac{\partial^2 C}{\partial x^2} \tag{2.2}$$

For anisotropic materials however, the diffusion flux through the thickness is not only dependent on the change in concentration in that direction [6]:

$$-J_x = D_{11}\frac{\partial C}{\partial x} + D_{12}\frac{\partial C}{\partial y} + D_{13}\frac{\partial C}{\partial z} \tag{2.3}$$

meaning that the change in concentration in the y and z-direction also influence the permeant transfer in x-direction and the diffusion coefficient is different for different directions. In most experiments the flow is desired to be one-dimensional, assuming the flow will be independent of y and z, and only a concentration gradient exists in the x-direction. The equation for the diffusion flux is then simplified to:

$$-J_x = D_{11}\frac{\partial C}{\partial x} \tag{2.4}$$

This is probably true for a spherical/cylindrical membrane, where the material boundary is essentially infinite except for the thickness, hence only a gradient in the thickness direction will exist. However, during experiments this is not entirely the case, still it is assumed that D_{11} is measured.
The diffusion coefficient is unknown and depends on membrane material, permeant and temperature. Increasing pressure causes a higher concentration gradient, hence a higher flux. Increasing temperature causes the energy of the permeant to increase, therefore increasing the chance of finding free volume to flow into.
The solubility coefficient is measured as the permeant concentration in the solid at the gas-solid interface, divided by the the partial pressure of gas:

$$S = \frac{C_i}{p_i} \tag{2.5}$$

The rate of transfer of gas per unit area can also be written as a function of the diffusion coefficient, solubility coefficient S and the pressure gradient over the thickness of the material:

$$J = D \cdot S \cdot \left(\frac{\Delta p}{t}\right) \tag{2.6}$$

where S is the solubility $[mol/(Pa \cdot m^3]$, Δp is the pressure difference on opposite sides of the material $[Pa]$ and t is the thickness $[m]$. The multiplication of the diffusion coefficient with the solubility coefficient yields the permeability coefficient:

$$\underline{P} = D \cdot S \tag{2.7}$$

With $\underline{P}$ the permeability $[mol/(m \cdot Pa \cdot s)]$. These three parameters are often determined experimentally by a time-lag experiment where the diffusivity is determined by measuring the time it takes until the permeant has diffused through the solid barrier, taking the thickness into account:

$$D = \frac{t^2}{6 \cdot time} \tag{2.8}$$

The amount of permeant passing the solid barrier as a function of the sample thickness, surface area, time and pressure difference is also measured and relates to the permeability, $\underline{P}$. With $\underline{P}$ and D known, the solubility S can be calculated.
There are no analytical methods to determine the permeability of a material, exposed to a certain permeant. At most an empirical relation is given by the Arrhenius equation, which describes the temperature dependence of the solubility, diffusivity and hence the permeability of a material by a specific permeant:

$$D = D_0 \cdot e^{\frac{E_d}{R \cdot T}} \tag{2.9a}$$

$$S = S_0 \cdot e^{-\frac{\Delta H_s}{R \cdot T}} \tag{2.9b}$$

$$\underline{P} = D \cdot S = \underline{P}_0 \cdot e^{\frac{E_A}{R \cdot T}} \tag{2.9c}$$

In these equations the subscript 0 is used for the pre-exponential term for when $1/T = 0$ (i.e. T goes to infinity), it is a constant and it has the same unit as its coefficient. E_d is the activation energy for diffusion as is ΔE_A for permeation $[J/mol]$, is influenced by the size of the permeant (not the mass) and describes the required energy for the permeant molecule to enter a free space (vacancy/interstitial) in the solid structure. Both pre-exponential terms and the activation energies are characteristics of the material-permeant pair. R is the gas constant $[J/(mol \cdot K)]$ and T is the temperature $[K]$. ΔH_s is the partial molar enthalpy of adsorption, which is the sum of the enthalpies of the gas molecule condensating into the solid and the gas molecule mixing into the solid:

$$\Delta H_s = \Delta H_{cond} + \Delta H_{mix} \tag{2.10}$$

Essentially, the exponential terms in the Arrhenius equations describe the chance of the permeant gas to succeed in reaching the next gap in the solid. As the temperature of the permeant decreases, so will its vibrational energy, and therefore the chance of the change of reaching the next gap, resulting in a lower permeation. The activation energy cannot be determined analytically and experiments need to be performed at a wide temperature range to make a proper estimate of the constant. Although the equation gives the sense that it is true for every value of T, it is noted by Mckeen [20] that caution should be taken when extrapolating too far outside of the measured data range. This is also acknowledged by Stokes [26], who states that permeability experiments are often performed at a temperature which does not correspond to reality, which should be considered when using the resulting data.
If multiple permeability experiments at different temperatures are performed, the natural logarithm of the results can be plotted against the inverse of the absolute temperature and using a linear regression through the points, P_0 can be found by taking the exponent of the axis intercept ($P_0 = e^y$ at x=0) and ΔE_A is the slope of the linear regression multiplied by the gas constant. An example of an Arrhenius plot is shown in Figure 2.1.

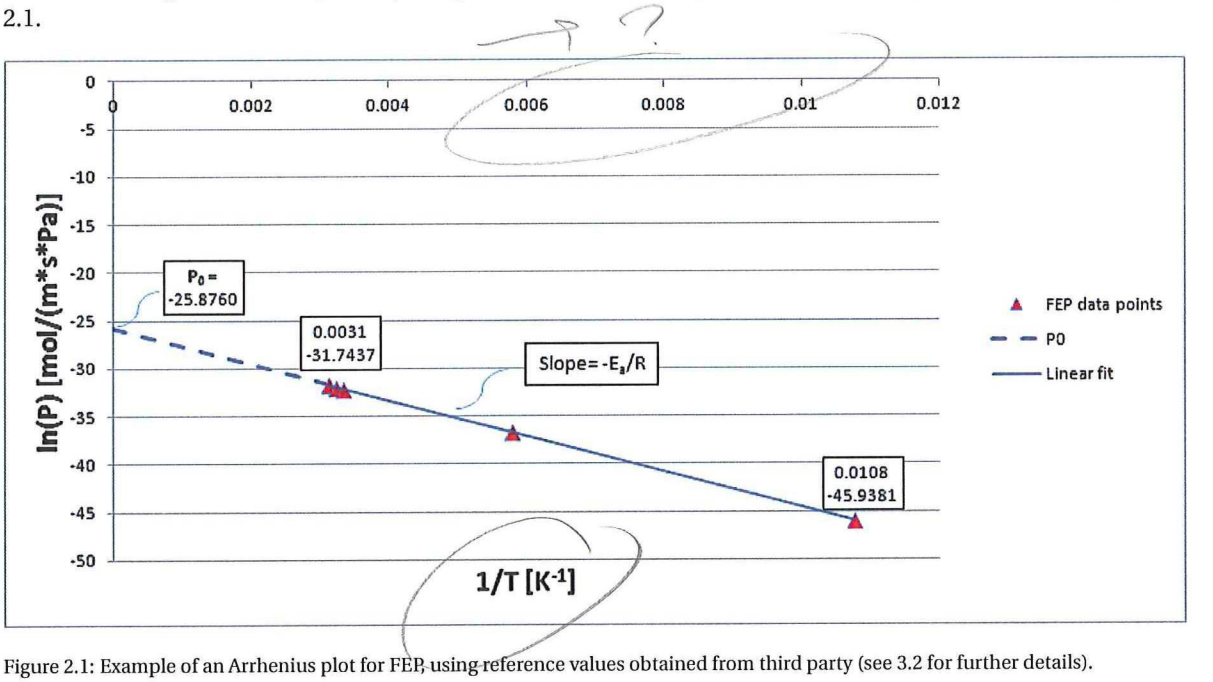

Figure 2.1: Example of an Arrhenius plot for FEP using reference values obtained from third party (see 3.2 for further details).

The Arrhenius plot and the equations for the diffusivity and solubility may give the impression that permeability only depends on temperature and on constants which are entirely based on the physical properties of the material-permeant pair. This would be the ideal scenario, but in fact the constants are affected by pressure: depending on how the permeant interacts with the polymer molecules the permeability may depend on pressure as shown in figure 2.2.

2.1.2. Permeability test devices

To determine the permeability of a material-permeant pair, experiments need to be performed. In literature the experimental setup is mostly based on a test standard from ASTM, D1434-82(2009)e1 [2]. This test standard describes two methods of determining the permeability of a material, by means of volumetric and manometric measurements. The volumetric method measures the change in volume downstream of the sample due to the added permeant gas, the manometric method measures the change in pressure over time downstream of the sample using mercury.
The volumetric apparatus is shown in the Figure 2.3 below. It shows how the specimen is clamped between two cell halves, and made airtight with an O-ring and a gasket. The upstream gas pressure is controlled with a gas pressure regulator and the test temperature is controlled with a constant temperature bath. A good overview of a volumetric apparatus in practice is shown in Figure 2.4. As can be seen from Figure 2.4, an exact copy of the apparatus setup as explained in the test standard is almost never applied in literature and

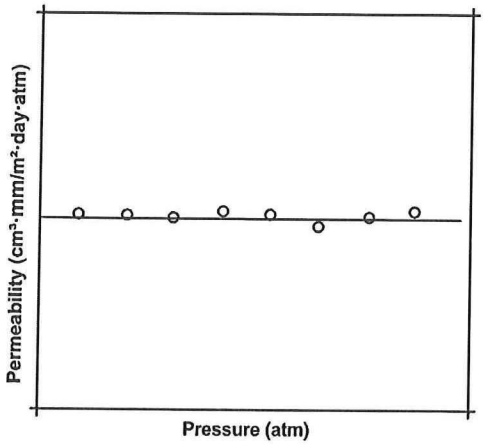

(a) Permeability coefficient depending on pressure in ideal case.

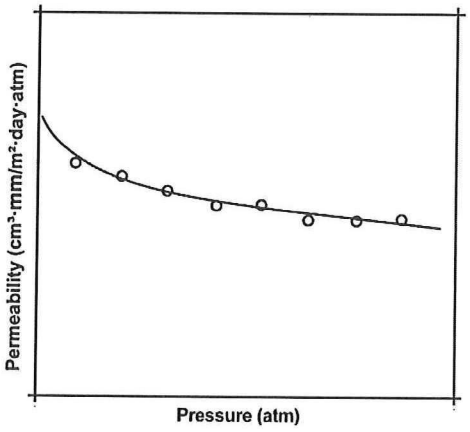

(b) Permeability coefficient depending on pressure when the penetrant plasticizes a rubbery polymer.

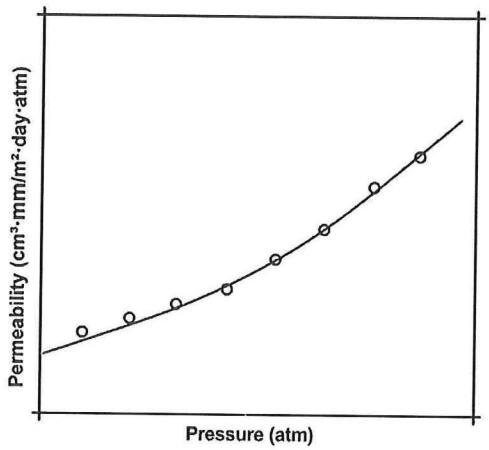

(c) Permeability coefficient depending on pressure in ideal case.

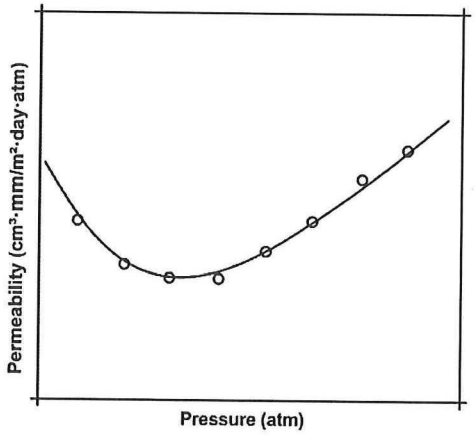

(d) Permeability coefficient depending on pressure when the penetrant plasticizes a rubbery polymer.

Figure 2.2: Possible effects of pressure on the permeability [20]

many modifications are made. The basis however stays more or less the same: two aluminium cells with the material clamped in between, and a gasket and a O-ring preventing any leaks at the material-setup interface.

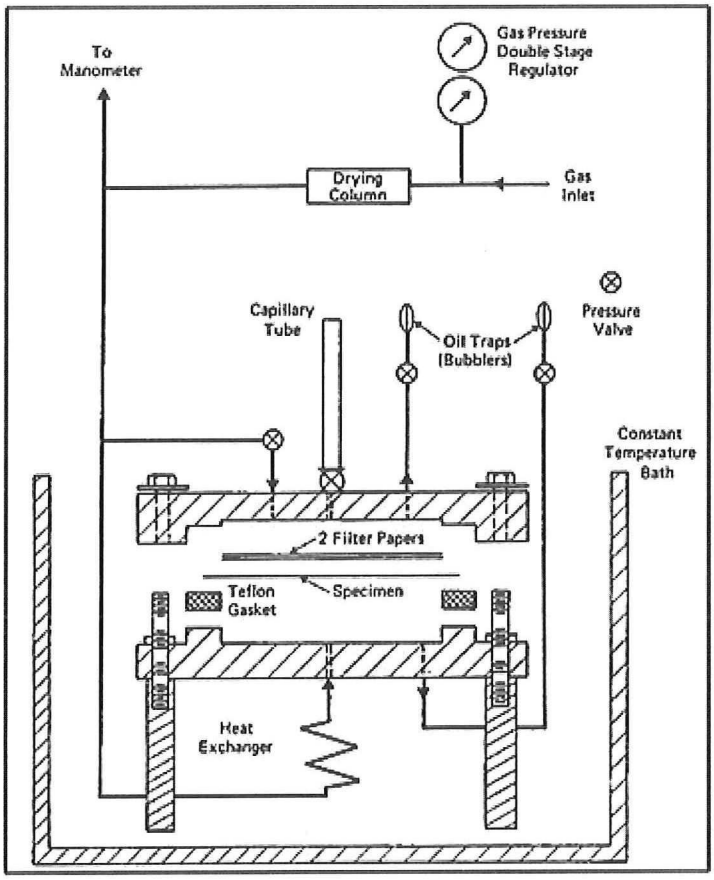

Figure 2.3: The volumetric gas permeability apparatus from the ASTM test standard [2]

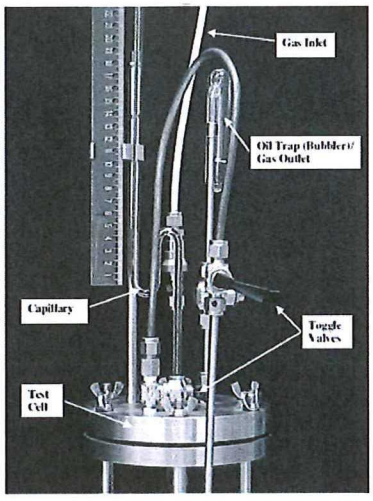

Figure 2.4: Volumetric gas permeability apparatus [14]

The displacement of a liquid slug in the glass capillary due to a change in volume is measured over time. Because the cross-sectional area of the capillary is known, it can be calculated how much gas was transmitted through the material as a function of time. Choi and Sankar [5] showed that small changes in ambient pressure can cause significant changes in slug position measurements, and therefore errors in the permeability calculations. By closing the downstream chamber with an aluminium plate and measuring the

slug position over time and the ambient pressure, it was possible to establish a correction factor. This correction factor k is calculated by dividing the change in slug position by the change in ambient pressure. Now the corrected slug position h can be calculated with:

$$h_{corrected} = h_{measured} + k \cdot \Delta p \tag{2.11}$$

where Δp is the change in ambient pressure. The position of the capillary (horizontal or vertical), does not matter according to Nettles [21]- [22].
The manometric test method is for the larger part the same - it uses the same apparatus - as the volumetric method. The difference is that the change in pressure is measured instead of the change in volume. In the standard test method described by ASTM, this change in pressure is measured using a column of mercury. Because mercury is highly toxic, this is by some considered not to be a safe option and therefore the measurement method is either disregarded or pressure transducers are used instead.
Not described in the test standard, but often used instead of the volumetric or manometric method, is the mass spectrometer. Although this device is quite expensive, permeated gas can be accurately analyzed. The machine uses the magnetic separation principle to separate and collect the helium particles, resulting in a sensitivity of $1 \cdot 10^{-11}$ $[cm^3/s]$ at $0°C$ and 101325 $[Pa]$ according to manufacturers.
Lastly, the lag-time apparatus, as described in section 2.1, can be used for the measurement of permeability [20] [30]. A sweep gas takes the permeant to a mass spectrometer for analysis. With this method not only the permeability is determined, but also the diffusivity and solubility. The setup for such an apparatus is shown in figure 2.5.

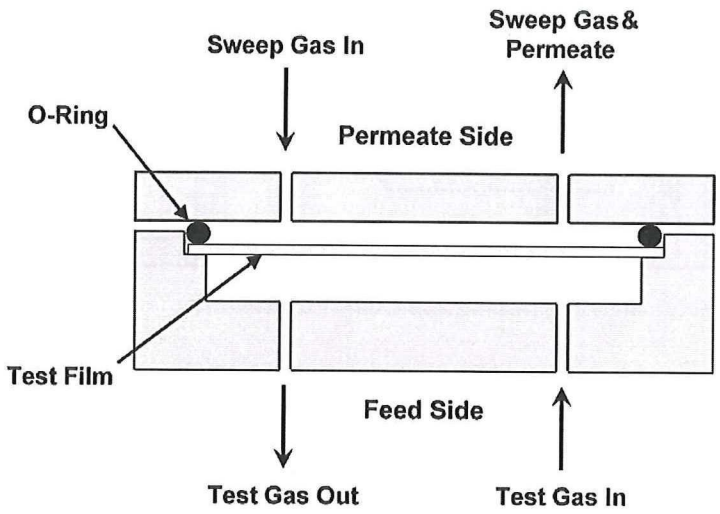

Figure 2.5: Sketch of the time-lag measurement method

2.2. Load environment of cryogenic tanks

The load environment of a reusable pressure vessel containing liquid hydrogen is quite harsh. For a mission the pressure vessel is filled with liquid hydrogen at a temperature of about 21 K, so the liquid and vaporized hydrogen will pressurize the tank and at the same time the temperature will also induce stresses. At re-entry the tank is empty and will heat up due to friction with the atmosphere. For the X-33 reusable launch vehicle (RLV) test program by NASA, which included a composite quarter scale multilobe tank, it was stated that the tank requirements were [4]:

- pressure difference from 0.36 to 2.48 bar;
- maximum strain of 6000 microstrain;
- thermal operation from 21K up to 450K;
- perform 600 missions.

The CHATT program deviates slightly as it is estimated there that the pressure will go as high as 3.8 bar and the temperature will be as high as 480 K.
This section will elaborate on the load environment in the subsections about the mechanical loads, thermo-mechanical loads, preconditioning (i.e. cyclic load) and a combination of loads. These subsections will include the effect of the load environment in question on the permeability.

2.2.1. Mechanical loads

The liquid hydrogen will heat up by its surroundings and hydrogen gas will boil off, which will pressurize the tank. As it is assumed the tank is thin-walled, the generated stresses in an element of the tank wall are in-plane. In case of a cylindrical vessel, the resulting equations for the stresses, in hoop direction and axial in the central section direction respectively, will be:

$$\sigma_h = \frac{p \cdot r}{t} \tag{2.12a}$$

$$\sigma_a = \frac{p \cdot r}{2t} \tag{2.12b}$$

Where σ is the stress $[N/m^2]$, subscripts h and a denote the hoop and axial direction respectively, p is the applied pressure $[N/m^2]$, r the radius of the vessel $[m]$ and t the wall thickness $[m]$. An example of a pressure vessel and the applied biaxial strain on element is shown in Figure 2.6.

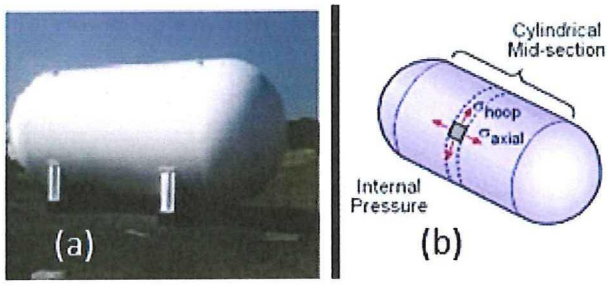

Figure 2.6: (a) Cryogenic pressure vessel; (b) Biaxial stress state of an element

The calculation of the stress is important as the maximum stress should not be exceeded and because it is directly related to the strain, which will be of great importance to the design: the tank wall material will become more brittle at lower temperatures and will become prone to cracks. In order to know the effect of these mechanical loads on the structure and its performance, numerical models can be made and experiments can be performed. Normally, coupon testing of dog bone specimens would suffice to obtain material properties, such as strength, stiffness and maximum strain. However, these tensile tests do not seem to be adequate anymore in order to assess the mechanical load environment of the tank wall during operation. Hannon et al. [12] argues that biaxial loading during operation can cause failure of the tank wall at lower applied strain levels than those determined by uniaxial coupon testing. Also Stokes [26] states that in this field too much research has been done using the common uniaxial tensile test, and that the biaxial loading scenario may imply lower failure load allowables than expected. Hence a biaxial test device is necessary to simulate the stresses in the tank wall and cruciform test specimen need to be designed to test the biaxial load upon. The design of the cruciform specimen is of importance as this has a major effect on the stress homogeneity in the test area. Numerical and experimental studies have been carried out, in order to acquire the best shape for the cruciform specimen. Fillets seem to work well and was currently also used in permeability tests and biaxial loads simultaneously [19] - [25]. Furthermore it was advised by Ferron and Makinde [9] to use slots in the legs in order to reduce the lateral stiffness of the arms as to give the leak test area (during a gas permeability test) the ability to deform unrestrictedly by the biaxial load. A specimen with these adjustments is shown in Figure 2.7
The influence of (biaxial) loading on the permeability of the tank wall have been investigated by NASA [8], Van Pelt [9], Kumazawa et al. [10], Stokes [11] and Raffaelli [12]. Results from NASA and Stokes, who used a tetra-axial load system (8 load tabs), show how permeability does not change until right before the strain limit of the material, where the permeability rises with a couple of orders of magnitude and is probably caused by micro-cracking or even connected micro-cracks. Kumazawa used a biaxial load and showed a

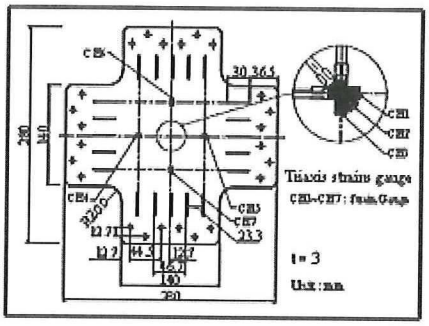

Figure 2.7: Cruciform test specimen with dimension and strain gauge locations [24]

linear increase with load, as shown in figure 2. From this figure it can be deduced that the load ratio is of great importance to the permeability, yielding the highest values at a ratio of 1 and the lowest at a ratio of 0 (i.e. uniaxial load). It is because of this effect Stokes has argued not to use uniaxial tests for biaxial problems. Also Hannon et al. [13] argues that biaxial loading during operation can cause failure of the tank wall at lower applied strain levels than those determined by uniaxial coupon testing. Kumuzawa also showed hysteresis: when gradually unloading, the permeability is slightly higher than during the increase in loading. Friction and viscoelasticity near the matrix cracks are thought be responsible for this effect. Van Pelt used a uniaxial load and permeability decreased up to 0.6%, at which point the test ended. Rafaelli used specimens with a curve and pressurized these to induce strain, but an increase in pressure (and therefore strain) yielded a decrease in permeability or stayed the same.

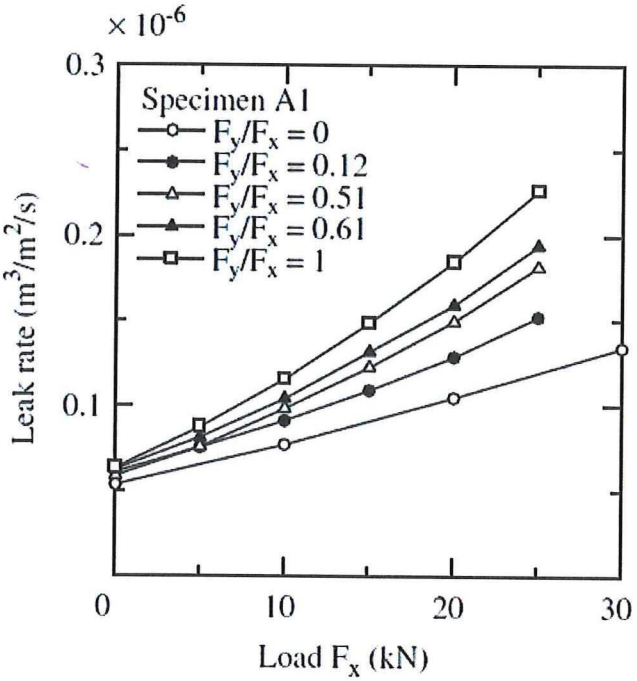

Figure 2.8: Relation between biaxial load and permeability [19]

2.2.2. Thermo-mechanical loads

The liquid hydrogen with a temperature of 21 K also introduces a thermal load into the structure. The amplitude is defined by the coefficient of thermal expansion (CTE) of the material. For most materials the CTE is positive, meaning an extension of the material for when it is heated and contraction when it is cooled. The anisotropic nature of carbon fibre reinforced plastic (CFRP), having a combination of plastic with a positive CTE and carbon fibres with a negative CTE, causes internal stresses. The internal stresses caused by

a sudden temperature drop and (repeated) exposure to cryogenic conditions may cause formation of microcracks and delaminations. This leads to degradation of the structure with respect to its mechanical properties and a possible leak path for the fuel to come out of the tank.
Residual stresses will develop in the plies of the laminate when cooling down. First the residual strain needs to be defined [16]:

$$\{\epsilon_{res}\}_k = \{\epsilon_{UD}\} - [T] \cdot \{\epsilon_{lam}\} \tag{2.13}$$

where ϵ_{res} is the computed residual strain of a single ply, ϵ_{UD} is the strain of a unidirectional laminate, ϵ_{lam} is the measured strain of the laminate and [T] is the transformation matrix to transform the strain of the laminate to the principal strain directions of the local ply. The residual stress σ_{res} can be calculated with the stiffness matrix [Q] of a ply:

$$\begin{Bmatrix} \sigma_{res1} \\ \sigma_{res2} \\ \tau_{res12} \end{Bmatrix}_k = \begin{bmatrix} Q_{11} & Q_{12} & 0 \\ Q_{22} & Q_{12} & 0 \\ 0 & 0 & Q_{66} \end{bmatrix} \begin{Bmatrix} \epsilon_{res1} \\ \epsilon_{res2} \\ \epsilon_{res12} \end{Bmatrix}_k \tag{2.14}$$

In the book of Mckeen [20] many polymers were tested on permeability at different temperatures, generating Arrhenius plots for the solid-permeant pairs. However, test temperatures did not go lower than 260 K most of the time, hence extrapolating any value to this temperature can be done assuming the relation still holds, but it is recommended by the author to do the test at the desired temperature.
It was shown by Aoki et al. [14] that the temperature has a large influence on the crack onset of composites: for an intermediate modulus carbon fibre epoxy composite the crack onset at liquid helium (LHe) temperature started at 50% of the force as that for RT.

2.2.3. Preconditioning

Preconditioning is done either i) to introduce a known damage state, for example achieved by three-point bending or loading (bi-)axially, or ii) to simulate a number of missions by repeating the load conditions a number of times. The first method is interesting as it allows the calculation of leak flow through connected micro-cracks and some analytical and numerical calculations have been successful at predicting the leak through these cracks []. The second method seeks to find the relation between the number of missions and the degradation of the material resulting in a change in permeability. Mechanical and thermo-mechanical cyclic loads are mostly separately applied in this method, although the combined case would be the most realistic. Still, by applying one variable at a time, the shown change in permeability can entirely be attributed to the single variable. Concerning the cyclic mechanical load it is again advised to use a bi-axial load, as it is more realistic and will significantly influence the number of cracks in the composite material.
In study performed by Henaff-Gardin, Lafarie-Frenot and Gamby [13], the effect of thermal cycling was analyzed on T300/914 carbon/epoxy laminates. The lower limit of the thermal cycle was chosen to be constant at 77 K and the upper limit was chosen to be 293 K, 323 K, 363 K or 403 K. It was shown that the number of cracks was strongly dependent on the height of the upper limit temperature and that thermal cycles in the range of 77-293 K resulted in very few cracks. Furthermore, it was shown that the maximum crack density was achieved after the first few cycles. Despite this, NASA studied the effect of thermal cycles in the range of 19 K-293 K. Few cracks were observed (1-1.4 cracks per cm), which were only present in the outer ply. When additional strain (0.13% in longitudinal direction and 0.21% in hoop direction) was applied during the lower limit temperature the crack density increased to 6.0 and 1.9 cracks per inch respectively and cracks were also present within the laminate. Applying the same amount of strain at RT and without thermal cycling resulted in no or few cracks [1]. Bechel, Negilski and James [3] found the same: thermal cycles performed in the range of 77 K-293 K did not lead to cracks. Only if the upper limit temperature was increased and the number of cycles was larger than 400, then cracks started to show. Kessler [18] performed permeability test on the material IM7/977-2 for the X-33 and included thermal cycling. Elevated temperature went up to 400K, as this is part of the load environment. Cooling and heating rates are shown in the figure below. Results showed no increase in crack density or permeability after 10 cycles, but it was noted that during the tensile tests the failure of the material was more violent than normal, probably due to material embrittlement.

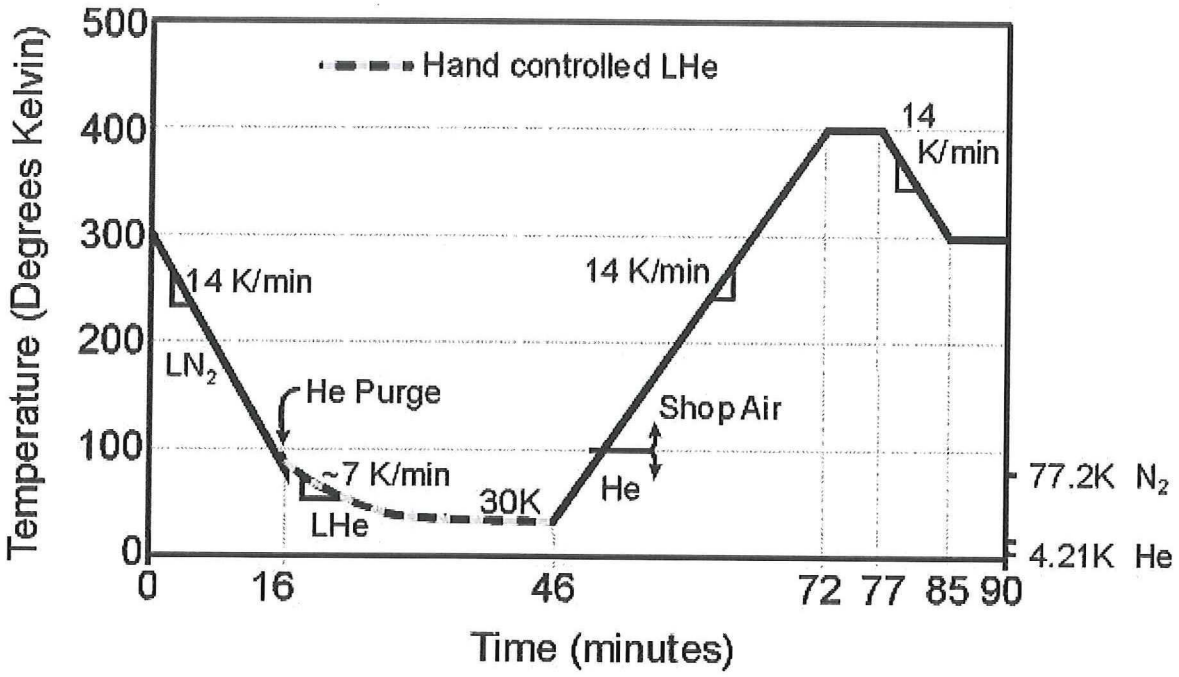

Figure 2.9: One thermal cycle of a specimen [18]

2.2.4. Combination of loads and preconditioning

Although testing the effects on permeability of all variables separately is possible, the best way to simulate the actual use of the tank is by combining the loads and preconditioning in an experiment: the low temperature causes cracks to form at a lower strain, and by applying tensile strain during a permeability measurement allows the cracks to remain open. Mechanical cycling at cryogenic temperature is also important in that sense.

However, the test setup is very demanding, and this is probably why not many studies have been performed with these conditions. The study performed by Raffaelli [23] also included a test where the samples are cycled thermally and the permeability test is performed at 77 K and is mechanically loaded by an out-of-plane deflection. Results show permeability decreases with temperature as expected, but is unaffected by the out-of-plane load. Furthermore, thermal cycles also seem to decrease the permeability, which is attributed the better performing indium seal at cryogenic temperature. However, as his reference is also performed at cryogenic temperature, this can't be a proper explanation. Raffaelli does acknowledge that his test setup is not sensitive enough.

Stokes [26] tested composite specimens which were mechanically cycled at liquid hydrogen (LH_2) temperature and also tested at that temperature. His provided graphs suggest that permeability at RT is similar to permeability at LH2 temperature, although it must be said that the data provided by Stokes are rather unclear.

The test setup at NASA, as used by Gates, Grenoble and Whitley [10] and Grenoble and Gates [11] and as shown in figure 2.10, allows for gas permeability tests at cryogenic conditions and uniaxial loads. The gas permeability is not measured through the thickness however: the hydrogen gas is inserted at the edge of the laminate and leak is measured at the centre. This method was chosen by the researchers because inducing incremental damage in the longitudinal ply was hard to achieve by cyclic loading prior to the permeability test and as such a blockade would remain. The goal of the research was to demonstrate a relationship between the damage state, as was introduced by mechanical cycling prior to the test, and the leak rate through the laminate. Permeability tests were performed at room temperature and cryogenic temperatures at incremental increasing uniaxial loads. Test results showed a correlation between crack density and leak rate, an increase in leak rate with increasing load, and a decrease in leak rate for decreasing temperatures. Furthermore, the difference in leak rate became smaller between tests conducted at RT and CT when the mechanical load was increased, suggesting more cracks or larger crack openings. It was also concluded that the leak rate increased at CT compared to RT. However, although the edge permeability method is presented as a good alternative to the through-the-thickness permeability method, there is no indication by the

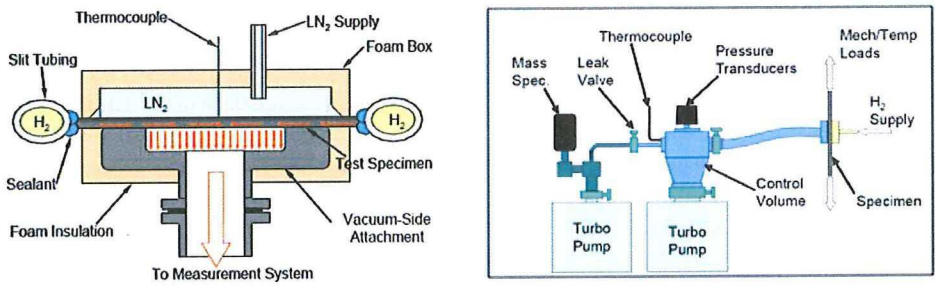

Figure 2.10: Measurement setup as used by Gates, Grenoble and Whitley [10]

authors how this method is justifiable: the center ply is still intact and therefore the leak path might be partly through the damaged plies and partly diffuse through the thickness. The path taken is also unknown.
An apparatus for measuring the gas permeability of tubular specimens is used by Yokozeki et al. [32]. As shown in Figure 2.11, the tubular specimen was immersed in a cryostat filled with LN2 and is loaded in tension. The static tensional load is applied at 0.5 mm/min. Helium gas is inserted under a 'skirt' attached to the specimen. The specimen is subjected to vacuum, creating a pressure difference of 1 atm. by which the helium is able to permeate through the specimen. The inside of the specimen is connected to a helium leak detector, probably a helium mass spectrometer.

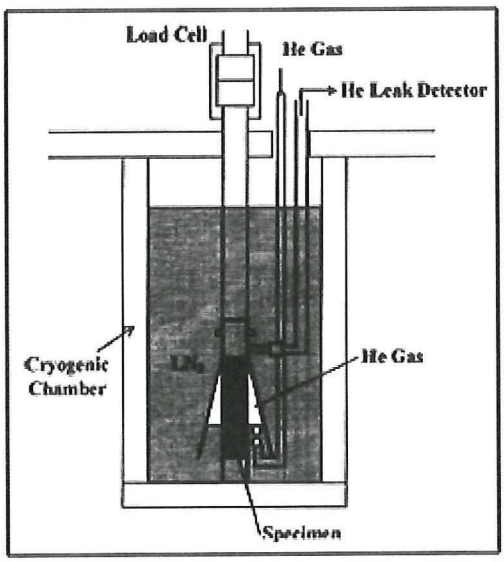

Figure 2.11: Overview of the test setup at the Institute of Aerospace Technology in Osawa, Japan [32]

2.3. Materials

Since the CHATT project is focusing on type IV pressure vessels (i.e. fibre reinforced plastic tank wall with polymer liner), two types of materials are considered for this research: composite materials, required for the tank wall and carrying the loads, and liner materials, with the purpose of acting as a barrier material to the gaseous hydrogen. In this section the material properties will be discussed.
One of the most significant material properties for pressure vessels is the CTE. In the case of composites, the CTE value is different for fibre and matrix, possibly leading to microcracks and/or delaminations when the material is exposed to cryogenic temperatures. In a study performed by Timmerman et al. [29] the crack density was observed to increase when the CTE of the carbon fibre became more negative, i.e. the mismatch became large. It is therefore desired to have similar CTEs for all constituents to avoid the formation of cracks due to the mismatch in the CTE.
Although the CTE is important, it is pointed out by Raffaelli [23] that stiffness is more important: a higher stiffness means a lower strain at the same mechanical load, leading to less crack formation and higher

achievable loads in the tank. Therefore intermediate modulus carbon fibres (slightly negative CTE) are better than glass fibres (low modulus, smallest difference in CTE). Raffaelli and Timmerman do agree that there is a limit in the stiffness and that a too stiff fibre, like the M40J and M35J fibres, results in a too negative CTE, a too large mismatch in CTE and therefore a higher chance of microcracking. These materials are also very brittle, meaning they have a lower failure strain value, especially at cryogenic temperature. A composite that is regularly used for gas permeability properties is an intermediate modulus carbon fibre with an epoxy matrix, IM7/977-2. As this material was chosen for the test with the X-33, it is still subject for research. Other carbon/epoxy-systems researched are IM7/8552, IM600/#101 and IM600/#133.
According to Mckeen [20] and Karimi [17], fibres in a composite can be considered as an added barrier for the permeant: the permeant has to take longer route around the much less diffusive fibres, which is called the tortoise effect. Various fibers have been tested by Humpenoder [15], and indeed the fibers decrease the permeability of the composite as can be seen in figure 2.12. In addition, also the filament diameter matters: increasing the diameter increases the time to diffuse through the polymer.

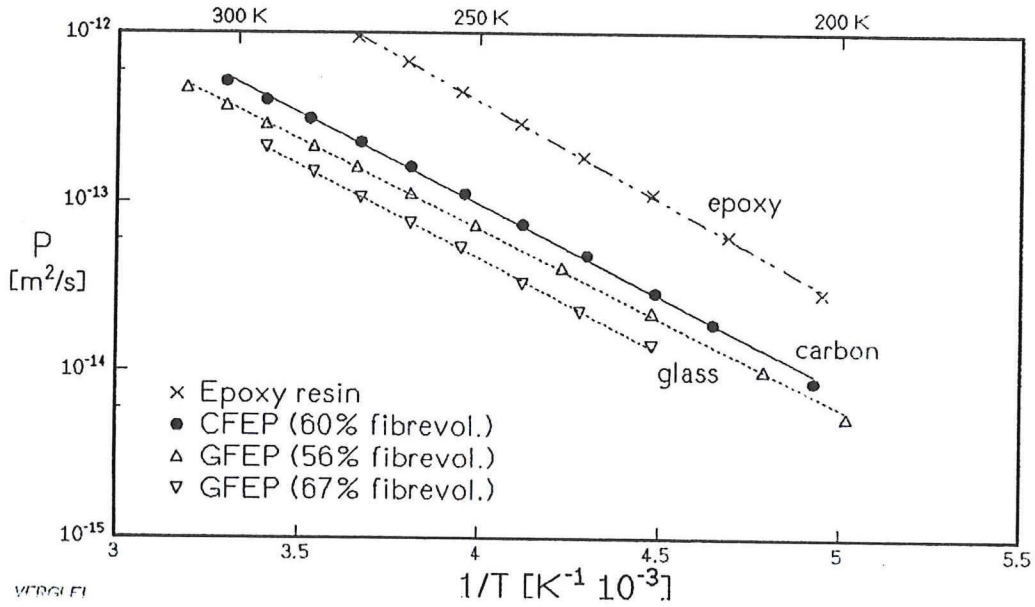

Figure 2.12: Helium permeability of epoxy resin and three fibre reinforced epoxies. [15]

Finally, the mode I strain energy release rate, G_{IC} is also said to be of importance to a composite, as a higher value of this reduces the chance of interlaminar cracks and delamination [13].
Desired properties of the liners, which will act as the barrier for the liquid hydrogen, are high ductility at cryogenic temperatures, and low CTE and Poisson's ratio as the composite wall. A low CTE is of importance so the liner will not deform too much, avoiding a possible collapse. A similar Poisson's ratio is important as it will allow the liner and composite wall to deform due to the pressure at the same rate, avoiding friction as much as possible. Furthermore, polymers have a high intermolecular bonding which is stronger than intermolecular bonding of metals, leading to a lower atomic diffusion than for metals [7]. This would make the choice of a polymer liner justifiable. In a study done by Tapeinos and Koussios [28] multiple possible liners are tested for microcracking initiation under bent strip testing at cryogenic conditions. Interest was shown in fluoropolymers as liner candidate materials, as they have low friction and non-stick properties, which are good properties as friction effects between composite and liner need to be minimal; friction would cause additional strain in the liner to occur and increases the chance of failure of the protective liner. According to Mckeen [20] these fluoropolymers have also permeability values that are valuable.
Also Liquid Crystal Polymers (LCP), Vectra A130 and A950 were tested by Tapeinos and Koussios [28]. LCPs are of interest as they have excellent barrier properties and high mechanical properties in the direction of orientation. Because of this, Dingemans et al. [8] have developed a thermoset LCP based on Vectra which can act as matrix. This TLCP will have a low CTE and is oriented like the fibre, hence the temperature shock will cause no/less damage to the tank wall and keep excellent barrier properties.

3

Apparatus and measurement method

3.1. Permeability apparatus

3.1.1. Apparatus design

For the design of the apparatus the ASTM Standard was used as a reference. Of the apparatus as described in the Standard, the oil bubbler was replaced by a Swagelok exhaust vent and the constant temperature bath was ignored as the temperature did not fluctuate in the room.
The two cell halves are constructed out of aluminium, for it is easy to manufacture. The upstream chamber (bottom half) is equipped with a gasket and the downstream chamber (upper half) with a O-ring with the same inner diameter. The specimen is clamped in between these two halves, with the gasket and O-ring defining the test area. The O-ring is made of material Viton and the gasket of NBR. According to Sturm et al. [27], permeability values of these seals range between $2.19 \cdot 10^{-18}$ and $7.14 \cdot 10^{-18}$ $[mol/(m \cdot s \cdot Pa)]$ with helium as the permeant, making them excellent seals. The diameter of the test area is decided to be 88 mm: this equals the inner diameter of available gaskets and O-rings and allows for a measurable amount of helium to pass through the specimen in a reasonable amount of time. A groove is made into the aluminium for the O-ring and gasket to fit. The O-ring will protrude 0.5 mm out of this groove, but the applied pressure force will compress the ring to make a good seal. The specimen is clamped by tightening eight bolts at the outer edge of the apparatus. Both cells have an inlet/outlet line and exhaust vent, which can be closed by a valve. The helium gas pressure was applied by a cylinder of helium gas connected to the apparatus with a flexible, stainless steel reinforced PTFE hose and a pressure regulator. All threaded items, except for the eight bolts, were tightened with PTFE-tape wrapped around the threads to minimize leaks. Two versions are made of the downstream cell half, one having a flat surface while the other has the test surface reduced by 5 mm to allow bending of the test specimen. An overview of the apparatus and its components is shown in figure 3.1.

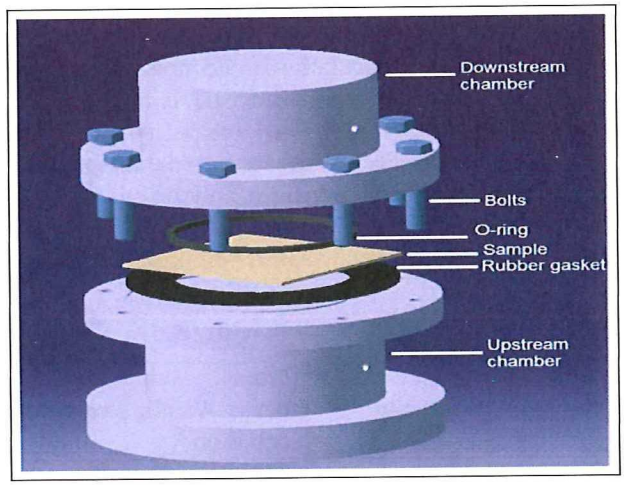

Figure 3.1: Exploded view of the apparatus with a specimen

3.1.2. Measurement method trade-off

In order to obtain the permeability value of a material, a measurement method needs to be chosen that is able measure the amount of gas permeating through the material in time. As was explained in Section 2.3, four methods have been developed previously to measure the permeability: the volumetric method, the manometric method, the mass spectrometry method and a time-lag method. A trade-off is performed in order to determine which experimental setup is best. The four methods all use the same basis.
With the volumetric method, as described in the ASTM standard, the permeability of a material is acquired by measuring the change in volume that is caused by the gas that has permeated through the material. A thin capillary with a ruler next to it is used to determine the volumetric change. The setup is quite simple and no additional (expensive) electronic devices are employed. Rather, the setup requires the user to do visual measurements. This limits the accuracy of the measurements, but this can be overcome by using a capillary with a small diameter and performing the measurements during a long time interval, decreasing the measurement error. Another disadvantage is the effect of atmospheric pressure changes on the position of the liquid slug, as was mentioned in 2.3. A relation can be found between the liquid slug position and the atmospheric pressure, hence the values of permeability can be adjusted for and the error is kept to a minimum.
The manometric method, as described in the ASTM standard, determines the permeability by measuring the change in pressure in the downstream chamber. As discussed in the previous chapter, the use of mercury as mentioned in the test standard is quite hazardous, so it would be safer to use a pressure transducer instead. The accuracy of the permeability value then depends on the accuracy of the pressure transducer and the accuracy of the empty cell measurement of the downstream chamber. According to the test standard the free volume also needs to be determined with mercury, but this is rather avoided by employing a model of the apparatus.
Lastly, the mass spectrometry method determines the amount of particles that pass through the specimen by mass spectrometry. Although this method should be very accurate, the costs are very high, about 30000 Euro.
Considering the costs, the mass spectrometry method is least attractive due to its high investment costs. The manometric method is with respect to the volumetric method more expensive, but should be easier to use as the pressure change measurement will be automated. However, if fully automated measurements need to be done, also the atmospheric temperature and pressure need to be recorded. As this adds to the expenses, these will be measured manually. Because of this the advantage of the manometric pressure over the volumetric method is gone, as the disadvantages of the volumetric method can be overcome. Hence, the volumetric method is chosen to determine the permeability of the specimen, for it is the least expensive, simplest to design and should achieve accurate results if the atmospheric effect is compensated for and a sufficiently thin capillary is used.
Also the test gas is of importance to the test apparatus and a proper gas should be chosen for the purpose of this research. As the pressure vessel will be designed to store hydrogen, using this gas would give the most accurate results. However, it is also highly flammable, introducing a risk. Helium is also often used as it is safer (inert gas) than hydrogen and has a similar molecular diameter. Calculation of the molecular size of hydrogen and helium by three different methods is shown in table 3.1. Because permeation is often treated as a viscous motion and based on the viscous calculation of the molecular diameters of hydrogen and helium, the permeability measurements may be conservative if helium is used instead of hydrogen. This is also confirmed by Humpenoder citeHump98, who showed that permeability is higher at RT for hydrogen, but as temperature decreases, permeability will decrease less rapid than for hydrogen (figure 3.2). Mainly because of safety reasons, the permeant of choice is helium, and the purity of the gas used in the experiments is 99.9%. A suitable pressure regulator for the applied helium pressure is The Omega R83-200, because it is designed for a gas such as helium and will have minimum leakage.

Table 3.1: Molecule diameters in picometer of helium and hydrogen [5]

Gas	From Viscosity	From Van der Waal's equation	From heat conductivity
Helium	19	26	23
Hydrogen	24	23	23

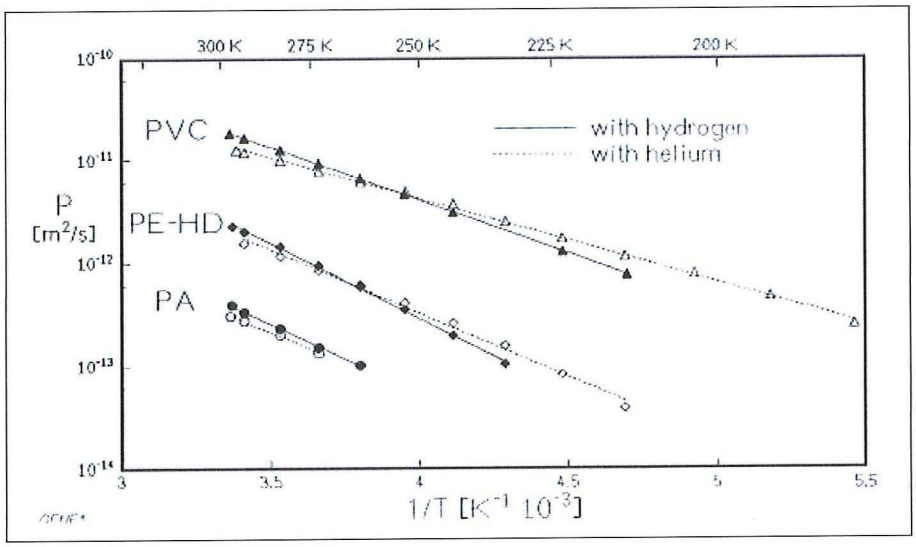

Figure 3.2: Helium and hydrogen permeability of PVC, PE-HD and PA [15]

3.1.3. Data acquisition

With the volumetric method chosen, a capillary tube needs to be connected to the outlet in order to measure the volumetric change. For this purpose a PTFE-tube was connected to the outlet in which a boronsilicate glass capillary with an inner diameter of 2 mm was inserted. In order to make a good connection without any leaks, the tube and capillary were adhered to each other. As a liquid slug, isopropyl alcohol was used, dyed with ink. Although any other low density liquid could have been used with equal results according to [21] including water, an alcohol is a good solvent for the dye (ink). Because isopropyl alcohol is not very toxic, this is used as the liquid slug. The tube is filled with the liquid slug, up to the connection with the capillary. A ruler is fixed in place next to the capillary, so the measurements are 0.5 mm accurate at best. It was considered to also employ a capillary tube with a smaller diameter, reducing the time required for an experiment and increasing the precision, but:

- a good connection with the feed tube would be even harder to make;
- a smaller diameter would result in a too fast test for the fluoropolymers, rendering accurate manual measurements almost impossible;
- switching between capillary tubes would result in a damaged feed tube-cell connection with possible leakage.

Therefore it was decided to use one capillary diameter only.
As permeation is a function of applied gas pressure on the specimen, the applied helium pressure is monitored with a pressure transducer. An Omega PX-309, capable of measuring the relative pressure up to 21 bars, is attached to the pressure regulator. The transducer is connected to a computer through a National Instruments 9219 input module and data is logged every second. The atmospheric pressure is measured with a digital barometer in hectopascals.
During a permeability test, the liquid slug position, atmospheric pressure and atmospheric temperature were manually logged. The pressure difference between the helium pressure and the atmospheric pressure was acquired every second during the entire measurement. With these values the volume-flow rate, the Gas Transmission Rate (GTR), permeance and permeability can be calculated, for which the equations are respectively:

$$V_r = slope \cdot a_c \tag{3.1a}$$

$$GTR = 10^{-6} \cdot V_r \cdot p_0 / (A \cdot R \cdot T) \tag{3.1b}$$

$$P = GTR / (p - p_0) \tag{3.1c}$$

$$\underline{P} = P \cdot t \tag{3.1d}$$

Where V_r is the volume flow rate of the permeated gas $[mm^3/s]$, Slope is rate of rise of the slug in the capillary $[mm/s]$, a_c is the cross-sectional area of the capillary $[mm^2]$, GTR is the Gas Transfer Rate $[nmol/(m^2 \cdot s)]$, p_0 is the ambient pressure $[Pa]$, A is the transmitting area of the specimen $[mm^2]$, R is the universal gas constant, 8314.31 $[L \cdot Pa/(K \cdot mol)]$, T is the ambient temperature $[K]$, P is the permeance $[fmol/(m^2 \cdot s \cdot Pa)]$, p is the upstream gas pressure $[Pa]$, $\underline{P}$ is the permeability $[amol/(m \cdot s \cdot Pa)]$, t is the thickness of the specimen $[mm]$.

3.1.4. Apparatus calibration and error determination

It is necessary to evaluate the design by inspecting the apparatus for any leaks. The downstream chamber is the most critical part, because if leaks exist at this point, the volume of permeated gas will not change and the liquid slug will not move. In case of a small leak, the liquid slug might move, but less than it should have moved without a leak. Hence, in order to test the seals of the downstream chamber, the apparatus was set up with a 3 mm thick aluminium specimen and applying vacuum on the downstream chamber. Upon closing the vacuum pump valve, the system pressure value was monitored for 15 minutes during which no pressure increase was measured.
The positive result with the vacuum test is only partly satisfactory:

- The leak path is different: from outside the apparatus to the inside;
- The result is only valid for air, not necessarily for helium which has a much smaller molecule diameter.

Because of this, a second test is conducted to see if any pressure leaks arise at 8 bars of helium pressure. To do this, a specimen is mounted with a hole at the center. This will cause the entire apparatus to be pressurized and leaks are detected with a soap solution. Although this is a good indication for faulty connections (badly applied PTFE tape, cell misalignment etc), very small defects will not be detected. However, considering the amount of helium that passes through the actual specimens will be very small, the chance that it immediately diffuses out of the cell through the tiny hole that is present is also very small. So it is likely there is an error in the measurement because of this, but it is assumed to be negligible.

Measurement accuracy
Every component of the data acquisition setup has an tolerance which needs to be taken into account during the data analysis. These tolerances have been provided by the supplier and are listed in Table 3.2 below. By implementing the values into the equations for permeability a worst case lower and upper boundary can be determined, and will be shown in the results. The tolerance of the test area is unknown and it assumed that the CNC machine made a perfect cut with a diameter of the specified 88 mm. It is furthermore assumed that four thickness measurements are enough to gain an average thickness of each sample. It is therefore assumed that the measurement accuracy only depends on the measurement device and not on the sample itself.

Table 3.2: Tolerance of each element of the data acquisition setup.

Part	Value	Unit
Slug measurement	0.5	[mm]
Thickness	0.005	[mm]
Temperature	0.05	[K]
Barometer	3%	[-]
Transducer	0.25%	[-]
Capillary diameter	10%	[-]

3.1.5. Data analysis

Outlier identification and removal
Although sufficient time was allowed to the helium to fully saturate the sample, many results show a peak value at the first measurement and some also show a drop at the last measurement. The peak value is hard to explain, as rather the opposite was expected: as it takes time for the sample to get saturated with helium, no measurements are expected during the first minutes and hence sufficient time is taken before the actual measurements start. But as the peak value does influence the trend to quite an extend, an outlier detection script is implemented to analyze the data and remove the outliers.

In this script the linear trend is first established with the provided slug height data. Then the residuals (the difference between the measured data point and the trend line) are calculated. By calculating the standard deviation of the measurements a test criterion can be set up, judging the measurement to be an outlier or as a normal value within the set confidence level of 95%. When the outliers have been removed, a new linear trendline is established without the outliers. This is then used for the calculation of the permeability.
The trendline is established with a linear fit function in Matlab, and is based on least-square fitting. The standard deviation is calculated with:

$$s = \sqrt{\frac{\sum_{n=1}^{n} y_i^2 - \left(\sum_{n=1}^{n} y_i\right)^2 / 2}{n-1}} \tag{3.2}$$

With n being the number of observations and y_i the value of an observation.

Area increase for deflected specimen
Due to the deflection of the sample caused by the helium pressure, the surface area exposed to the helium as well as the surface area downstream will increase. By determining the deflection of the specimen, the change in area can be established. According to Timoshenko [] the analytical expression for the deflection of clamped anisotropic circular plates under uniform pressure is:

$$w(r) = \frac{q \cdot (r_s^2 - r^2)^2}{24 \cdot (D_{11} + D_{22}) + 16 \cdot (D_{12} + 2 \cdot D_{66})} \tag{3.3}$$

then the surface area A can be written as:

$$A = \int_r^0 2\pi r \cdot ds \tag{3.4}$$

with arc length ds given to be:

$$ds = \sqrt{1 + \left(\frac{dw}{dr}\right)^2}\, dr \tag{3.5}$$

The same equations also apply for isotropic materials.

Atmospheric pressure correction
According to [5] the atmospheric pressure change influences the slug position measurements. This makes sense: as the glass capillary is open at the top, an increase in the atmospheric pressure forces the liquid to go downward until a balance between atmospheric pressure and downstream pressure is achieved. A correction factor for this phenomenon can be deduced by calculating the volume decrease caused by the increase in pressure. To do this, it is assumed that it is a reversible adiabatic process and the ideal gas law can be used:

$$P_1 \cdot V_1^{\gamma} = P_2 \cdot V_2^{\gamma} \tag{3.6}$$

$$V_2 = V_1 + A_c \cdot \Delta h \tag{3.7}$$

$$\Delta h = \frac{-V_1 + \left(\frac{p_2 \cdot V_1^{\gamma}}{p_1}\right)^{1/\gamma}}{A_c} \tag{3.8}$$

Where P is the pressure, V is the volume and the subscripts 1 and 2 denote the before and after condition respectively in the downward chamber. γ is the adiabatic index and is assumed to equal 1.4: although helium has a higher adiabatic index of 1.667, the amount of helium in relation to air in the downstream chamber is negligible. Δh finally is the change in slug height. P_1 and P_2 are known through measurements, the initial volume V_1 is estimated by adding all the empty segments of the downstream chamber. With this it is estimated that the initial volume is 2900 mm^3. Because the correction with this equation is dependent on the pressure ratio, the correction will not be exactly constant, but will about -0.0075 mm/Pa for the glass capillary with a diameter of 2 mm. If for example, the starting pressure would be 101300 Pa and the decrease in atmospheric pressure is 50 Pa during the test, the change will be 1.662 μL, equivalent to about 0.38 mm in slug movement. Compared to a test performed with e.g. PFA, of which the permeability is relatively high,

this accounts to about 0.5% of the total slug movement, which is neglegible. Whereas for a lesser permeable material, where the total slug movement is much lower, the effect of atmospheric pressure changes can go up to 2%.
In the case the second aluminium cell is used, which has an empty chamber for the sample to deflect, the correction factor is tenfold higher at about -0.077 mm/Pa and depends on the amount of volume taken by the deflected sample. This means that influence of atmospheric pressure change is much higher for a test where deflection is involved. The amount of volume taken by the deflected sample is explained and calculated in section 3.1.5.
The correction value was also attempted to be measured experimentally by setting up the apparatus with an aluminium sample and all valves closed. According to this method, the correction is -0.13 mm/Pa. However, as it was necessary to wait for a very long time until the pressure had changed enough to get a good reading, the temperature had changed by more than $1°C$. This caused the experiment to be faulty, as the temperature affects the volume in the downstream chamber. Therefore, the theoretical value for the atmospheric pressure correction is chosen to test any improvement to the obtained measurement data.

Liquid slug pressure correction
In the equation used in the ASTM test standard for permeability, it is assumed that the pressure in the downstream chamber equals the atmospheric pressure. However, this assumption is not correct for this situation as the feed tube to the capillary has a u-bend in order to store the liquid slug in. As the liquid slug is pushed up the glass capillary, the weight of the column (see Figure 3.3) that has moved up will add to the pressure together with the atmospheric pressure. Hence, the pressure in the downstream chamber is:

$$p_{down} = p_{atm} + \rho \cdot g \cdot h_{meas} \cdot \left(1 + A_{cap}/A_{tube}\right) \tag{3.9}$$

where ρ is the density of the liquid slug, isopropyl alcohol, h_{meas} the measured liquid slug movement, A_{cap} the capillary area and A_{tube} the feed tube area. In practice this results in a maximum error of about 800 Pa. This also has an effect on the permeability by the decrease in pressure difference between the pressure in the upstream chamber and downstream. Therefore, the pressure difference as given by the pressure transducer should be corrected as well:

$$\Delta p_{actual} = p_{transducer} - \rho \cdot g \cdot h_{meas} \cdot \left(1 + A_{cap}/A_{tube}\right) \tag{3.10}$$

Where Δp_{actual} is the actual pressure difference between the two chambers, and $p_{transducer}$ is the measured pressure difference by the pressure transducer. However, these effects are minor as the difference between the atmospheric pressure and the calculated pressure of the downstream chamber will not exceed 1000 Pa, hence is less than 1%.

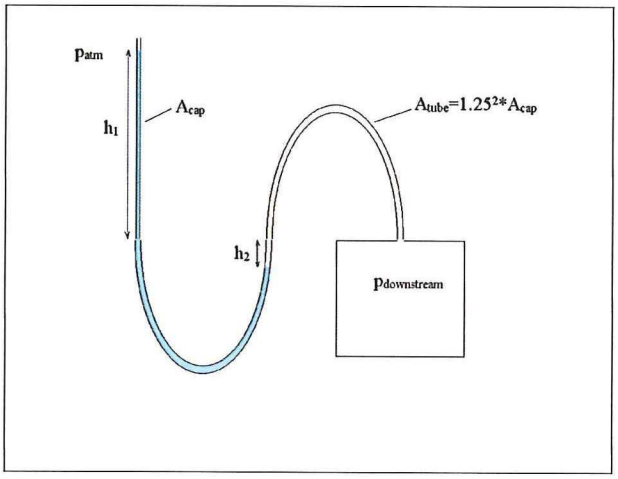

Figure 3.3: Program structure

Thickness decrease
The applied out of plane pressure cause a decreased thickness of the samples. As the permeability is calculated as a function of thickness, it is desirable to know how much the thickness is affected by the

pressure load. For a specimen that is not allowed to deflect, it is assumed that only the polymer matrix influences the decrease in thickness, as the fibers are all in-plane. In this case Hooke's law is employed:

$$t^* = \left(\frac{p}{E}\right) \cdot t \tag{3.11}$$

with t^* being the new thickness $[mm]$, E being the stiffness modulus of the polymer $[N/m^2]$, p the pressure applied $[N/m^2]$ and t the original thickness $[mm]$. In the case of an undeflected specimen, the decrease in material thickness can be ignored as even a flexible material such as a fluoropolymer only has a thickness decrease of 0.1% due to the pressure applied.
For a round specimen where a deflection is allowed, it is assumed that the volume of material deflected remains unchanged, meaning that the edges are perfectly clamped. So to get the decreased thickness of the deflected specimen, the increased surface area A_2 of the deflected specimen needs to be acquired.

$$t_2 = \frac{A_1 \cdot t_1}{A_2} \tag{3.12}$$

where t is the thickness, A the area, and subscripts 1 and 2 denote the conditions before pressure is applied and while pressure is applied respectively. A_2 can be calculated as shown in equation 3.4. For composites and LCPs the area increases by less than a percent due to the small deflection and can therefore be ignored. The influence on the more flexible fluoropolymers is larger, in the range of 4-5% and therefore cannot be ignored.

Decreasing deflection correction
As was noticed from the figures of the original samples, the pressure difference decreases over time in most of the cases and is likely the cause of a leak in the upstream side of the system. Although the pressure regulator was supposed to keep the applied pressure constant during measurements, it did not function as desired: during one test the pressure valve was closed and the upstream bleed valve was opened prior to stopping the program running pressure transducer, yet the pressure measurement still pointed to the same value as before. Hence, the measurements performed with the pressure regulator controlling the pressure were faulty. The cause of this could not be found and it was decided to continue by controlling the pressure with the pressure regulator with coarse adjustment valve present at the top helium tank. Sadly, the regulation was difficult and although the pressure changes were mostly in the order of 0.1 bar, a correlation between a drop in pressure difference and a drop in permeability seems to be present. This can be explained by the increase in volume of the downstream chamber by a decrease in deflection of the sample due to a decrease in pressure difference.
Therefore it was decided to find a correction for this increase in volume by making a FEA model in Abaqus and generating the deflection of the sample for a range of pressures and compare this to the analytical expression of Timoshenko (equation 3.3). As model and analytical expression were in good agreement, a program was created in MatLab (see Appendix B) that uses the analytical expression to find the change in volume due to the change in pressure. In order to find the volume occupied by the deflected sample, the area under the curve is integrated with respect to y as the region is rotated about the y-axis. Therefore the radius r needs to become a function of the deflection w to calculate the volume:

$$V = \int_0^{w_{max}} A(y)dy = \int_0^{w_{max}} \pi(r(w))^2 dy \tag{3.13}$$

By reusing this formula at multiple pressures a relation is established between the pressure change and volume occupied, which is found to be linear as is shown for the quasi-isotropic AS4/8552 sample in figure 3.4.

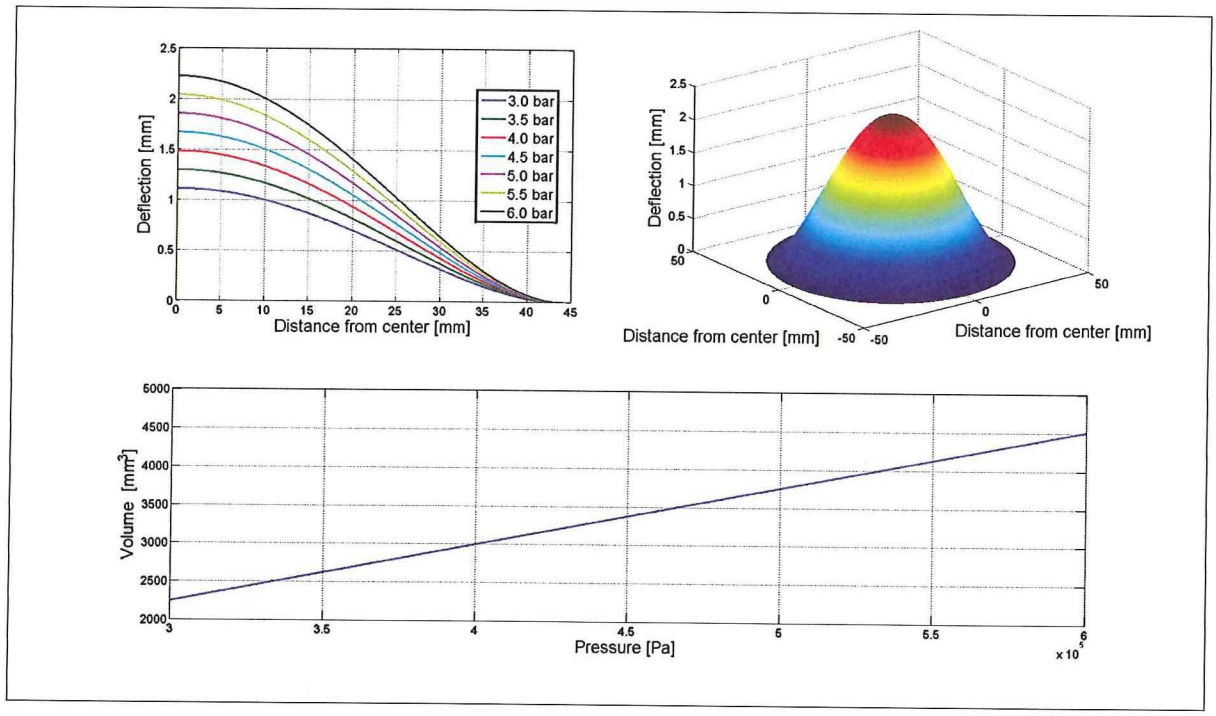

Figure 3.4: Deflection of a quasi-isotropic AS4/8552 sample at various pressures. Shown are the cross section of the sample when deflected, an overview of a deflected sample at 6 bar and the volume occupied by the deflected sample as a function of pressure.

Data analysis program structure

With all required calculations have been established, a Matlab program was developed. A good overview of how this program works is shown in figures 3.5 and 3.5 on the next pages. As can be seen in these flowcharts, the permeability is calculated with and without outlier detection and data corrections. This was performed to gain insight in the adjustments made by the program.

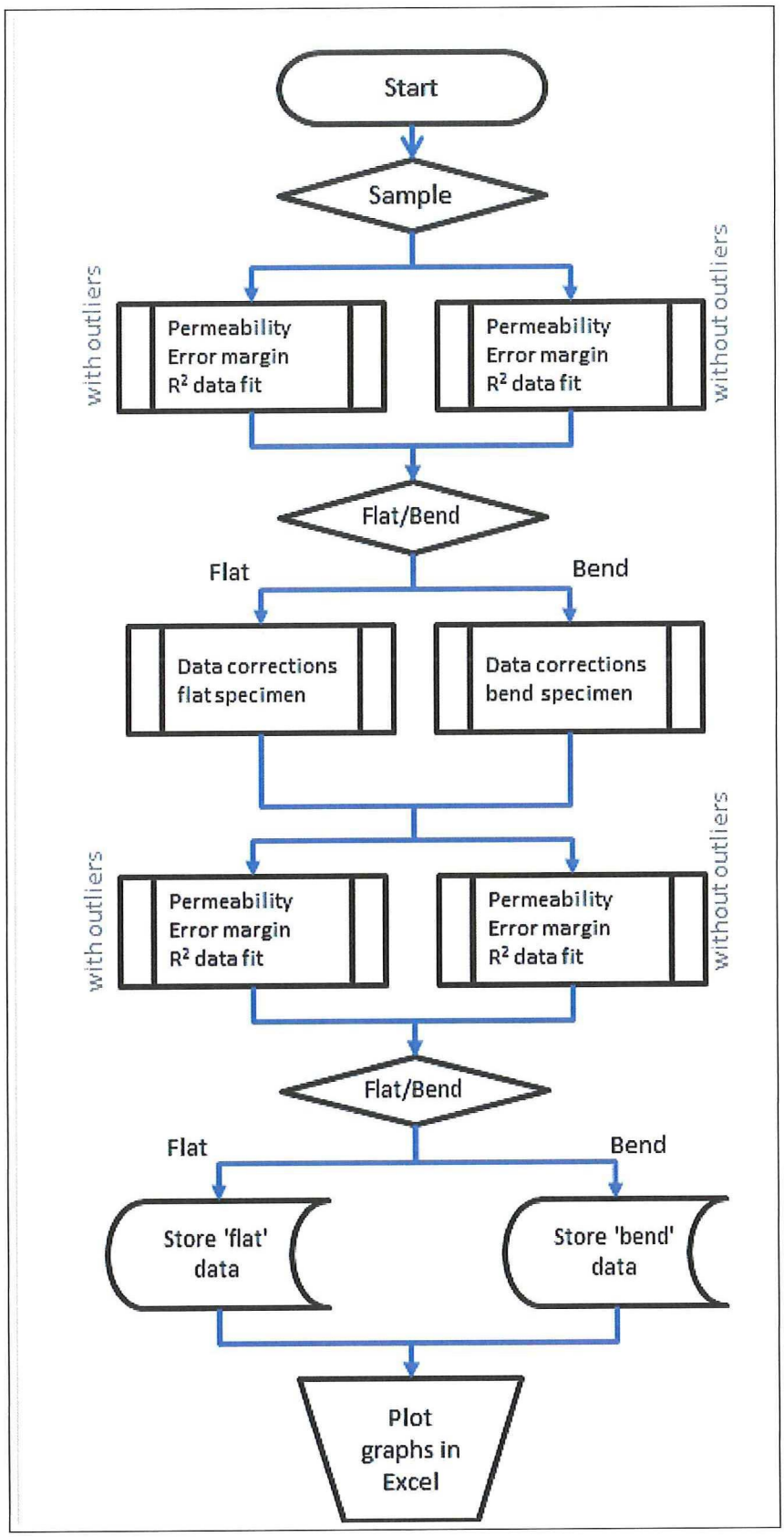

Figure 3.5: Flowchart of the Matlab program that analyzes the data.

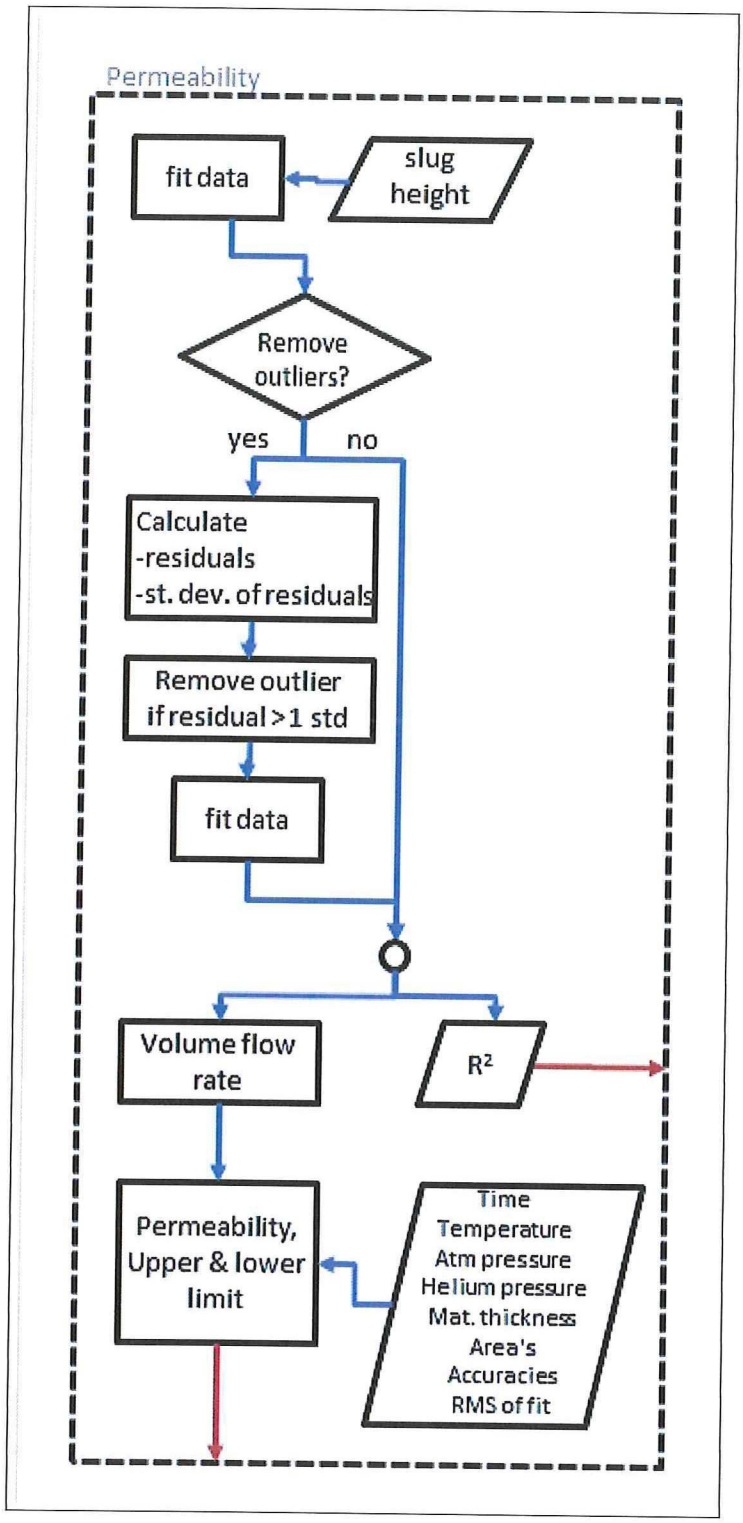

Figure 3.6: Flowchart of the Matlab program that calculates the permeability, the upper and lower limit, and the goodness of fit of the data.

Measurement setup
Also a flowchart of the entire measurement setup is provided, as shown in figure 3.7. The red arrows depict the required manual operations for the data acquisition.

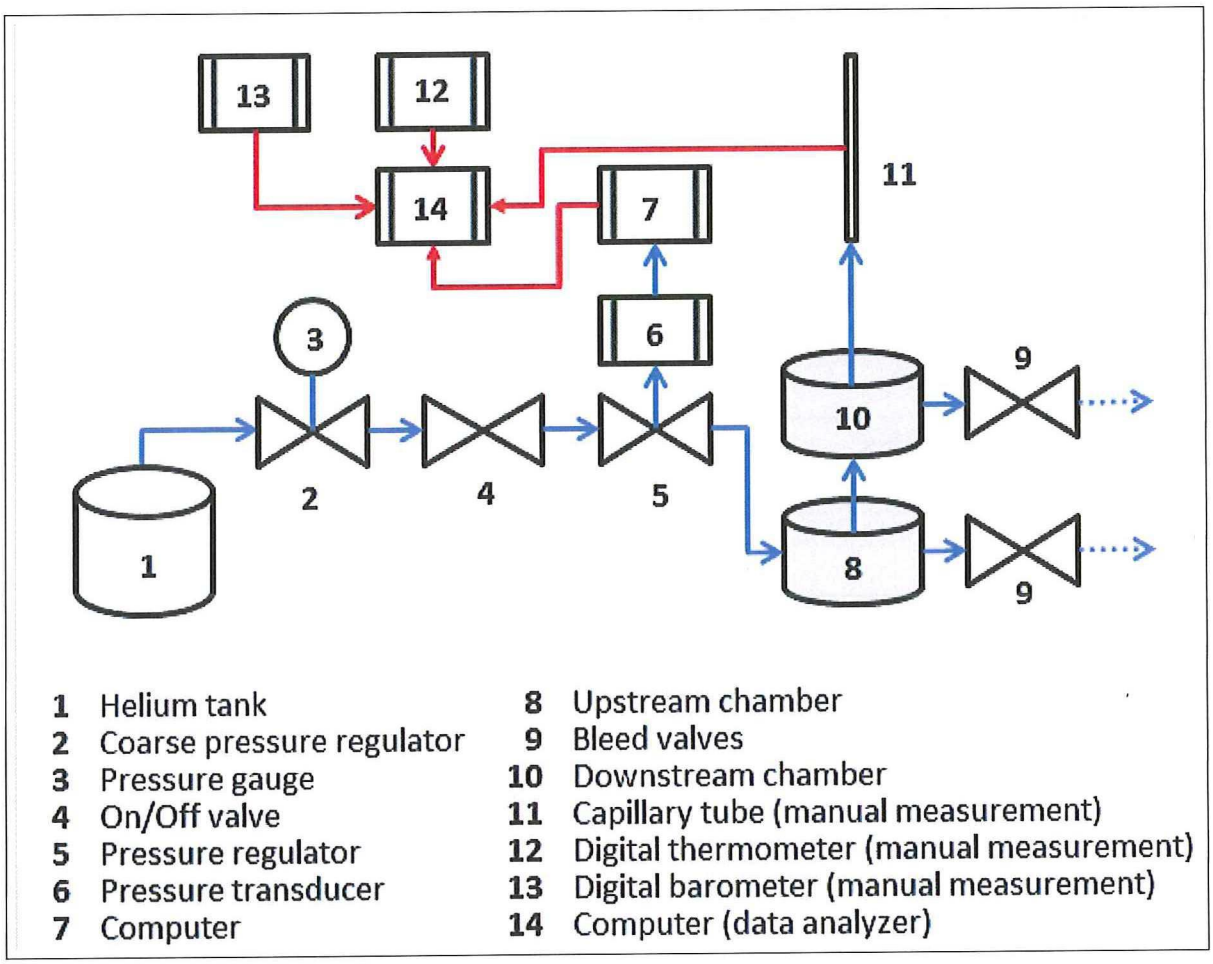

Figure 3.7: Flowchart of the entire setup.

3.2. Materials

Three types of materials are considered in this research, which are either candidate tank wall or liner materials:

- Carbon fiber reinforced plastic AS4/8552;
- Fluoropolymers;
- Liquid crystal polymers.

Material properties of above materials can be found in Appendix C.
Samples of the fluoropolymers and LCPs were send to LabThink for permeability research, as to acquire representative values to compare own results with. However, LabThink provided test data with units other than used in the ASTM standard which is used in this research. Hence, the provided values were rewritten from $cm^3 \cdot cm/(cm^2 \cdot s \cdot cmHG)$ to $mol/(m \cdot s \cdot Pa)$. The conversion factors 22415 cm^3/mol, obtained from the ideal gas law, and $7.5 \cdot 10^{-4}$ $cmHg/Pa$ have been used. The resulting reference values can be found in the subsections below. As the reference data are provided in a range from 93 K up to 318 K, Arrhenius plots can be made from which the permeability coefficients and activation energies can be deduced. This shall be used to estimate the volume loss in a pressure vessel with a polymer liner. The liner is assumed to:

- have a total surface area of 10 m^2;

- have a thickness of 1 mm;
- not be influenced by the mechanical load;
- act as a barrier without the composite;
- be pressurized at a constant 4.8 or 6.7 bar. Atmospheric pressure is at 1 bar;
- have the same temperature as the boiled of gas.

Results of the helium volume loss per hour shall be given as a function of temperature for the LCPs and the fluoropolymers. In addition, the result of the FEP liner is compared to the hydrogen loss in time for the same tank, with the permeability coefficient and activation energy values derived from the Arrhenius plot from Figure 3.8, and is given in Table 3.3. As the permeability values given for the material which had helium as the permeant are given in $[mol/(m \cdot s \cdot Pa]$, while the permeability values given for hydrogen are in $[mm^3/(m \cdot s \cdot Pa]$, the former will be rewritten so units will match. This is done with the ideal gas law, which is still quite accurate at very low temperatures for helium as is shown in Appendix C.

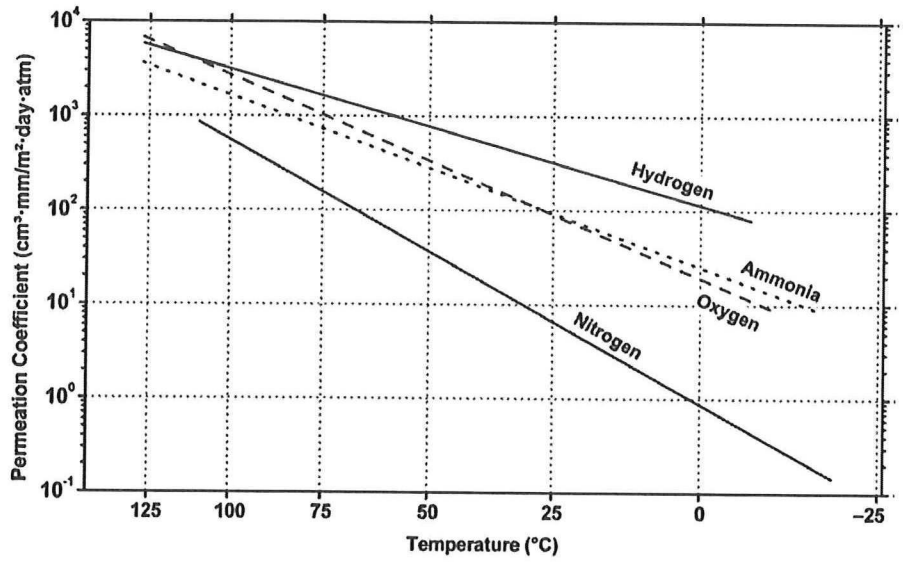

Figure 3.8: Arrhenius plot of FEP with hydrogen as the permeant [20]

Table 3.3: Permeability values deduced from 3.8 for FEP with hydrogen as the permeant

	E_A J/mol	P_0 $mm^3/(m \cdot s \cdot Pa)$
FEP	30169.12	$6.76 \cdot 10^{-3}$

3.2.1. AS4/8552

The AS4 fiber is an intermediate modulus carbon fiber and because of that is a good choice for the tank wall structure. The matrix is the 8552 toughened epoxy, which is a well known high performance thermoset polymer. There is a CTE mismatch between fiber and matrix, but with choosing an intermediate modulus fiber there is a good balance between stiffness and CTE properties. Another reason this material is chosen, is because its properties resembles the composite material used in other research, such as in the research performed by NASA on the X-33 (IM7/977-2,-3). The composite laminates were manufactured with preimpregnated AS4/8552 unidirectional sheets by hand layup in three different layup sequences:

- Completely unidirectional: $[0]_8$;
- Quasi-isotropic: $[0/45/-45/90]_s$;
- Angleply: $[30/-30]_{2s}$.

After layup, the specimens need to be cured in the autoclave. The vacuum table is build up as shown in Figure 3.9. As can be seen in this figure, kapton foil and flat aluminium sheets of the same shape as the specimens have been used to acquire smooth surfaced specimens. This is a necessity, as a smooth surface ensures a good connection between the O-ring and the composite specimen without leakage.

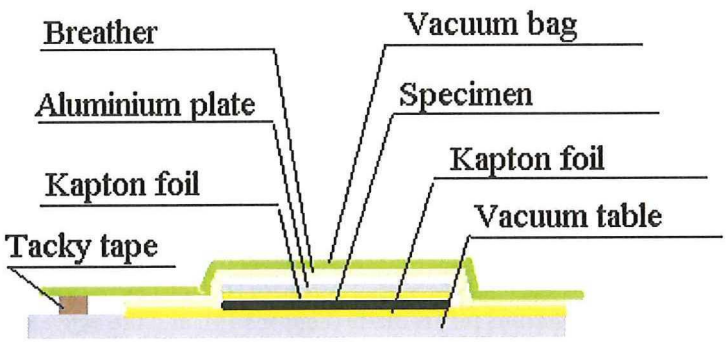

Figure 3.9: Vacuum table build up.

The cure cycle was acquired from the supplier (Hexcel) and is shown graphically in Figure 3.10.

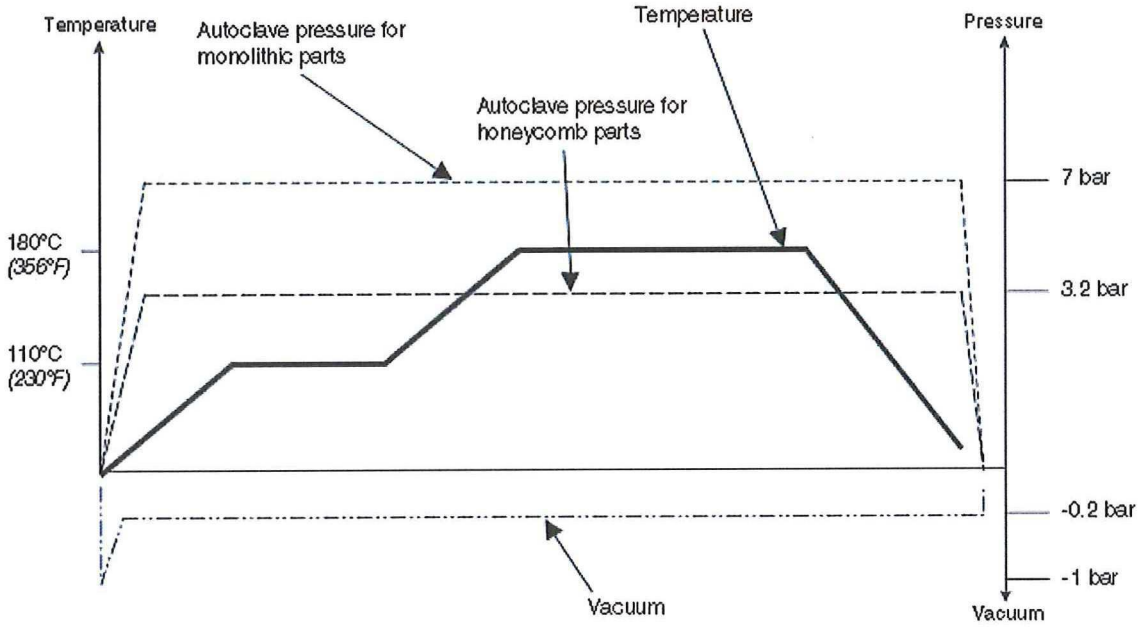

Figure 3.10: Cure cycle of the AS4/8552 composite as provided by Hexcel

As shown in figure 3.10, the autoclave is first heated up to 110° to promote flow of the resin and the composite is then cured at 180°C for two hours at 8 bars (absolute) pressure. Cool down is performed at 5°C per minute.
The final circular shape of the specimens, with a diameter of 110 mm, was acquired by machining. Although this may induce some splintering at the edges, this does not influence the measurements as there is enough clearance from the edge to the edge of test area.

3.2.2. Fluoropolymers

Fluoropolymers are selected for this research as these are flexible (even at low temperatures), have a low density and the polymer is relatively easy to manufacture.

Three fluoropolymers were chosen: FEP, PFA and PTFE. As they were delivered in plates of 3 and 4 mm thick, it was decided to machine the plates to an equal thickness of 2 mm and polish them afterwards.

Table 3.4: Reference permeability values for the fluoropolymers

Temperature [°C]	PFA $[mol/(m{\cdot}s{\cdot}Pa)]$	FEP $[mol/(m{\cdot}s{\cdot}Pa)]$	PTFE $[mol/(m{\cdot}s{\cdot}Pa)]$
45	$1.56{\cdot}10^{-14}$	$1.63632{\cdot}10^{-14}$	$1.13337{\cdot}10^{-14}$
35	$1.36{\cdot}10^{-14}$	$1.35523{\cdot}10^{-14}$	$9.44646{\cdot}10^{-15}$
26	$1.16{\cdot}10^{-14}$	$1.12702{\cdot}10^{-14}$	$8.00088{\cdot}10^{-15}$
-100	$3.21{\cdot}10^{-16}$	$1.19796{\cdot}10^{-16}$	$1.14475{\cdot}10^{-16}$
-180	$2.11{\cdot}10^{-19}$	$1.12032{\cdot}10^{-20}$	$1.97194{\cdot}10^{-20}$

With the values from Table 3.4 an Arrhenius plot is made (Figure 3.11), and the activation energy E_A and the permeability constant $\underline{P}_0$ are determined. The accuracies of the data provided in Table 3.4 is unknown as it was not provided by the contractor. The fit through the datapoints in figure 3.11 is perfect ($R^2 = 1$). It was tested what the effect would be of some small (5% errors) in the data received, however the fit remained almost unaffected by it and the same is also applicable for the activation energy and permeability constant.

Table 3.5: Activation energies and permeability constant of the fluoropolymers

	E_A	$\underline{P}_0$
	$[J/mol]$	$[mol/(m{\cdot}s{\cdot}Pa)]$
PFA	12255	$1.61{\cdot}10^{-12}$
FEP	15513	$5.78{\cdot}10^{-12}$
PTFE	14491	$2.72{\cdot}10^{-12}$

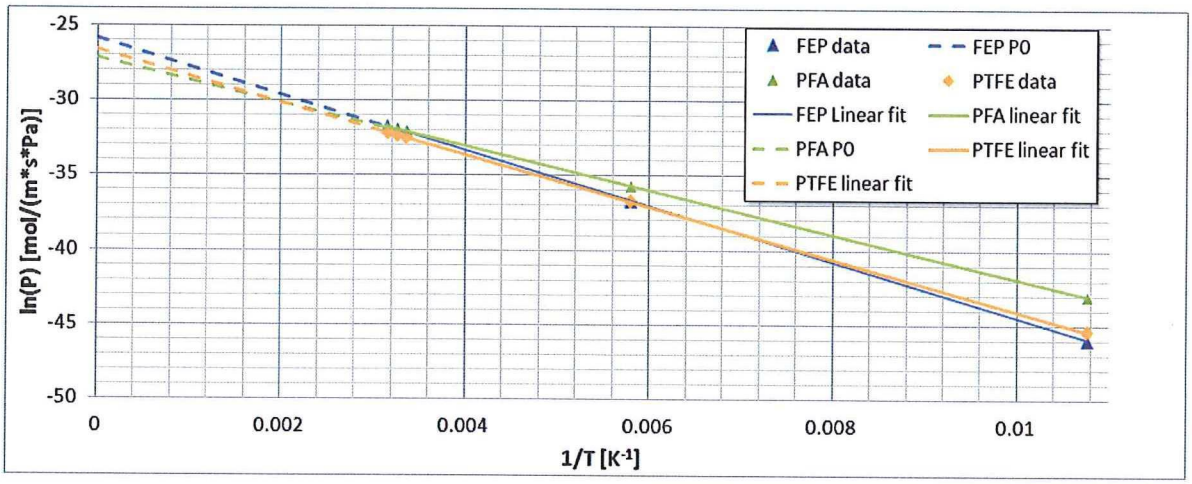

Figure 3.11: Arrhenius plot of reference data of fluoropolymers FEP, PFA and PTFE.

3.2.3. Liquid crystal polymers

With the values from Table 3.6 an Arrhenius plot is made (Figure 3.12), and the activation energy E_A and the permeability constant $\underline{P}_0$ are determined and provided in table 3.7.

Table 3.6: Reference permeability values for the LCP's

Temperature [°C]	Vectra A130 $[mol/(m{\cdot}s{\cdot}Pa)]$	Vectra A950 $[mol/(m{\cdot}s{\cdot}Pa)]$
35	$5.69{\cdot}10^{-17}$	$5.92286{\cdot}10^{-17}$
26	$4.30{\cdot}10^{-17}$	$4.39362{\cdot}10^{-17}$
-100	$3.95{\cdot}10^{-20}$	$2.56992{\cdot}10^{-20}$
-180	$1.43{\cdot}10^{-20}$	$8.69355{\cdot}10^{-21}$

Table 3.7: Activation energies and permeability constant of the LCP's

	E_A	P_0
	$[J/mol]$	$[mol/(m \cdot s \cdot Pa)]$
A130	23863	$6.34 \cdot 10^{-13}$
A950	25409	$1.21 \cdot 10^{-12}$

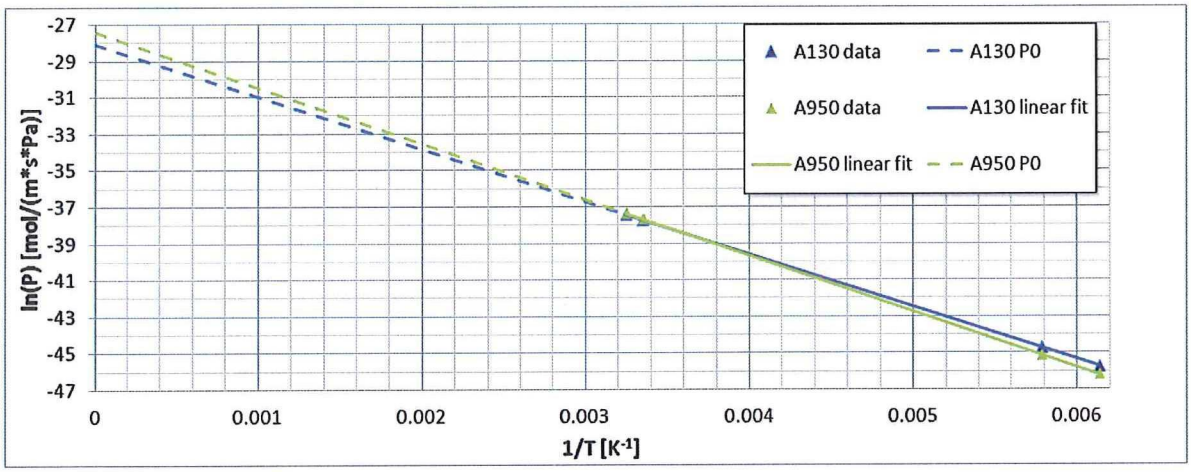

Figure 3.12: Arrhenius plot of reference data of fluoropolymers FEP, PFA and PTFE.

3.3. Experiments

3.3.1. Introduction

This section explains the experiments performed and the reason of the selected setup. Results are compared with the basic permeability test which is performed prior to the other tests. This test will leave the material unaltered: no thermal cycles, no mechanical load.

3.3.2. Thermal cycling

As the thermal cycles as established by NASA and Lockheed Martin ranges between 10K and 450K for the actual pressure vessel, the optimal test cycle is between these temperatures. However, with only liquid nitrogen available, the lowest temperature that can be reached is 77K. This should have little impact on the test results, as it was shown in literature that the elevated temperature has a larger influence than the cryogenic temperature. According to the demands set for the multilobe tank of CHATT, an elevated temperature of 480K is desired. Hence, the temperature range of the cycles will be 77K-480K.
Regarding the number of tests, it has not been established how many times the pressure vessel needs to be reused (although it is specified that the RLV as a whole will perform 600 missions) and tests performed at NASA range from 3 cycles up to 30. Also shown in section 2.2.3 was that the number of cycles either affected the permeability after a few cycles, after many (400+) cycles or no effect was observed within the number of cycles executed. Therefore, the number of cycles is limited to eight: if the material or layup sequence will show no increase in permeability in this number of cycles, it will probably take many more cycles. If permeability is affected much, the material or layup sequence should be reconsidered or rejected entirely.
The thermal cycle is shown graphically in figure 3.13.
As it was observed that the samples tend to deform out of plane during the cryogenic phase of the thermal

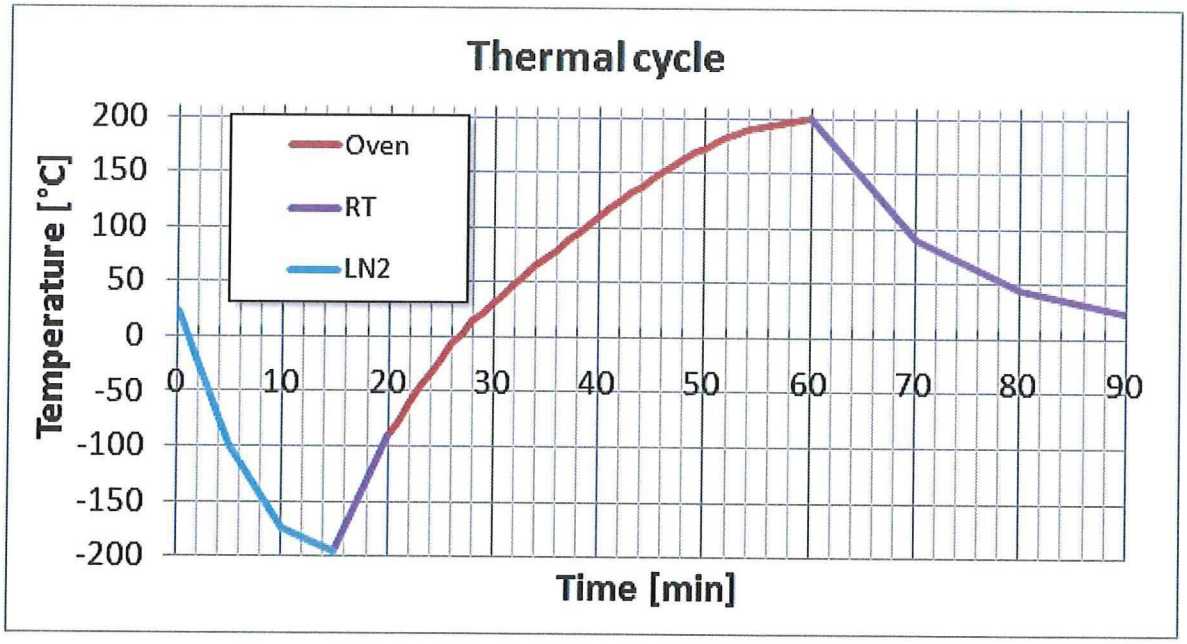

Figure 3.13: Temperature of a specimen during a cryogenic cycle measured with a K-type thermocouple, except for the cryogenic phase, where the temperature of the sample is assumed to have the temperature of the liquid nitrogen.

cycle, it was decided to limit the out of plane deflection by fixing the samples in between aluminium sheets. The pack was kept together with tape, and the force exerted by this was enough to greatly limit the samples from deforming out of plane and low enough to simultaneously keep the in plane friction low, allowing the sample to deform in that direction.
Before and after the thermal cycles the surface is observed for cracks using an optical microscope at magnification settings of 5x, 10x and 20x. And although the damage state after the thermal cycles is of interest, it may not be assumed that the sample is perfect prior to the cycles, hence the damage state is also checked before the samples are pretreated. In order to observe the same location before and after the thermal cycles, a template was created that was fixed to the sample. Both the template and the sample were marked so they could be aligned. The use of a liquid fluorescent penetrant would make the crack detection easier, but would also pose a problem if not fully removed prior to the thermal cycles and the permeability test: the elevated temperature may cause the penetrant and the sample to burn and damage the sample. Furthermore the penetrant may decrease the permeability as it has filled the cracks. Because of this is was decided not to utilize the penetrant for crack determination.
After the thermal cycles were performed the permeability measurements were executed as normal.

3.3.3. Mechanical load

The mechanical loads acting on the pressure vessel are the hydrostatic load from the liquid hydrogen and the gas pressure of the gaseous hydrogen present in pressure vessel. It is assumed the load is uniform and a biaxial in plane load is applied. As explained in section 2.2.1 the effect of the pressure load is then tested optimally with a biaxial test device and accompanied specimen. Unfortunately, such devices are not available at the TU Delft, but it was still desired to find a relation between applied load and permeability. As discussed in section 2.2 Rafaelli used a slightly bulged composite (about 4 mm out of plane) and applied a high pressure to it and measured the permeability as a function of the applied pressure. Also VanPelt [31] used a similar idea, but also applied a uniaxial load. It was decided to apply a similar strategy, with the difference of not having a bulge in the material or applying a uniaxial load. This decision makes the strain distribution not uniform, but the strain distribution of the slightly bulged specimen was not uniform either. Although the strain will not be uniform, results are still able to show a relation between strain and permeability.
For this experiment a second downstream cell was used where room was left for the sample to deform. It is desired to know the strain in the sample and this can be found analytically and numerically. However, experimental determination of the strain would be best. Some options achieve this were considered:

1. Regular strain gauge;
2. Wireless strain gauge;
3. Co-cured optical strain gauge;
4. Adhered optical strain gauge.

The problem with the wired strain gauges (options 1 and 4) is that they introduce a possible leak path. This can be solved by stripping the wire as much as possible (e.g. removing protective sleeves) and filling the space between the wire and the cell with a filler (i.e. an adhesive). Still a couple of problems remain: it is unknown if the adhesion is good enough between the surface to guarantee no leak will occur, the adhesive may adsorb the permeant and the replacement of the wire will be difficult. The wireless strain gauge would be a good alternative, but the sensor is "credit card" sized and therefore not usable in this setup, it is too large and an obstruction for the permeant. Finally co-curing the optical sensor is an interesting idea, but it disturbs the composite fiber orientation and also affects the surface smoothness as the optical fiber is relatively thick compared to the composite lamina. Because it was believed that a trustworthy permeability measurement was more important than an accurate knowledge of the strain in the sample, no strain measurement is performed and strain is only analytically and numerically determined.
The numerical model is created with Abaqus. Only a quarter of the actual specimen is modelled, as the specimen is axisymmetric, which allows for the same amount of elements on a smaller surface area, resulting in a higher accuracy model. Because it is axisymmetric, the boundary conditions at the cut sections are assumed to be $u_x = \kappa_x = 0$ at the cut on the y-axis and $u_y = \kappa_y = 0$ at the cut on the x-axis. As the O-ring is fully compressed into the aluminium cell, the boundary condition at the connection with the O-ring is assumed to be clamped. The elements used are 3D shell elements (type C3D8R). The pressure varies from 1 bar for the fluoropolymers up to 3.8 bars for the composites and Vectra. The result of the output is compared to an analytical solution, which is based on the deflection calculated in equation 3.3. With the deflection known at every point of the specimen, the curvature κ can be calculated:

$$\kappa_x = -\frac{\partial^2 w}{x^2} \tag{3.14a}$$

$$\kappa_y = -\frac{\partial^2 w}{y^2} \tag{3.14b}$$

$$\kappa_{xy} = -2\frac{\partial^2 w}{x \cdot y} \tag{3.14c}$$

Then, assuming the midplane strain is zero, the strain through the thickness can be calculated with:

$$\begin{bmatrix} \epsilon_x \\ \epsilon_y \\ \gamma_{xy} \end{bmatrix} = z \cdot \begin{bmatrix} \kappa_x \\ \kappa_y \\ \kappa_{xy} \end{bmatrix}$$

As the deflection and strains of the analytical solution are in good agreement (<5%) with the numerical solution, the analytical solution is considered to give satisfying results.
Tests were performed at the usual 3.8 bars for the composites and LCP's, but at 1 bar for the fluoropolymers to limit the deflection within the boundaries of the cell.

3.3.4. Varying pressure test

The goal of the pressure test is demonstrate the dependence of pressure on the permeability of the selected materials. According to theory, as explained in section 2.1.1, it is quite unpredictable how the permeability is affected by the pressure and this test will give some insight. In this test the samples are not allowed to deflect and only the pressure will be increased from 3.8 bar, up to 5.7 bar of pressure in steps of 0.5 bar. The upper limit of 5.7 bar is obtained by applying a safety factor of 1.5 to the design specification of 3.8 bar.

4

Results

4.1. Introduction

In this chapter the results of the gas permeability tests are shown and analysed. The results are provided for each material group, and in case of the deflected specimen tests, also the analytical calculated strain is given. Results are shown graphically (to give a good overview), as well as numerically (for further investigating the numbers). The unit for permeability used in this chapter is chosen to be $[fmol/(m \cdot s \cdot Pa)]$ as the f for $femto$ (10^{-15}) increases the readability of the graphs and tables. Individual permeability measurement results of successful tests are provided in Appendix D. In the last section of this chapter, an example is provided how much hydrogen will actually leak out of a hypothetical tank, with the assumptions as stated in the previous chapter.
Finally, an overview of the successful permeability tests conducted for each material and for each condition is shown in table 4.1. As can be seen, there are no test results for the unidirectional composite layup due to removal of faulty data. Also, no data is provided for the thermal cycled samples for PTFE and A130, as well as for pressure tests of the materials A950 and all composite layups. These tests were skipped because of time concern, as these tests require a very long time to prepare and perform.

Table 4.1: Overview tests

	Base	Bended	Pressure	Cycled
FEP	3	3	15	4
PFA	8	8	15	4
PTFE	3	3	10	-
A130	2	5	5	-
A950	1	1	-	1
UD	-	4	-	1
Angleply	1	5	-	2
Quasi isotropic	1	11	-	1

4.2. Composites

The results of the permeability measurements for three layups of the AS4/8552 CF-epoxy systems are given graphically in figure 4.1. As earlier mentioned, there is no reference data available for this material and unfortunately there have not been successful tests for the base test of the UD layup. Nevertheless, it can be assumed that the undamaged base material should have very similar results as for the angleply and quasi-isotropic layups.

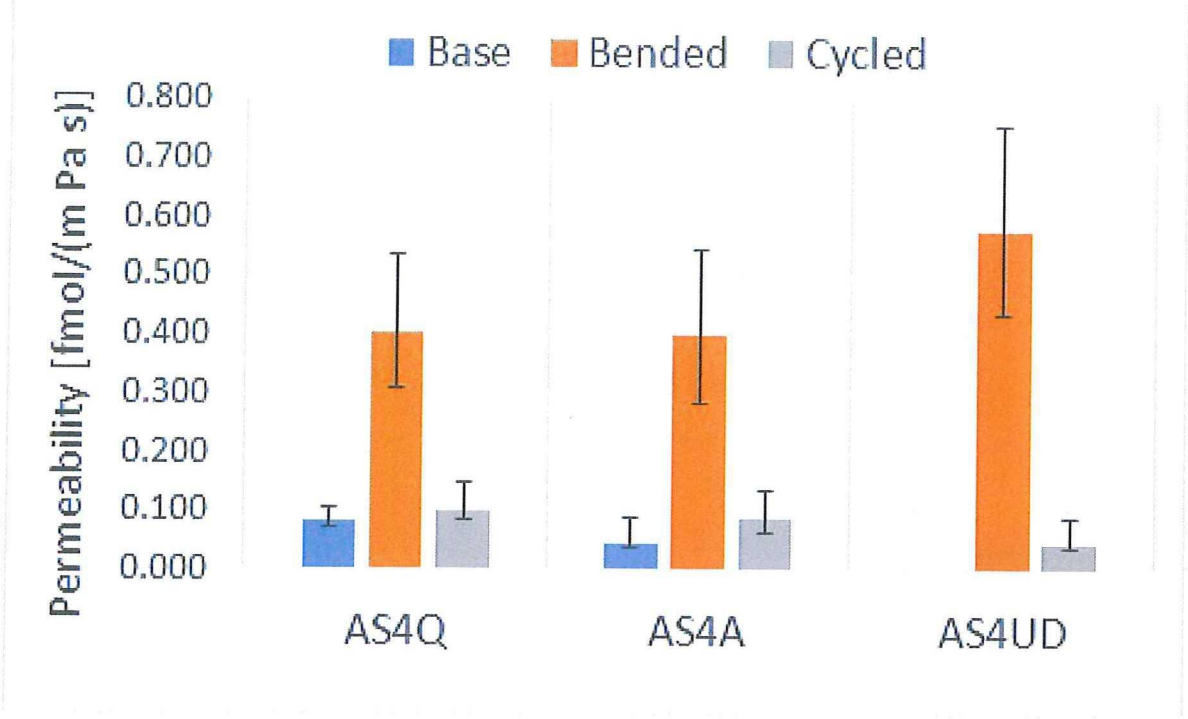

Figure 4.1: Bar chart of the permeability measurement results for AS4/8552, including error margin.

Table 4.2: Table of the permeability measurement results for AS4/8552, including error margin.

	Base			Bended			Cycled		
	Mean	Upper	Lower	Mean	Upper	Lower	Mean	Upper	Lower
AS4Q	0.082	0.108	0.072	0.403	0.534	0.309	0.098	0.147	0.086
AS4A	0.044	0.088	0.039	0.399	0.545	0.285	0.086	0.134	0.064
AS4UD				0.576	0.754	0.435	0.044	0.088	0.039

Comparing the tests with each other, it is noticed that strain has a very large effect on the permeability with respect to the base samples and thermally cycled samples. The error is high for bended samples, caused by the large difference in measurements. The effect of the thermal cycles is less prominent however and remains close to the permeability of the base experiments.
The strains applied are shown in table 4.3 and are calculated with the equations as was given in section 3.3.3. The strains transverse of the fibers are most important, as this will cause microcracking and flow of permeant through the specimen. Only the maximum strain parallel to the fibers, which is known to be 1.7%, can be used to compare the values of the table with. It is discovered that the deflection of all three layups are the same and therefore also produce the same strains in a ply. These strains are well below the maximum strain allowed in fiber direction, but it is unknown how close the strain was compared to the transverse strain. Nevertheless, no visible cracks were discovered after the tests. Also provided is a strain distribution plot of the ply in which the maximum strain occurs (figure 4.2). This strain distribution is similar for all other materials, except for the difference in amplitude. According to this figure the strain distribution is far from uniform and maximum strain in parallel and transverse direction are always maximum at the center as expected.

Table 4.3: Maximum strains of the composite materials at a pressure of 3.8 bar.

Material	ϵ_1	ϵ_2	γ_{12}
Unidirectional	0.218%	0.218%	0.436%
Angleply	0.218%	0.218%	0.436%
Quasi isotropic	0.218%	0.218%	0.436%

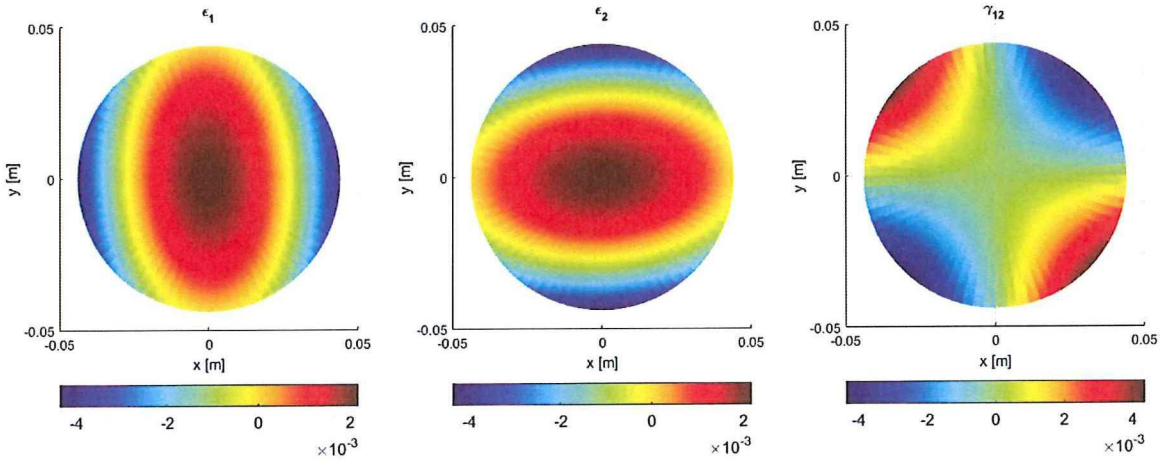

Figure 4.2: Example of the strain distributions in a ply of the Angleply layup at a pressure of 3.8 bar

4.3. Liquid Crystal Polymers

The results for the LCP's are split in three graphs. The first (figure 4.3) shows the permeability values of the reference, base and thermal cycle tests, temporarily ignoring the results of the bended samples. It is noticed that the outcome of base result is 2.0 and 2.5 times larger than the reference for A130 and A950 respectively. The effect of the cyclic thermal load is more pronounced for the A950 LCP than for the composite, although the error on it is large. The second figure (figure 4.4) includes the same results as the first graphs, but now also includes the results of the bended samples. The effect of straining the LCP is very large compared with the other data. The last graph (figure 4.5) shows the effect of pressure increase on the permeability of A130. It is found that the relation is not linear, but follows a parabolic line. Multiplying the permeability with the pressure applied and dividing by the thickness of the sample gives the GTR, which shows a similar behaviour (figure 4.6).

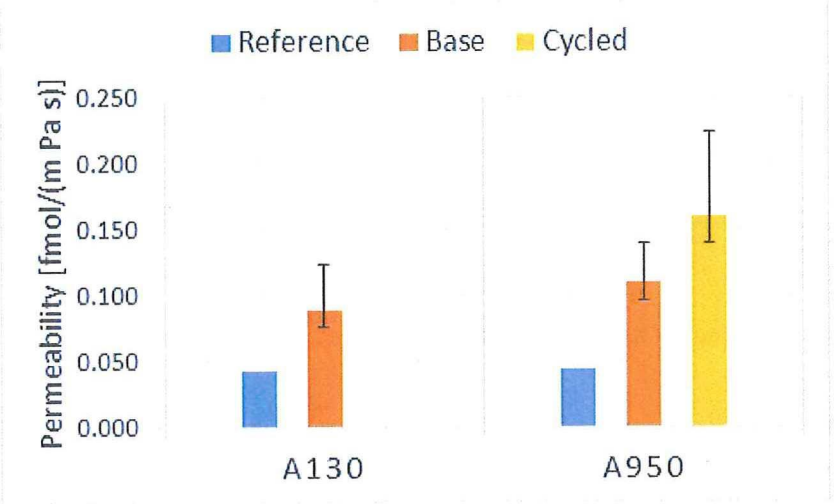

Figure 4.3: Bar chart of permeability measurement results (reference, base and cycled specimens) for the LCP's Vectra A130 and A950, including error margin.

Just as with the composite, the strain in transverse direction, ϵ_2 is most important to the anisotropic LCP's. However, only the maximum elongation parallel to the fiber direction is known, so the values of table **??** can only be compared to the maximum strain at break of 2.1%.

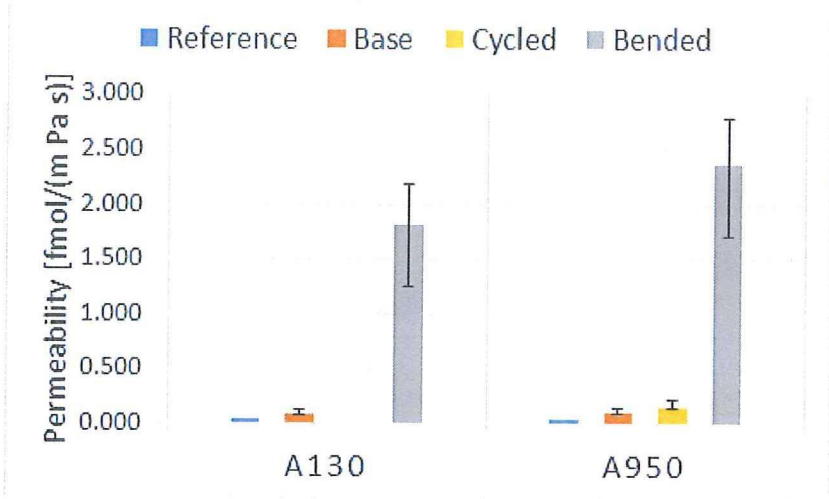

Figure 4.4: Same as figure 4.3, but now also including results for bended specimens.

Table 4.4: Table of the permeability measurement results for the LCP's Vectra A130 and A950, including upper and lower limit of the error.

	Reference	Base			Bended			Cycled		
		Mean	Upper	Lower	Mean	Upper	Lower	Mean	Upper	Lower
A130	0.043	0.088	0.124	0.077	1.816	2.188	1.255			
A950	0.044	0.110	0.139	0.096	2.370	2.792	1.707	0.160	0.223	0.139

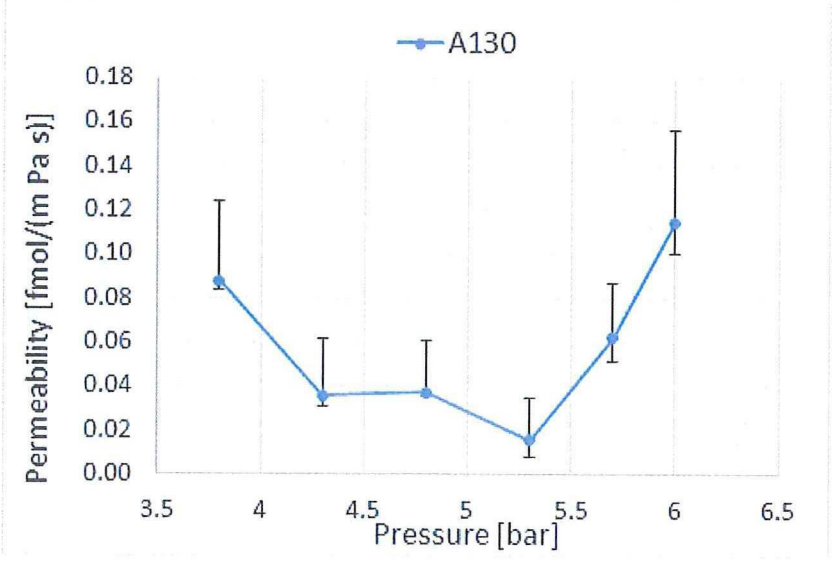

Figure 4.5: Graph of the permeability of Vectra A130 as a function of pressure.

4.4. Fluoropolymers

The results of the fluoropolymers is shown graphically in figures 4.7 and 4.8. The first graphs shows the permeability values for reference, base, bended specimen and thermally cycled specimen. It is noticed how the base test results of PFA and FEP are about 30% higher than the reference values, while the PTFE value seems to be spot on. The bending and the thermal cycling of the specimen also show a difference between PFA and FEP, and PTFE: the values decrease for FEP and PFA with respect to the base experiment, while bending causes an increased value for PTFE. However, the values don't differ much and the measurement error is large. The second graph contains the outcome of pressure test for all three fluoropolymers. As the lines are near flat, especially for PTFE, permeability is almost unaffected by pressure in this range. For completeness sake, the GTR of the fluoropolymers is also provided in figure 4.10, having a similar shape as

Table 4.5: Table of the permeability measurement results as a function of pressure for the LCP Vectra A130. Upper and lower limit of the error are included.

Pressure	A130		
[bar]	Mean	Upper	Lower
3.8	0.088	0.124	0.083
4.3	0.036	0.061	0.031
4.8	0.037	0.061	0.035
5.3	0.016	0.035	0.008
5.7	0.062	0.087	0.051
6.0	0.115	0.156	0.100

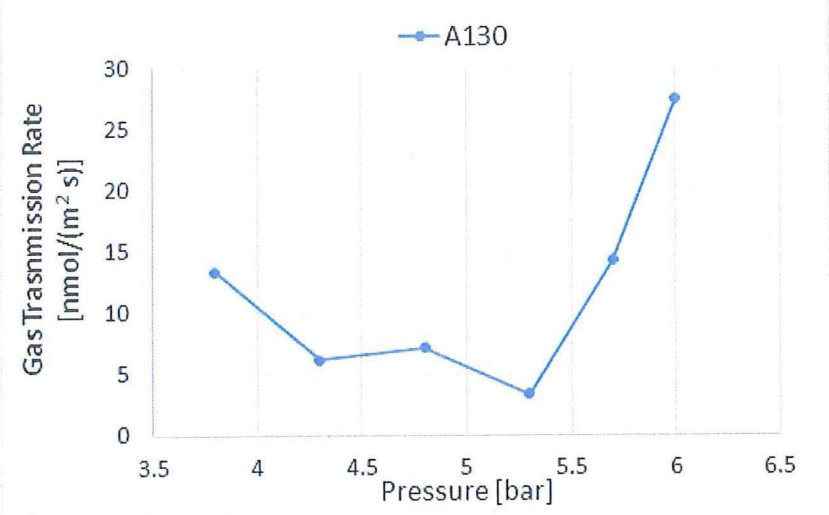

Figure 4.6: Graph of the GTR as a function of pressure of Vectra A130.

Table 4.6: Maximum strains of the LCP materials at a pressure of 3.8 bar.

Material	ϵ_1	ϵ_2	γ_{12}
A130	0.324%	0.324%	0.648%
A950	0.391%	0.391%	0.782%

for the permeability.

Table 4.7: Permeability measurement results values, including upper and lower limit error, for the fluoropolymers PFA, FEP and PTFE.

	Reference	Base			Bended			Cycled		
		Mean	Upper	Lower	Mean	Upper	Lower	Mean	Upper	Lower
PFA	11.598	16.434	18.979	14.330	13.306	13.715	11.101	10.554	12.283	9.200
FEP	11.270	14.975	17.325	12.977	11.404	11.885	9.466	8.872	10.824	7.693
PTFE	8.001	7.777	9.053	6.782	9.445	10.715	7.257			

In table 4.8 the maximum strains are given for all three materials. As can be seen, the strain is much lower than the maximum strain of such polymers, which is in the order of 300%. The strain applied is however much higher than the strains applied to the composites and LCP's, to about ten times.

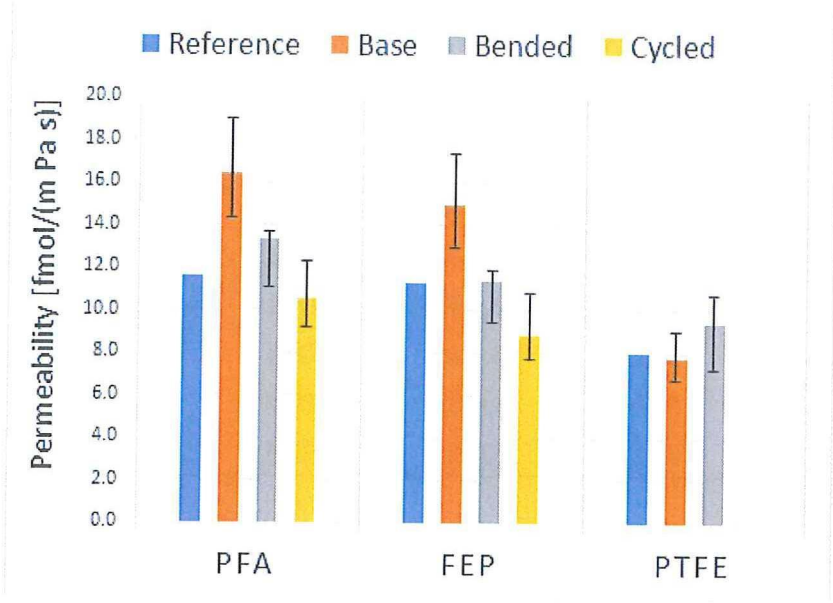

Figure 4.7: Bar chart of permeability measurement results, including error margin, for the fluoropolymers PFA, FEP and PTFE.

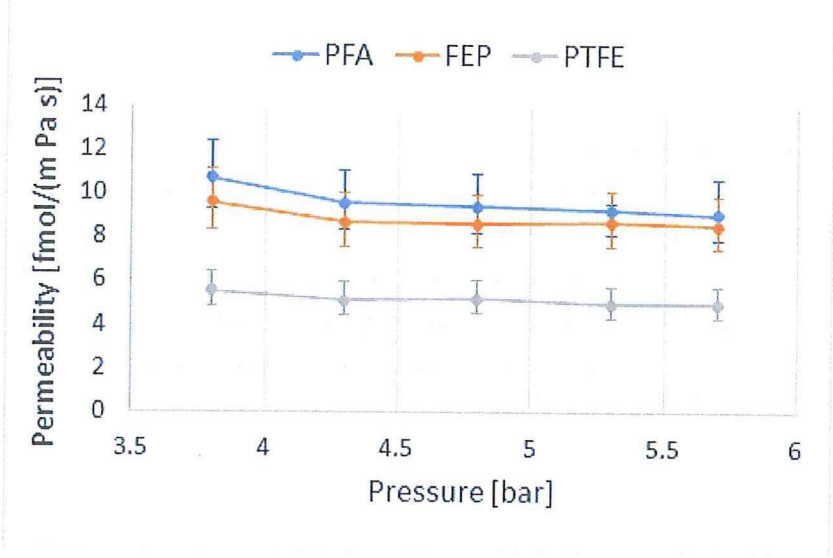

Figure 4.8: Graphs of the permeability as a function of pressure, including error margin, for the fluoropolymers PFA, FEP and PTFE.

Pressure	PFA			FEP			PTFE		
[bar]	Mean	Upper	Lower	Mean	Upper	Lower	Mean	Upper	Lower
3.8	10.683	12.390	9.315	9.610	11.130	8.376	5.548	6.455	4.839
4.3	9.540	11.070	8.315	8.684	10.047	7.573	5.122	5.942	4.467
4.8	9.374	10.846	8.171	8.609	9.926	7.508	5.201	6.021	4.535
5.3	9.251	9.550	8.068	8.697	10.061	7.584	4.948	5.719	4.316
5.7	9.034	10.635	7.865	8.516	9.823	7.427	4.953	5.728	4.320

Figure 4.9: Permeability measurement results values as a function of pressure, including upper and lower limit error, for the fluoropolymers PFA, FEP and PTFE.

4.5. Expected He and H_2 volume loss of pressure vessel

As explained in section 3.2 a pressure vessel is assumed to exist and includes a liner. The volume loss per hour of a fluoropolymer and a LCP liner material with the assumptions as explained in methodology is shown in figures 4.11 and 4.12 respectively. Regardless of material type, the loss per hour is near zero at 21 K

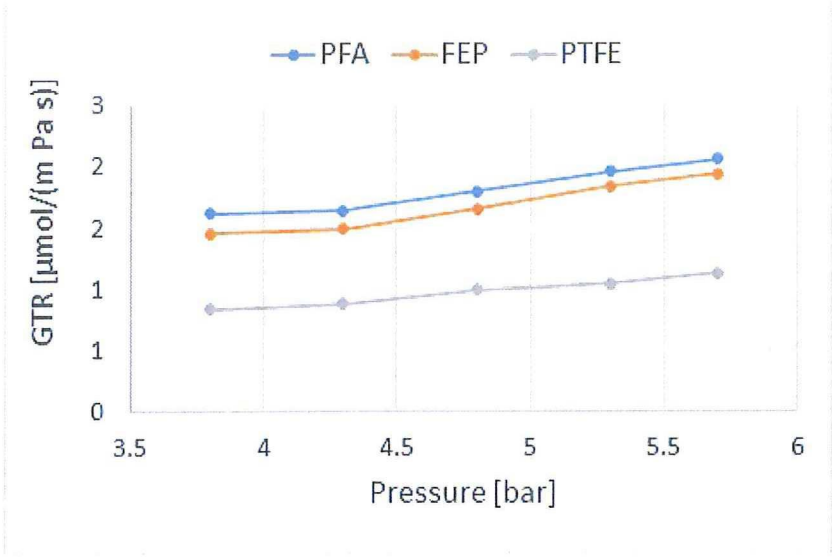

Figure 4.10: The GTR as a function of pressure for the fluoropolymers PFA, FEP and PTFE.

Table 4.8: Maximum strains of the fluoropolymer materials

Material	ϵ_1	ϵ_2	γ_{12}
PFA	3.05%	3.05%	6.09%
FEP	4.24%	4.24%	8.48%
PTFE	3.04%	3.04%	6.07%

according to the Arrhenius equation. At a higher temperature of 93 K, which was the lowest temperature at which the reference material was tested, the loss per hour is negligible.

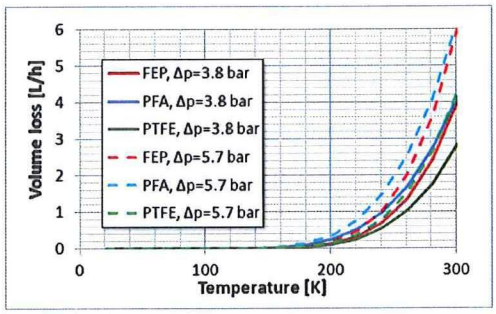

(a) Helium loss per hour as a function of temperature, within the range of 21 K to 300 K.

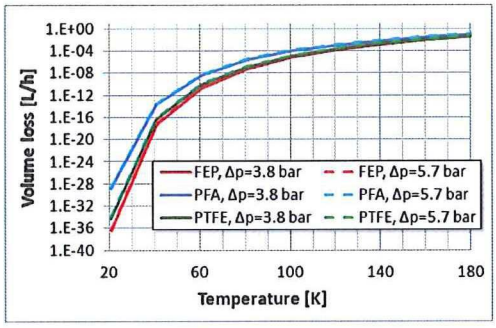

(b) Same figure as (a), but zoomed in on the temperature range 21 K to 180 K.

Figure 4.11: Helium loss per hour as a function of temperature for the fluoropolymers FEP, PFA and PTFE at pressure differences of 3.8 and 5.7 bar.

Also the loss per hour of helium is compared with reference data of hydrogen and compared with each other in figure 4.12. The loss of hydrogen for the material FEP is lower than for helium, to about eight times lower at RT, to a factor 36 at 21 K.

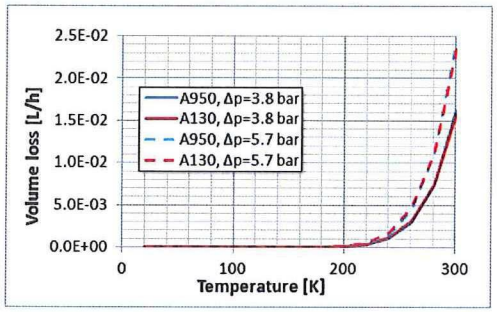

(a) Helium loss per hour as a function of temperature, within the range of 21 K to 300 K.

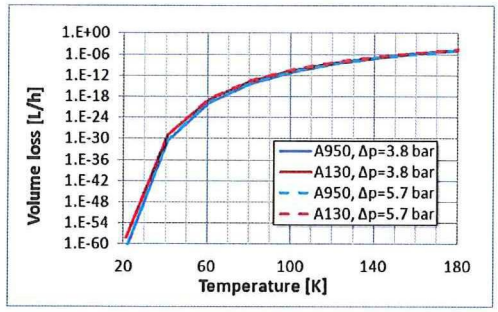

(b) Same figure as (a), but zoomed in on the temperature range 21 K to 180 K.

Figure 4.12: Helium loss per hour as a function of temperature for the LCPs A130 and A950 at pressure differences of 3.8 and 5.7 bar.

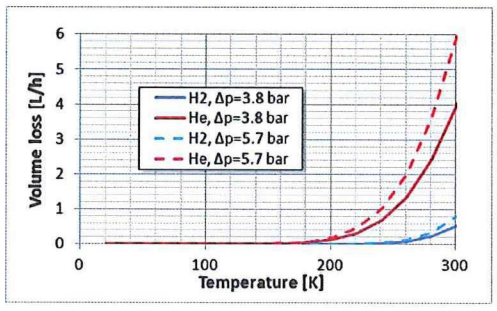

(a) Difference between hydrogen and helium loss per hour for FEP as a function of temperature, within the range of 21 K to 300 K.

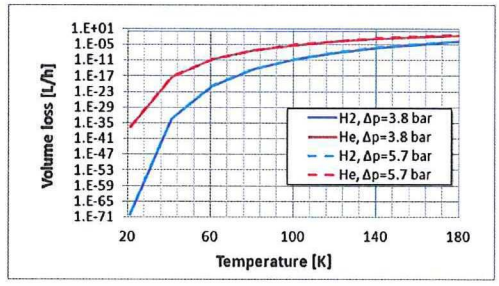

(b) Same figure as (a), but zoomed in on the temperature range 21 K to 180 K.

Figure 4.13: Difference between hydrogen and helium loss per hour for FEP as a function of temperature for the LCPs A130 and A950 at pressure differences of 3.8 and 5.7 bar.

5

Discussion

5.1. Introduction

This chapter will discuss both the methodology and the results obtained. The methodology discussion will encompass the apparatus, data acquisition, materials and the test procedures, as the choices made in these areas have lead to the final results that were acquired. The discussion about the methodology will therefore mainly consider how the choices have influenced the measurements and what possible limitations they have. Finally the obtained results are examined and how these need to be interpreted.

5.2. Apparatus

Although the design of the apparatus was based on the ASTM test standard as discussed in 3.1.1 and many of the articles used this standard for the design of their own apparatus, the standard does not say whether or not it is able to work with anisotropic materials such as the composite and LCP used in this research: as these materials are prone to microcracking, the suggested O-ring may not be able to contain the permeant in the cell, causing a loss of permeant on the downstream side of the sample. This leak path is impossible to locate on the current apparatus using a soapy solution or a pressure test: the soapy solution cannot be applied directly to the sample O-ring interface, as this is located within the apparatus and cannot be reached. The soapy solution can be applied to the outer ring and to the holes for the bolts, but as the small amount of leaked permeant will distribute itself over the free volume available and the area to apply the soapy solution to is quite large, a possible leak will not be found. Furthermore, *if* a leak is found, it is still unknown from which side of sample the leaked permeant is coming from: a small leak from the upstream side does not influence the measurement, but a leak on the downstream side does. A pressure test is not possible in this setup, as only the pressure is known on the upstream side. A helium sniffer would be easier to use and increases the chance of finding small leaks, still it is not known which side the leak is located on. Furthermore, such a helium sniffer was not available to use.
The purging of the upstream chamber with helium is done at high pressure, but it is not really known if the air in the chamber is completely replaced by the helium. If not, then the partial pressure of helium is lower than the measured pressure which is used for the calculations. In this case, the permeability is underestimated.

5.3. Data acquisition

The volumetric method seemed like a simple and good way to measure the permeability, but in practice there quite a number of factors that can influence the measurement and make it more complex. First of all, the atmospheric pressure changes affect the measurement performed. Also human interference with the apparatus, even proximity to the capillary for longer periods of time, was noticed to increase the slug height. It was attempted to correct for the affect the atmospheric pressure has on the measurements by incorporating an analytical expression for pressure balance which improves the received data, but it is unknown what the accuracy of this correction. Another issue is the manual measurement technique: as the height of the liquid slug needs to be measured with the naked eye, the precision of measurement is about 0.5 mm. This value can be considered as reasonable when the total slug movement is high, such as for the

fluoropolymers where the slug movement is about 70 mm. However, for LCPs the slug movement was about 20 mm in about six hours time, meaning that the measurement error due to manual slug measurement is about 5%. Also the capillary in itself has a quite large inaccuracy of 10%. The acquired data therefore shows a large error range for materials with a low permeability and it therefore is hard to quantify the material's permeability.
Unfortunately there are also some aspects which influence the data acquisition in an unknown measure. Firstly, all materials are able to adsorb the permeant, and because the helium was trapped in the downstream chamber for several hours in the case of a LCP-test. It is therefore possible that some of the helium was lost due to adsorption. Possible adsorption locations are the PTFE feed tube to the capillary and the capillary fluid. The amount of permeant lost is assumed to be very small, as the difference in partial pressures is very small from the downstream side to the atmosphere, but if given enough time this may influence the permeability measurement significantly. Secondly, the liquid slug evaporates in time. This is a fairly slow process (estimated at 1 to 2 mm of liquid loss per day), but again: due to the long time required for a LCP test this may be of importance. Lastly, the temperature is not taken into account: during longer measurements, in some cases the temperature changed by about $0.5°C$, which has an unknown influence to the system.

5.4. Materials

As mentioned, the fluoropolymers were delivered at different thicknesses (3 and 4 mm) and were scratched. The decision was made to decrease the thickness to an equal 2 mm and to polish the fluoropolymers afterwards as to make a good comparison between the materials at an equal thickness. However, machining may have irreversibly damaged the surface, e.g. by introducing microcracks. By visual inspection it is clear that the surface remains damaged despite polishing, as the surface had a matte finish to it. This may have lead to the higher measured permeability values for FEP and PFA. The reason PTFE is not affected might be explained by the better surface quality that was acquired. The LCPs on the other hand had a good surface quality at visual inspection, but machining the square sheets to circular samples lead to the peeling of the unfilled polymer type near the edges. Although it was not observed that these strands continued into the measurement area, causing a leak path past the O-ring, microscopic defects may still have been present affecting the measurement performed. As can be seen in figure [], small strands of polymer have been peeled of the surface that lies within the measurement area.
Regarding the material thickness selection, it must be noted that the choice of using LCPs at a thickness of 2.5 mm was wrong: as the permeability of this material type is very low in general, thinner samples would have lead to a higher flow of helium through the specimen and therefore more accurate results in less time.
The choice of fluoropolymers as a liner was mainly based on its flexibility at low temperatures and the manufacturability. The CTE however is much higher than the CTE of the composite, which may cause concerns: assuming the liner is not adhered to the tank wall, the liner will first shrink due to the low temperature of the liquid hydrogen and then expand again due to the pressure of the liquid hydrogen, as graphically shown in figure 5.1. It is not known if the expansion is within the strain limits and no cracks or tears will form. Another issue might be the structural stability of the liner when it is contracting, as it may buckle and fail. Increasing the thickness of the liner material may enhance its structural stability but at the cost of added weight, undermining the advantage of composite over metals. Adhering the liner to the composite wall would be a solution, but this would require the adhesion to be able to cope with the shear forces at very low temperatures, which would be difficult as the adhesive would become brittle.
Furthermore, fluoropolymers are well-known for their low friction properties and it is very hard to adhere anything to it. Therefore the fluoropolymers needs to be pretreated with a chemical etchant in order to make adhesion possible.
The CTE of the LCP's is lower than the fluoropolymers, and the CTE's in flow and transverse directions almost equal the CTE's of a unidirectional composite lamina. However, the composite consists of a layup with multiple orientations, so in the end there will be a mismatch in the transverse direction mostly and so a larger contraction of the liner will occur with respect to the contraction composite tank wall in transverse direction. However, unlike the fluoropolymers the LCPs are less flexible. Another issue is the manufacturability as Vectra LCP's are injection moulded and the flow direction of the LCP determines what the orientation of the polymer will be: Orientation control will be difficult for a double curved contour.

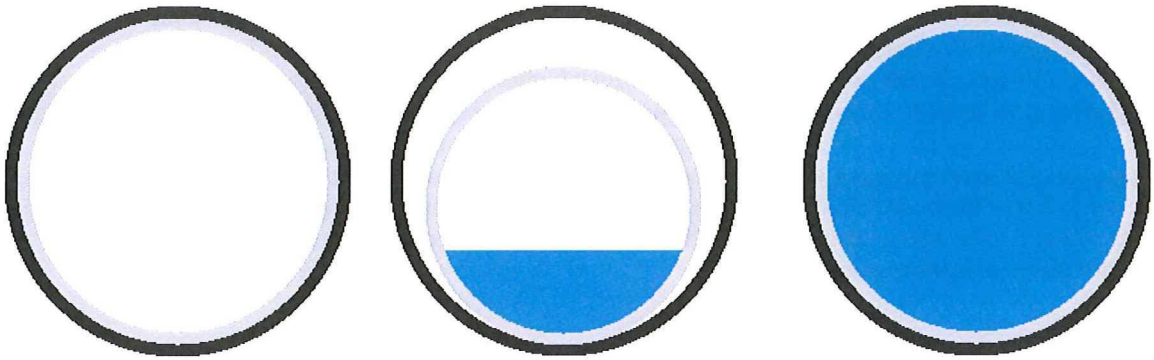

Figure 5.1: Graphic representation of the liner shrinkage and expansion due to the liquid hydrogen.

5.5. Test setup

In the test where deflection of the specimen is allowed, it is known that the strain distribution is heterogeneous and therefore the permeability cannot be coupled to a single strain state value. A maximum strain value gives some information regarding the gravity of the deformation, but still no conclusions can be made in regard to the material permeability. Furthermore, it would have been better if a similar strain state was achieved for all materials tested, but this is impossible due to anisotropic nature of the composites and LCP's compared to the isotropic nature of the fluoropolymers. Therefore only materials from within a material group can be compared to each other and qualitative conclusions can be drawn when comparing the material groups.
The thermal cycling performed on the test specimen is a reasonable representation of an actual thermal load on the tank. However, the damage state of the material due to the thermal cycling could not be determined. Although photographs were made of the specimen at predetermined locations, before and after the cycles, at various magnification settings of the microscope, no damage caused by the cycles could be observed. The observation technique is to blame for this, as it is very difficult to spot cracks without a fluorescent liquid penetrant. A liquid penetrant would make cracks visible, but also needs to be applied *before* the thermal cycle and measurements takes place (in order to know the initial damage state of the specimen), and because the penetrant is difficult to remove it may influence the measurement or burn and damage the specimen in the oven. A second problem of the observation technique is that it is difficult to relocate points of interest after the cycles. And although a template was used to find the points of interest after the thermal cycles, at higher magnifications (20x - 40x) it was nearly impossible to find the exact area again. Another issue with the thermal cycling test is the amount of time required to pretreat the samples, which is quite high, and the amount of cycles performed, which is just too low to be represent the total lifetime of a pressure vessel of a RLV. Finally, the test is of limited value as in reality the cycle would involve both a temperature *and* a mechanical load. So a separate test for both temperature and a mechanical may show their separate contributions to the permeability, but it is possible that it underestimates the actual problem.

5.6. Test results

The amount of tests performed for each variable is unfortunately too low to incorporate some statistical analysis and to gain more insight of the repeatability of the tests performed. Furthermore, the error margin on most measurements is large and because of this some results cannot be interpreted well as they are of the same order of magnitude. For instance, bending and thermaly cycling the fluoropolymers show a different outcome than during the base test, but due to the large error margin the actual difference in permeability may be a lot smaller than the averages currently depict. Similarly, a lower permeability was found for the angleply composite compared to the quasi isotropic composite (which would be a correct observation, as according to [] the optimum angle is 25°), but the low amount of observations as well as the large measurement error do not allow this conclusion to be made in this research. Corrections applied to counteract some effects that distorted the measurements only improved the data in a minor fashion - a couple of percent at most. The removal of outliers, probably caused by mistakes in the manual observations or extreme temporary atmospheric changes improved the data set in many cases, but still by a low amount.

Despite this, the test results still are able to provide some information, especially when comparing the material types with each other.
Although the permeability of fluoropolymers is much higher than for the composites and LCP's, they all are negligibly small at 21 K. Despite not having any data to validate the permeability at such low temperatures it can be assumed that the Arrhenius equation will largely correspond with reality as the energy of the permeant will decrease much due to the low temperature. Hence the earlier statement about the permeability of the materials at 21 K will still hold true. Furthermore, it was assumed in the calculations that only a liner needs to be permeated through, while in reality also a composite tank wall will be present, further decreasing the volume flow.

6

Conclusions

6.1. Apparatus

The apparatus with the flat surface is essentially the correct device with which a permeability test should be performed, hence everyone uses a similar device. However, with a very small molecule as helium is (and for that matter, also hydrogen) details are important. As explained in the discussion on this matter, there is a concern for leakages which cannot be determined. This makes the reliability of the apparatus less than is desired and may be a cause of an underestimation of the permeability of the materials tested.
Although the original pressure regulator was replaced with one that is more suited for helium, it was discovered after multiple tests that it was not able to regulate the pressure at all. Although it was argued that the small decrease in pressure in time would not affect the measurements much, it probably did for the bended specimens: the liquid slug movement decelerated and is caused by the decrease in deflection of the specimen, but also by less permeation as the strain also decreased.
With respect to the size of the apparatus it can be concluded that the test surface area was too small for low permeability materials such as LCPs and composites, with the current data acquisition system used.

6.2. Data acquisition

As explained in section 5.3 the data acquisition system is too inaccurate and too imprecise for low permeability materials. The correction functions scripted in Matlab are cute, but do not solve the actual problem. Also the accuracy of the correction in itself is disputable and it would be better to avoid. These issues reduce the reliability of the acquired data and make it harder to quantify the permeability characteristic of the materials to the point where they only qualitatively can be compared. Hence it must be concluded that the data acquisition should be improved in order to achieve more accurate results in order to quantify the permeability of materials and the influence of variables (such as pressure and temperature) on them.

6.3. Materials

Regarding the material treatment it is concluded that the decision to decrease the thickness by milling it down was wrong: the surface quality decreased and it is very probable this influenced the permeability as a result.

6.4. Test setup

Four different test setups were considered. Of these the base test and increased pressure test were conducted as required and the results can be used reasonably. The outcome of the bended specimen test was less straightforward, as permeability cannot be directly correlated to a certain amount of strain applied to the specimen as the strain distribution was heterogeneous. As the magnitude of the influence of the strain can therefore not be established, it must be concluded that the test setup for the purpose is flawed.
Regarding the setup of the thermally cycled specimens it is difficult to state what the cause is of the difference in outcome for A950 and the fluoropolymers: while there is a noticeable increase in permeability

of A950, there is also a noticeable decrease in permeability for PFA and FEP. The difference may be caused by the anisotropic LCP microcracking because of the thermal cycles and the induced strain, while the isotropic fluoropolymers may have re-ordered and improved the microstructure, decreasing the permeability. However, this could not be confirmed with an optical microscope, even possible damage to the A950 specimens could not be found, let alone a micro-structural change.

6.5. Test results

It can be concluded from the permeability measurements that:

- bending the composite specimens introduces a strain that has a noticable effect on the permeability;
- the unidirectional layup is more affected by the strain than the other layup sequences;
- the effect of thermal cyclic loads on the composites could not be established with certainty, although a slight increase is observed for the quasi isotropic and angleply layup sequences;
- bending the LCP specimens also have a large influence on the permeability of the material. Although the strain applied was 50% to 100% higher than for the composites, the measured increase in permeability is over 2000%. Hence these LCP's are more sensitive to strain;
- the thermal cyclic load is a probable cause of the observed increase in permeability of Vectra A950;
- the permeability of Vectra A130 is a function of the pressure and shows a parabolic shape, meaning that helium probably plasticizes the polymer;
- the measured permeability of PFA and FEP of the base test is higher than its reference values and is attributed to the microstructural damage caused by milling down the specimens to an equal thickness;
- bending PFA and FEP caused a decrease in permeability to occur, but an explanation is not known for this behaviour. At the very least it can be concluded that fluoropolymers are far less influenced by strain than the other materials tested;
- thermal cycling caused an inexplicable decrease in permeability of the fluoropolymers tested;
- the permeability of fluoropolymers is less dependent and maybe even not dependent on the pressure applied in the pressure range of 3.7 to 5.8 bar. Helium, apparantly, plasticizes these fluoropolymers to a lesser degree.

Based on the volume loss of a hypothetic tank under the given assumptions of section 3.2 it is concluded that:

- volume flow out of the tank becomes negligible at 21 K, regardless of liner material used;
- the hydrogen flow is less than the helium flow out of a FEP liner.

From the observed influences of strain and thermal cycling on the liners and the notion that permeation goes to zero as temperature nears zero, it can be concluded that the mechanical stability of the liner under mechanical and thermal load is more important than the bulk material permeability.

7

Recommendations

7.1. Introduction

In this chapter recommendations will be given based on the discussion and conclusions. The subjects are the same as for the discussion and conclusions, so recommendations will be given regarding the apparatus design, the data acquisition, the candidate materials and the tests respectively. These recommendations includes the suggested improvements to this project, but will also point out possible topics for future research in the broader perspective of the research subject.

7.2. Apparatus

Some modifications to the original design of the apparatus are recommended. The material of the O-ring employed may have been too hard, increasing the chance of not having a leak-tight setup, especially when the surface is not entirely smooth as was the case with the materials tested in this research. It is proposed to employ a much softer material for the O-ring, such as silicon. The silicon O-ring can be manufactured straight onto the specimen using a mould, ensuring a good connection. Another modification is to add a second O-ring with a larger diameter, basically allowing a free volume to remain between the two O-rings. If a helium sniffer is purchased, this can be employed to detect a leak at the O-ring, giving more information about the success of the test. Ideally, the helium flow could be reversed, giving an immediate result regarding the reliability of the O-ring. Also the repeatability of the tests can be improved by applying a uniform pressure to the upper cell of the apparatus. This will ensure the same amount of force is applied to the specimen each time, reduces the chance of a skewed load and improves the speed at which the test can be set up. Finally, the purging process can be improved by applying a vacuum to the system before applying helium pressure: this will result in a better known concentration of helium applied at the specimen, and no helium will be wasted in the process.

7.3. Data acquisition

Although the data acquisition was fine for short test runs and relatively permeable materials such as the fluoropolymers were, for materials with low permeabilities the tests took much time and were less accurate. The best solution would be to purchase a mass spectrometer, which is the most accurate system available. However, it also comes at a steep price, which is a large disadvantage. A cost driven solution would then be found in the improvement of the current volumetric measurement method. This can be achieved by reducing the capillary diameter to as low as 0.5 mm (hence a system that is 16 times more precise) for low permeability materials. The 0.5 mm accuracy reading the liquid slug position manually can be improved with automated measurements: already a test was performed with a camera plugged to a Raspberry Pi, which was able to take measurements at a specified interval including the pressures and temperature, and also is able to make a picture of the current slug position. More details concerning this device is given in Appendix E.

The precision helium pressure regulator did not work as it was supposed to in this project, unfortunately no reason was found why it did not function. According to the manufacturer it is installed correctly and the device should be suitable for regulating helium pressure. Nevertheless, it was not and it should be either

fixed or replaced.
The above improvements of the volumetric measurement method are reasonable for tests performed at room temperature. If the test will be done at low (sub zero) or even cryogenic temperatures, then according to the Arrhenius equation the permeabilities will become so low that the test will take a very long time. Furthermore, some additional problems will arise: as the temperature in the downstream cell drops, the trapped air will decrease in volume, sucking the liquid slug out of the capillary into the cell. Additionally, the moisture in the air will freeze, possibly forming a blockade in a tube. In this case it is really recommended to use a mass spectrometer.

7.4. Materials

For future tests with the current permeability test setup it is advised to test films for low permeability materials such as Vectra, as this would decrease the time required to saturate the barrier material with permeant and the time required to accurately measure the volume of gas permeated. In addition, a thick material should not be decreased in thickness by milling or sanding it down to the desired thickness: this inherently damages the material surface, likely introducing measurement errors.
As discussed, there seems to be connection between the morphology and resulting anisotropy to the material's permeability when mechanically loaded. It would be interesting to study this relationship, as it would give valuable information which kind of material is suitable as a barrier.
As the structural stability, when subjected to a thermal and mechanical load, are important material characteristics for a liner in the pressure vessel, these should be studied when designing a pressure vessel with a liner. Therefore materials should be selected having a CTE comparable to that of the composite and is able to cope with the compression when cooled down and should be flexible to cope with the strain generated by the hydrogen pressure. First, materials should be selected based on their CTE, maximum strain and glass temperature. In order to acquire the knowledge for the demands at cryogenic temperature, tensile tests should be performed at cryogenic temperatures with a cryostat and a uniaxial test bench. Although the uniaxial load underestimates the maximum strain of the actual biaxial load, the test will be less complex and gives useful data with which a finite element model can be generated to check a candidate design of the pressure vessel. Finally a scaled pressure vessel should be manufactured and filled repeatedly to test the structural stability.
An alternative solution to the liner can also be investigated: as shown, LCPs have excellent barrier properties and have similar CTE compared to carbon fibers, and according to Dingemans et al. [8] it can be modified to become a thermoset liquid crystal polymer (TLCP). This means that this polymer can act as the matrix instead of the common epoxy in the composite, nullifying the original disadvantage of the CF/epoxy composite: microcrack initiation due to CTE mismatch, and loss of hydrogen and risk of failure because of that. At NASA such a material has already been used in a pressure vessel, with successful results. It would therefore be very interesting to develop a new TLCP - the material used by NASA is trademarked and cannot be manufactured by any other than Ticona - which can be used for the CHATT program.

7.5. Test setup

For the test conditions, it should be investigated how the humidity influences the permeability measurement of a sample. Therefore samples need to be pre-treated by drying them in a vacuum oven at low temperature. Afterwards, tests can be conducted as normal and an effect may be observed. Additionally, this can be done prior thermal cycling as well, as crystallized moisture may affect the microstructure. Another variable of importance is the applied pressure, which should always be set to the designed pressure load or to the pressure including a safety factor. Finally, the amount of tests performed should be increased to at least ten, so enough statistical data is available to judge the reliability and repeatability of the measurements.
The material permeability measurement while mechanically loaded is of importance, as was also mentioned in section 7.4, as the mechanical load can be of great influence to the permeability. Therefore a biaxial testing machine should be acquired and a biaxial specimen should be developed.
Regarding the effect of cryogenic temperature on permeability, tests need to be conducted together with a biaxial load in order to be of any interest: at 21 K the permeabilities of all material-permeant pairs will be negligibly small anyway, and by adding a biaxial load the embrittled sample is likelier to acquire cracks and a flow of permeant. At such a low temperature it is also recommended to use hydrogen as the permeant instead of helium, as the permeants are only comparable at room temperature. The setup for such a test is much more complex and much needs to be taken into account. Lastly, as the permeability is expected to be

very low during such a test, the use of a mass spectrometer would become mandatory.

A

Material properties

A.1. Fluoropolymers

As the data sheet of the supplier was incomplete, it was chosen to use averages provided by CES Edupack 2015.

Table A.1: Mechanical and thermal properties of fluoropolymers PFA, FEP and PTFE

Property	PFA	FEP	PTFE
E [GPa]	0.483	0.345	0.476
G [GPa]	0.168	0.119	0.166
ν [-]	0.435	0.441	0.45
ρ $[kg/m^3]$	2140	2140	2170
T_g [K]	378	361	386
T_m [K]	573	548	600
α $[10^{-6}K^{-1}]$	120	94	145
Conductivity $[W/(m \cdot K)]$	0.252	0.252	0.252

A.2. Liquid crystal polymers

Because the stiffness depends on material thickness, the stiffness in flow direction is calculated by interpolating between stiffnesses for known thicknesses. The stiffness in transverse direction was not provided, but a measure of anisotropy was and is used to calculate the transverse stiffness.

Table A.2: Mechanical and thermal properties of Vectra A130 and A950

Property	A130	A950
E_{11} [GPa]	18.75	16.2
E_{22} [GPa]	8.52	4.42
G_{12} [GPa]	2.45	5.35
ν	0.46	0.42
T_m	553	553
α_{11} $[10^{-6}K^{-1}]$	6	4
α_{22} $[10^{-6}K^{-1}]$	23	38

A.3. AS4/8552

Material properties are as provided by Hexcel.

Table A.3: Mechanical and thermal properties of UD AS4/8552

Property	Value	Unit
E_1	131.62	GPa
E_2	9.238	GPa
G_{12}	4.826	GPa
ν_{12}	0.3	-
t_{ply}	0.1875	mm

B

MATLAB Code

B.1. Excel to Matlab conversion tool

```
clc;
clear all;
close all;

fileID = fopen('LogFile-DataGenerator.txt','a+');

parentcd = cd;
dirs = dir(cd);
dirs = {dirs([dirs.isdir]).name};
dirs = dirs(3:length(dirs));

while ~isempty(dirs)
    xlsfiles = dir(strcat(cd,'\',dirs{1},'\*.xls'));
    xlsfiles = {xlsfiles.name};
    matfiles = dir(strcat(cd,'\',dirs{1},'\*.mat'));
    matfiles = {matfiles.name};

    for i = 1:length(xlsfiles)
        if sum(ismember(matfiles,...
                strcat(xlsfiles{i}(1:find(xlsfiles{i}=='x')-2),'.mat')))==1
            continue;
        end
        data1 = xlsread(strcat(cd,'\',dirs{1},'\',xlsfiles{i}),...
            'Measurements','A2:F19');
        EndData = find(isnan(data1(:,4)),1,'first')-1;
        DATA.time = data1(1:EndData,2);
        DATA.slug = data1(1:EndData,4);
        DATA.patm = data1(1:EndData,5);
        DATA.temp = data1(1:EndData,6);
        data2 = xlsread(strcat(cd,'\',dirs{1},'\',xlsfiles{i}),...
            'Calculations','B2:B19');
        DATA.pres = data2(1:EndData);
        data3 = xlsread(strcat(cd,'\',dirs{1},'\',xlsfiles{i}),...
            'SampleAndSetup','B16:B31');
        DATA.Area_cap = data3(2);
        DATA.Area_test = data3(4);
        DATA.t_avg = data3(15);
        DATA.sample = xlsfiles(i);
        save(strcat(cd,'\',dirs{1},'\',...
            xlsfiles{i}(1:find(xlsfiles{i}=='x')-2),'.mat'),'DATA');
        fprintf(fileID,'%s\t%s\r\n',datestr(now),xlsfiles{i});
        clear DATA
    end
     dirs(1)=[];
end
```

```
fclose(fileID);
```

B.2. Main program

```
% Permeability Corrections Test Unit

%% Initialization
clc
close all
clear all

%% Error factor
e.capillary   = 0.1;      % percentage
e.thickness   = 0.005;    % mm
e.sampleDiam  = 0;        % Unknown percentage error
e.meas        = 0.5;      % mm
e.patm        = 0.03;     % percentage
e.presDiff    = 0.0033;   % percentage
e.temp        = 0.05;     % Kelvin

%% Find and select sample
choice = questdlg('Run single sample or all samples?', ...
    'Single/All', ...
    'Single','All','Single');
if strcmp(choice,'Single')
    dirpath = uigetdir(cd,'Select folder with datasets...'); %start directory
    matfiles = dir(dirpath);                                    %everything inside the directory
    matfiles = {matfiles(~[matfiles.isdir]).name};                  %dont record the base director
    matfiles = matfiles(~cellfun('isempty',strfind(matfiles,'.mat')));    %only record .mat files

    [f,cancel] = listdlg('PromptString','Select a file:',...
                    'SelectionMode','single',...
                    'ListSize',[300 400],...
                    'ListString',matfiles);                  %Selecting the desired data file

    if cancel == 0
        error('process stopped by user')
    end

    load([dirpath,'\',matfiles{f}]) % Loads structure called DATA with all measurements

    % Corrections
    if matfiles{f}(end-4)=='F'
        DATA = PCTU_fcn(DATA,'flat','F');
        perm_c_e3 = perm_fcn(DATA,e);
    elseif matfiles{f}(end-4)=='B'
        DATA = PCTU_fcn(DATA,'deflection','B');
        perm_c_e3 = perm_fcn(DATA,e);
    end
else
    parentcd = cd;
    dirs = {'AS4UD' 'AS4Q' 'AS4A' 'A130' 'A950' 'PFA' 'FEP' 'PTFE'};
    parpool('local',2);
    fileF = fopen('Flats2.txt','a');
    fileB = fopen('Deflected2.txt','a');
    while ~isempty(dirs)
        matfiles = dir(strcat(cd,'\',dirs{1},'\*.mat'));
        matfiles = {matfiles.name};
        for i = 1:length(matfiles)
            load([cd,'\',dirs{1},'\',matfiles{i}]) % Loads structure called
                                                   %DATA with all measurements
            fprintf('%s\n',matfiles{i});
            try
            if matfiles{i}(end-4)=='F'
                [perm1,gof1,slugfit1] = perm_fcn(DATA,e,'NoOutliers');
                [perm2,gof2,slugfit2] = perm_fcn(DATA,e);
                DATA = PCTU_fcn(DATA,'flat','F');
                [perm3,gof3,slugfit3] = perm_fcn(DATA,e,'NoOutliers');
                [perm4,gof4,slugfit4] = perm_fcn(DATA,e);
```

```
                fprintf(fileF,['%s;%5.4E;%5.4E;%5.4E;%5.4f;'...
                    '%5.4E;%5.4E;%5.4E;%5.4f;'...
                    '%5.4E;%5.4E;%5.4E;%5.4f;'...
                    '%5.4E;%5.4E;%5.4E;%5.4f\r\n'],...
                    matfiles{i},perm1(2),perm1(3),perm1(1),gof1.rsquare,...
                    perm2(2),perm2(3),perm2(1),gof2.rsquare,...
                    perm3(2),perm3(3),perm3(1),gof3.rsquare,...
                    perm4(2),perm4(3),perm4(1),gof4.rsquare);
            elseif matfiles{i}(end-4)=='B'
                [perm1,gof1,slugfit1] = perm_fcn(DATA,e,'NoOutliers');
                [perm2,gof2,slugfit2] = perm_fcn(DATA,e);
                DATA = PCTU_fcn(DATA,'deflection','B');
                [perm3,gof3,slugfit3] = perm_fcn(DATA,e,'NoOutliers');
                [perm4,gof4,slugfit4] = perm_fcn(DATA,e);
                fprintf(fileB,['%s;%5.4E;%5.4E;%5.4E;%5.4f;'...
                    '%5.4E;%5.4E;%5.4E;%5.4f;'...
                    '%5.4E;%5.4E;%5.4E;%5.4f;'...
                    '%5.4E;%5.4E;%5.4E;%5.4f\r\n'],...
                    matfiles{i},perm1(2),perm1(3),perm1(1),gof1.rsquare,...
                    perm2(2),perm2(3),perm2(1),gof2.rsquare,...
                    perm3(2),perm3(3),perm3(1),gof3.rsquare,...
                    perm4(2),perm4(3),perm4(1),gof4.rsquare);
            end
            catch ME
                warning(matfiles{i});
            end
        end
        dirs(1)=[];
    end
    delete(gcp('nocreate'))
    fclose(fileF);
    fclose(fileB);
end
```

B.3. Correction functions

```
function [OUT] = PCTU_fcn(DATA,Function,Option)
%PCTU_fcn This function contains all the small functions necessary to
%correct the data acquired during permeability measurements.
%
%   As an input is required the DATA structure, containing the
%   measurements performed, and one of the selected functions.
%   Functions are:
%       'pressure' to correct for the change in atmospheric pressure during
%       the measurements;
%       'surface' to correct for an increase in surface area when the
%       sample is allowed to deflect;
%       'volume' to correct for the decrease in volume taken by the
%       deflected sample due to the decrease in applied pressure;
%       'thickness' to correct for the thickness decrease due to the
%       applied pressure;
%       'transducer' to correct for the acquired pressure difference
%       between applied pressure and atmospheric pressure, as the rise of
%       the liquid slug increases the pressure in the downstream chamber;
%       'deflection' to apply all corrections for a sample that is allowed
%       to deflect under load;
%       'flat' to apply all corrections for a sample that remains flat
%       under load.
    switch Function
        case 'pressure'
            OUT = C_pressure(DATA,Option);
        case 'surface'
            OUT = fcn_dS(DATA);
        case 'deflection'
            OUT = C_deflection(DATA,Option);
        case 'volume'
            OUT = fcn_dV(DATA.pres,DATA.sample{:});
        case 'thickness'
            if nargin == 3
```

```
                OUT = fcn_dt(DATA,Option);
            else
                OUT = fcn_dt(DATA);
            end
        case 'transducer'
            OUT = fcn_transducer(DATA);
        case 'flat'
            OUT = fcn_flat(DATA,Option);
        otherwise
            error('invalid function chosen');
    end
end

function [DATA] = C_pressure(DATA,Option)
%C_pressure Atmospheric pressure correction
%   Data structure DATA goes in.
%   Correction is made to DATA.slug
%   Output is DATA
    gamma   = 1.4;
    if strcmp(Option,'F')
        V1      = 2900; %mm3
        dh      = (-V1 + (DATA.patm(1).*V1.^gamma./DATA.patm(2:end)).^(1/gamma))./DATA.Area_cap; %mm
    else
        V1      = 33700-fcn_dV(DATA.pres,DATA.sample{1}); %mm3
        dh      = (-V1(1) + (DATA.patm(1).*V1(1:end).^gamma./DATA.patm(2:end)).^(1/gamma))./DATA.Area_c
    end
    DATA.slug(2:end) = DATA.slug(2:end)+dh;
end

function [DATA] = C_deflection(DATA,Option)
        DATA = PCTU_fcn(DATA,'pressure',Option);
        DATA = PCTU_fcn(DATA,'transducer');
        S_old = DATA.Area_test;
        DATA = PCTU_fcn(DATA,'surface');
        DATA = PCTU_fcn(DATA,'thickness',S_old);
end
%%
%
function [DATA] = fcn_transducer(DATA)
%fcn_transducer calculates the increased pressure in the downstream chamber due to the rise
%of the liquid slug. It is assumed that isopropyl alcohol is used as a
%liquid slug and the feed tube has a radius of 1.5 mm.
%   INPUT: DATA structure with DATA.patm, DATA.slug and DATA.Area_cap.
    rho_isopropyl = 786; %kg/m3
    p_down = DATA.patm + (rho_isopropyl*9.81.*(DATA.slug-DATA.slug(1))*(1+(DATA.Area_cap/(pi*1.5^2)))*1
    DATA.pres = DATA.pres - (p_down-DATA.patm);
    DATA.patm = p_down;
end

function [dV] = fcn_dV(pressure, material)
% Based on the pressure applied to one of the materials, a known relation
% between pressure and volume change ("slope" mm3/Pa) is applied.
% Values obtained with other piece of code, called Volume.m and uses the
% material properties as specified in Appendix A.
    pressure = pressure(2:end)-pressure(1:end-1);
    switch material(1:3)
        case 'AS4'
            slope = 7.502609e-03; %mm3/s AS4/8552 quasi, UD and angleply
        case 'FEP'
            slope = 4.161712e-01;
        case 'PTF'
            slope = 2.979221e-01;
        case 'PFA'
            slope = 2.990308e-01;
        case 'A13'
            slope = 6.693427e-03;
        case 'A95'
            slope = 8.079497e-03;
    end
    dV = slope.*pressure;
end
```

```
function [DATA] = fcn_dS(DATA)
    switch DATA.sample{1}(1:4)
        case 'AS4A'
            layup = [30 -30 30 -30 -30 30 -30 30];
            load AS4_8552.mat
        case 'AS4U'
            layup = zeros([1,8]);
            load AS4_8552.mat
        case 'AS4Q'
            layup = [0 45 -45 90 90 -45 45 0];
            load AS4_8552.mat
        case 'FEP-'
            layup = [0];
            load FEP.mat
        case 'PFA-'
            layup = [0];
            load PFA.mat
        case 'PTFE'
            layup = [0];
            load PTFE.mat
        case 'A130'
            layup = [0];
            load A130.mat
        case 'A950'
            layup = [0];
            load A950.mat
    end

    [ABD, ~] = CLT(layup,ones(size(layup)),ply);
    a = sqrt(DATA.Area_test/pi)/1000; % radius of test sample in [m]
    q = DATA.pres*1E5;
    %parpool('local',2);
    parfor i = 1:length(q) % parallel computing for-loop
        r = sym('r','positive');
        dzdr = diff(q(i)*(a^2-r^2)^2/(24*(ABD(4,4)+ABD(5,5))+16*(ABD(4,5)+2*ABD(6,6))),r);
        ds =sqrt(1+dzdr^2);
        dS = 2*pi*r*ds;
        S = real(double(int(dS,0,a))); %in m2
        Area_test(i) = S*1E6; %S back in mm2
    end
    %delete(gcp('nocreate')) %stop parallel computing
    DATA.Area_test = Area_test';
end

function [DATA] = fcn_dt(DATA,S_old)
    if nargin == 1
        S_old = DATA.Area_test;
        DATA = fcn_dS(DATA);
    end
    DATA.t_avg = S_old.*DATA.t_avg./DATA.Area_test;
end

function [DATA] = fcn_flat(DATA,Option)
    DATA = C_pressure(DATA,Option);
    DATA = fcn_transducer(DATA);
end
```

B.4. Permeability function

```
%% PERMEABILITY CALCULATION
function [perm,gof,slugfit] = perm_fcn(DATA,e,flag)

    %% Constants
    R           = 8314.3; %L/Pa/mol/K
    zeroC       = 273.15; %K
    ft          = fittype('a*x+b');

    %% Individual permeability calculations
```

```
        [fit1,gof1,fitinfo] = fit(DATA.time,DATA.slug,ft,'StartPoint',[1,1]);
    if nargin == 3 && strcmp(flag,'NoOutliers')
        Slope       = fit1.a/60;
        gof         = gof1;
        outliers    = zeros(size(DATA.time));
        slugfit     = fit1;
    else
        residuals   = fitinfo.residuals;
        I           = abs(residuals) > 1.0 * std(residuals);
        outliers    = excludedata(DATA.time,DATA.slug,'indices',I);
        [fit2,gof2] = fit(DATA.time,DATA.slug,ft,'StartPoint',[1,1],'Exclude',outliers);
        Slope       = fit2.a/60;
        gof         = gof2;
        slugfit     = fit2;
    end
    Time        = max(DATA.time.*(outliers==0))-min(DATA.time.*(outliers==0)); %Time without possible f
    for i = -1:1
        Slope       = (Slope*60*Time+i*2*e.meas+i*gof.rmse)/(60*Time);
        VFR         = Slope*DATA.Area_cap*(1+i*e.capillary);                                    %micr
        GTR         = 100*DATA.patm(1)*(1+i*e.patm)*VFR/(mean(DATA.Area_test)*R*mean(DATA.temp+zeroC-i*
        Permeance   = GTR/(mean(DATA.pres*1E5)*(1-i*e.presDiff));                               %mol/m2/
        perm(i+2)   = Permeance*(mean(DATA.t_avg)-i*e.thickness)*0.001;
    end
end
```

B.5. Deflected volume

```
% Volume.m calculates the deflection of a circular sample due to a uniform
% pressure. It then calculates what the slope is of this volume change wrt
% pressure, resulting in an outcome of mm3/Pa for each material type. These
% values are necessary for the function PCTU_fcn.m to work properly, as
% the pressure applied decreased in time and should be compensated for.
clc
clear all
close all
format compact
%%
a = 0.044;      % radius of sample in [m]
for i = 1:8
    clear ply
    % E_x, E_y, nu_xy, G_xy and t_ply are loaded.
            % Units used are Pa and m
    if i == 1
        name = 'AS4/8552 Quasi';
        load AS4_8552.mat
        layup = [0 45 -45 90 90 -45 45 0];
        q = 3E5:1E4:6E5; %applied pressure in [Pa]
    elseif i == 2
        name = 'AS4/8552 Angleply';
        load AS4_8552.mat
        layup = [30 -30 30 -30 -30 30 -30 30];
        q = 3E5:1E4:6E5;
    elseif i == 3
        name = 'AS4/8552 UD';
        load AS4_8552.mat
        layup = [0 0 0 0 0 0 0 0];
        q = 3E5:1E4:6E5;
    elseif i == 4
        name = 'PTFE';
        load PTFE.mat
        layup = 0;
        q = 0.5E5:.5E4:1.5E5;
    elseif i == 5
        name = 'PFA';
        load PFA.mat
        layup = 0;
        q = 0.5E5:.5E4:1.5E5;
    elseif i == 6
        name = 'FEP';
```

```
        load FEP.mat
        layup = 0;
        q = 0.5E5:.5E4:1.5E5;
    elseif i == 7
        name = 'A130';
        load A130.mat
        layup = 0;
        q = 3E5:1E4:6E5;
    elseif i == 8
        name = 'A950';
        load A950.mat
        layup = 0;
        q = 3E5:1E4:6E5;
    end
    material = ones(size(layup));
    [ABD, Qmat] = CLT(layup,material,ply);
    syms r w_s
    V = zeros([1,length(q)]);
    for j = 1:length(q)
        w = q(j)*(a^2-r^2)^2/(24*(ABD(4,4)+ABD(5,5))+16*(ABD(4,5)+2*ABD(6,6)));
        wmax = double(subs(w,0));
        r_fcn_w = unique(solve(q(j)*(a^2-r^2)^2/(24*(ABD(4,4)+ABD(5,5))+...
            16*(ABD(4,5)+2*ABD(6,6)))==w_s,r).^2);
        r_fcn_w(double(subs(r_fcn_w,wmax))>0.0001)=[];
        V(j) = min(pi*double(subs(int(r_fcn_w,0,wmax))));
    end
    dV = fit(q',V','a*x','StartPoint',1);
    fprintf('Material: %s\n',name);
    fprintf('Volume change is %e mm3/Pa\n',dV.a*1E9);
end
```

B.6. Classical Lamination Theory

```
function [ABD, Qmat] = CLT(layup,material,varargin)
%   CLASSICAL LAMINATE THEORY
%Output:    A, B and D.                                          (matrix)
%Input:     ply properties Ex, Ey, Gxy, nuxy, ply thickness(scalar)
%          layup sequence (i.e. [0 45 -45 90 90 -45 45 0]) (vector)

%   Written by Robert-Vincent de Koning
%   11-01-2012

%% Input arguments

if size(varargin,2) == 1
    f = varargin{1};
    core = 0;
elseif size(varargin,2) == 2
    f = varargin{1};
    core = varargin{2};
%     core = c.tcore;
else
    error('give material properties in an structure format please');
end


%% Material Properties layer

for i = 1:length(f)
    nuyx = f(i).Ey*f(i).nuxy/f(i).Ex;

%% Layer stiffness Calculation [Q]_x,y

Qxx = f(i).Ex/(1-f(i).nuxy*nuyx);
Qyy = f(i).Ey/(1-nuyx*f(i).nuxy);
Qxy = f(i).nuxy*f(i).Ey/(1-f(i).nuxy*nuyx);
Qss = f(i).Gxy;

Qmat(:,:,i) = [Qxx Qxy 0; Qxy Qyy 0; 0 0 Qss];
```

```
end

%% Transformed layer stiffness calculation [Q]_1,2
% input layer angle theta

R = [1,0,0;0,1,0;0,0,2];

for j = 1:length(layup)
    m = cosd(layup(j));
    n = sind(layup(j));

    T = [ m^2, n^2, 2*m*n  ;
          n^2, m^2, -2*m*n ;
         -n*m, m*n, m^2-n^2];



     MatQ12(:,:,j) = T\Qmat(:,:,material(j))*R*T/(R);
end
if core ~= 0
    MatQ12(:,:,length(layup)/2+2:length(layup)+1) = MatQ12(:,:,length(layup)/2+1:length(layup));
    MatQ12(:,:,length(layup)/2+1) = zeros(3,3,1);
end


%% Laminate stiffnesses calculation [A], [B], [D]
% input layer location/thickness
t = core;
h = zeros(size(layup));
for i = 1 : length(f)
t = t + sum(material == i)*f(material(i)).tply;
h = h + (material == i)*f(material(i)).tply;
end
if core ~= 0
    h = flipdim(cumsum([0 h(1:length(h)/2) core h(length(h)/2+1:length(h))])-t/2,2);
else
    h = flipdim([0 cumsum(h)]-t/2,2);
end


A = zeros(3,3);
B = zeros(3,3);
D = zeros(3,3);

for i = 1:length(h)-1

A = A + MatQ12(:,:,i)*(h(i)-h(i+1));
B = B + MatQ12(:,:,i)/2*(h(i)^2-h(i+1)^2);
D = D + MatQ12(:,:,i)/3*(h(i)^3-h(i+1)^3);

end

if isequal(layup(1:floor(length(layup)/2)),flipdim(layup(ceil(length(layup)/2+1):length(layup)),2))
    B = zeros(3,3);
end


ABD = [A B; B D];

end
```

B.7. Strain of deflected sample

```
clc
clear all
close all
format compact
%%
```

```
str = {'PFA','FEP','PTFE','A130','A950',...
    'AS4/8552 A','AS4/8552 UD','AS4/8552 Q'};
[choice,v] = listdlg('PromptString','Select a file:',...
                'SelectionMode','single',...
                'ListString',str);
switch choice
    case 1
        load PFA.mat    % E_x, E_y, nu_xy, G_xy and t_ply are loaded.
                        % Units used are Pa and m
        layup = [0];
        q = 100000;          % Pa
    case 2
        load FEP.mat
        layup = [0];
        q = 100000;
    case 3
        load PTFE.mat
        layup = [0];
        q = 100000;
    case 4
        load A130.mat
        layup = [0];
        q = 380000;
    case 5
        load A950.mat
        layup = [0];
        q = 380000;
    case 6
        load AS4_8552.mat
        layup = [0 0 0 0 0 0 0 0];
        q = 380000;
    case 7
        load AS4_8552.mat
        layup = [30 -30 30 -30 -30 30 -30 30];
        q = 380000;
    case 8
        load AS4_8552.mat
        layup = [0 45 -45 90 90 -45 45 0];
        q = 380000;
    otherwise
        error('Something went wrong...')
end

material = ones(size(layup));

a = 0.044;      % radius, in m
dr = 0:0.0001:a; %radius increment
dphi = 0:0.5:360; % angle increment

[ABD, Qmat] = CLT(layup,material,ply);

%% Find deflection
syms x y
w = q*(a^2-x^2-y^2)^2/(24*(ABD(4,4)+ABD(5,5))+16*(ABD(4,5)+2*ABD(6,6)));

th = (0:5:360)*pi/180;
[TH,R] = meshgrid(th,dr);
[X,Y] = pol2cart(TH,R);

%% Find strains for top of sample ply

kappa_x = subs(-diff(diff(w,x),x),{x y},{X Y});
kappa_y = subs(-diff(diff(w,y),y),{x y},{X Y});
kappa_xy = subs(-2*diff(diff(w,x),y),{x y},{X Y});
Kappa12(:,:,1) = kappa_x;
Kappa12(:,:,2) = kappa_y;
Kappa12(:,:,3) = kappa_xy;

t = length(layup)*ply(1).tply;
top = t/2;
h = top;
```

```
layer = 1;
Strain12 = zeros(size(X));
    for xinput = 1:441
        for yinput = 1:73
            Strain12(xinput,yinput,1:3) = StrainTrans(layup,layer,h(layer)*...
                squeeze(Kappa12(xinput,yinput,1:3)));
        end
    end
e1 = max(max(Strain12(:,:,1)));
e2 = max(max(Strain12(:,:,2)));
g12 = max(max(Strain12(:,:,3)));

figure(1)
subplot(1,3,1)
surf(X,Y,Strain12(:,:,1),'LineStyle','none')
set(gca,'FontSize',12)
title('\epsilon_1','FontSize',20)
xlabel('x [m]','FontSize',20); ylabel('y [m]','FontSize',20)
colormap(jet)
view(2)
colorbar('SouthOutside','FontSize',14)
axis square
subplot(1,3,2)
surf(X,Y,Strain12(:,:,2),'LineStyle','none')
set(gca,'FontSize',12)
title('\epsilon_2','FontSize',20)
xlabel('x [m]','FontSize',20); ylabel('y [m]','FontSize',20)
colormap(jet)
view(2)
colorbar('SouthOutside','FontSize',14)
axis square
subplot(1,3,3)
surf(X,Y,Strain12(:,:,3),'LineStyle','none')
set(gca,'FontSize',12)
title('\gamma_{12}','FontSize',20)
xlabel('x [m]','FontSize',20); ylabel('y [m]','FontSize',20)
colormap(jet)
view(2)
axis square
colorbar('SouthOutside','FontSize',14)
subtitle(['(\epsilon_1)_{max}=',num2str(e1),...
    '  (\epsilon_2)_{max}=',num2str(e2),'  (\gamma_{12})_{max}=',num2str(g12)],'FontSize',20)
```

B.8. Helium density calculation

```
function [rho] = HeDensity(p,T)
% p is in Pascals
% T is in Kelvin
% returned value rho is in kg/m3

%Calculation of Helium density according to the equation of state given by
%Robert D. McCarty (1973)
%   Equations 8 and 17 are used
p = p/101325; % to convert from Pa to Atm, as the equations need this.


b_i = [-0.00000050815710041,...
        -0.00011168680862,...
        0.011652480354,...
        0.074474587998,...
        -0.53143174768,...
        -0.95759219306,...
        3.9374414843,...
        -5.1370239224,...
        2.0804456338];

%Table 10
n_1i = [-3.6027735292E-5,...
        1.6079946555E-3,...
```

```
        -2.7441763615E-2,...
        1.4739506957E-1,...
        -4.3559344838E-1,...
        1.3447956078,...
        -1.7040375125,...
        9.0262674040E-1
        ];

n_2i = [1.9661380688E-6,...
        1.7122932666E-4,...
        2.3051000563E-4,...
        -9.6564739100E-4
        ];

n_3i = [-2.3326553271E-7,...
        4.0855110880E-7,...
        1.0900567964E-5,...
        -5.0060952775E-5,...
        1.1312765043E-4,...
        -1.2539843287E-4
        ];

n_4i = [5.6875644111E-3,...
        -1.4438146625E-1,...
        3.3768874851E-3,...
        ];

n_5i = [1.0754201218E-6,...
        -4.5264622308E-5,...
        3.8597388864E-5
        ];

n_6i = [-1.4802195348E-8,...
        4.1721791119E-7
        ];

gamma = -5.00E-4;

%Eq 8
B = sum(b_i.*T.^(1.5-[1:9]/2));

%Eq 17 (in parts)
C1 = sum(n_1i.*T.^(1.5-[1:8]/2));
C2 = sum(n_2i.*T.^(1.5-[1:4]));
C3 = sum(n_3i.*T.^(0.75-[1:6]/4));
C4 = sum(n_4i.*T.^(1-[1:3]));
C5 = sum(n_5i.*T.^(1-[1:3]));
C6 = sum(n_6i.*T.^(1-[1:2]));

syms r

R = 0.0820558; %mol/L/K

% Solve for density with equation 17
solve_r = solve(r*R*T*(1+B*r)+r^3*C1+r^4*C2+r^5*C3+r^3*exp(gamma*r^2)*C4+r^5*exp(gamma*r^2)*C5+r^6*C6==p,r);

rho=double(solve_r)*4.0026; %conversion to kg/m3
end
```

C

Ideal gas law - Helium density

With the Matlab-function as provided in Appendix B.8 the helium density can be accurately calculated. The ideal gas law, as given in Equation C.1 below, is found to be quite accurate as well, even at lower temperatures. Because the ideal gas law was used to convert units in permeability in Section 3.2, it is shown here that the use of it is justified as the difference between ideal gas law and the empirical relationship as given in the Matlab-function remains well below 5%.

$$\rho = \frac{p \cdot M}{R \cdot T} \tag{C.1}$$

where ρ is the calculated density of the helium in $[kg/m^3]$,M the molar mass of helium in $[kg/mol]$, p the pressure of the helium in $[Pa]$, R the universal gas constant of 8.3144598 $[(m^3 \cdot Pa)/(K \cdot mol)]$.

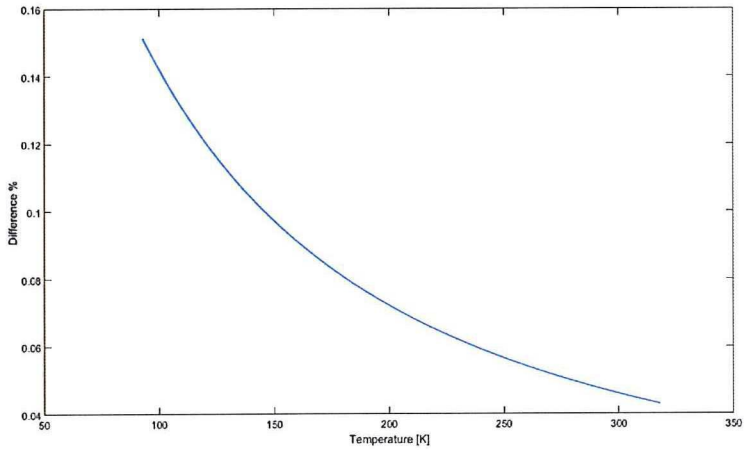

Figure C.1: Difference given as percentage between the ideal gas law and the empirical relationship.

D

Individual results

	No corrections				No corrections, outliers removed				Corrections applied				Corrections applied, outliers removed			
Sample	Perm	Upper	Lower	R^2	Perm	Upper	Lower	R^2	Perm	Upper	Lower	R^2	Perm	Upper	Lower	R^2
AS4UD-4_1 - 3.8bar 4cycles	4.603E-17	9.538E-17	4.018E-17	0.903	4.452E-17	8.782E-17	3.886E-17	0.970	4.638E-17	9.653E-17	4.048E-17	0.893	4.417E-17	8.790E-17	3.855E-17	0.964
AS4Q-2_3 - 3.8bar 0cycles	7.849E-17	1.054E-16	6.852E-17	0.989	8.132E-17	1.070E-16	7.099E-17	0.997	7.937E-17	1.066E-16	6.929E-17	0.988	8.205E-17	1.081E-16	7.163E-17	0.996
AS4Q-4_1 - 3.8bar 4cycles	9.488E-17	1.455E-16	8.283E-17	0.983	9.525E-17	1.433E-16	8.315E-17	0.995	9.516E-17	1.463E-16	8.307E-17	0.981	9.795E-17	1.466E-16	8.551E-17	0.994
AS4A-1_3 - 3.8bar 0cycles	1.764E-16	2.371E-16	1.540E-16	0.921	1.648E-16	2.136E-16	1.438E-16	0.967	1.677E-16	2.273E-16	1.464E-16	0.915	1.560E-16	2.036E-16	1.362E-16	0.965
AS4A-4_1 - 3.8bar 8cycles	1.092E-16	1.565E-16	9.530E-17	0.985	1.111E-16	1.574E-16	9.699E-17	1.000	1.126E-16	1.604E-16	9.830E-17	0.986	1.136E-16	1.609E-16	9.917E-17	1.000
AS4A-4_2 - 3.8bar 8cycles	5.552E-17	9.711E-17	4.846E-17	0.975	5.691E-17	9.681E-17	4.968E-17	0.990	5.623E-17	9.806E-17	4.908E-17	0.974	5.867E-17	9.844E-17	5.122E-17	0.993
A130-2_2 - 6bar 0cycles	6.781E-17	1.074E-16	5.911E-17	0.980	6.901E-17	1.066E-16	6.016E-17	0.993	6.680E-17	1.070E-16	5.824E-17	0.974	6.835E-17	1.065E-16	5.958E-17	0.989
A130-2_3.1 - 3.8bar 0cycles	9.357E-17	1.342E-16	8.158E-17	0.979	9.191E-17	1.280E-16	8.013E-17	0.997	9.073E-17	1.306E-16	7.910E-17	0.980	8.796E-17	1.236E-16	7.668E-17	0.996
A130-2_3.2 - 4.3bar 0cycles	4.703E-17	7.339E-17	4.100E-17	0.962	5.124E-17	7.474E-17	4.467E-17	1.000	3.482E-17	6.011E-17	3.035E-17	0.933	3.589E-17	6.128E-17	3.129E-17	0.969
A130-2_3.3 - 4.8bar 0cycles	4.617E-17	7.401E-17	4.025E-17	0.969	4.448E-17	6.728E-17	3.877E-17	1.000	4.017E-17	6.679E-17	3.502E-17	0.969	3.723E-17	6.071E-17	3.246E-17	0.996
A130-2_3.4 - 5.3bar 0cycles	1.983E-17	4.213E-17	1.729E-17	0.919	2.311E-17	4.331E-17	2.015E-17	0.987	1.224E-17	3.391E-17	1.067E-17	0.862	1.564E-17	3.515E-17	1.364E-17	0.975
A130-2_4 - 5.7bar 0cycles	7.147E-17	9.929E-17	6.231E-17	0.988	7.321E-17	9.929E-17	6.382E-17	0.998	6.034E-17	8.662E-17	5.260E-17	0.985	6.237E-17	8.674E-17	5.437E-17	0.998
A130-4_2 - 6bar 0cycles	1.140E-16	1.616E-16	9.940E-17	0.963	1.103E-16	1.513E-16	9.617E-17	0.992	1.167E-16	1.640E-16	1.017E-16	0.968	1.146E-16	1.560E-16	9.990E-17	0.993
A950-2_1 - 3.8bar 0cycles	9.784E-17	1.317E-16	8.531E-17	0.936	9.592E-17	1.261E-16	8.363E-17	0.978	1.117E-16	1.477E-16	9.741E-17	0.946	1.096E-16	1.416E-16	9.554E-17	0.983
A950-2_2 - 3.8bar 0cycles	1.065E-16	1.343E-16	9.288E-17	0.975	1.044E-16	1.314E-16	9.099E-17	0.989	1.112E-16	1.396E-16	9.698E-17	0.977	1.098E-16	1.373E-16	9.575E-17	0.991
A950-4_1 - 3.8bar 8cycles	1.506E-16	2.168E-16	1.313E-16	0.983	1.710E-16	2.371E-16	1.491E-16	1.000	1.495E-16	2.162E-16	1.304E-16	0.981	1.596E-16	2.232E-16	1.391E-16	0.992
PTFE-2_2 - 1bar 0cycles	7.432E-15	8.778E-15	6.482E-15	0.997	7.669E-15	8.944E-15	6.688E-15	0.999	7.488E-15	8.844E-15	6.531E-15	0.997	7.722E-15	9.004E-15	6.735E-15	0.999
PTFE-2_3.1 - 3.8bar 0cycles	5.519E-15	6.405E-15	4.814E-15	1.000	5.561E-15	6.430E-15	4.850E-15	1.000	5.541E-15	6.429E-15	4.833E-15	1.000	5.584E-15	6.455E-15	4.870E-15	1.000
PTFE-2_3.10 - 5.7bar 0cycles	4.957E-15	5.743E-15	4.323E-15	1.000	4.989E-15	5.773E-15	4.352E-15	1.000	4.945E-15	5.736E-15	4.313E-15	1.000	4.978E-15	5.764E-15	4.341E-15	1.000
PTFE-2_3.2 - 3.8bar 0cycles	5.525E-15	6.406E-15	4.819E-15	1.000	5.509E-15	6.449E-15	4.805E-15	1.000	5.531E-15	6.413E-15	4.824E-15	1.000	5.513E-15	6.454E-15	4.808E-15	1.000
PTFE-2_3.3 - 4.3bar 0cycles	5.175E-15	5.993E-15	4.514E-15	1.000	5.179E-15	5.989E-15	4.517E-15	1.000	5.128E-15	5.943E-15	4.473E-15	1.000	5.156E-15	5.982E-15	4.497E-15	1.000
PTFE-2_3.4 - 4.3bar 0cycles	5.138E-15	5.951E-15	4.481E-15	1.000	5.155E-15	5.964E-15	4.496E-15	1.000	5.093E-15	5.904E-15	4.442E-15	1.000	5.088E-15	5.902E-15	4.438E-15	1.000
PTFE-2_3.5 - 4.8bar 0cycles	5.245E-15	6.056E-15	4.575E-15	1.000	5.216E-15	6.038E-15	4.549E-15	1.000	5.276E-15	6.090E-15	4.601E-15	1.000	5.244E-15	6.069E-15	4.573E-15	1.000
PTFE-2_3.6 - 4.8bar 0cycles	5.139E-15	5.948E-15	4.482E-15	1.000	5.125E-15	5.930E-15	4.470E-15	1.000	5.169E-15	5.985E-15	4.508E-15	1.000	5.158E-15	5.973E-15	4.499E-15	1.000
PTFE-2_3.7 - 5.3bar 0cycles	4.856E-15	5.680E-15	4.235E-15	0.998	4.947E-15	5.722E-15	4.315E-15	1.000	4.844E-15	5.667E-15	4.224E-15	0.998	4.934E-15	5.710E-15	4.303E-15	1.000
PTFE-2_3.8 - 5.3bar 0cycles	4.974E-15	5.747E-15	4.339E-15	1.000	4.965E-15	5.739E-15	4.330E-15	1.000	4.973E-15	5.752E-15	4.338E-15	1.000	4.963E-15	5.729E-15	4.329E-15	1.000
PTFE-2_3.9 - 5.7bar 0cycles	4.928E-15	5.697E-15	4.298E-15	1.000	4.938E-15	5.696E-15	4.307E-15	1.000	4.930E-15	5.704E-15	4.300E-15	1.000	4.929E-15	5.692E-15	4.299E-15	1.000
PTFE-3_2 - 1bar 0cycles	7.703E-15	8.967E-15	6.718E-15	1.000	7.759E-15	9.019E-15	6.767E-15	1.000	7.772E-15	9.047E-15	6.779E-15	1.000	7.832E-15	9.100E-15	6.831E-15	1.000

	No corrections				No corrections, outliers removed				Corrections applied				Corrections applied, outliers removed			
Sample	Perm	Upper	Lower	R^2	Perm	Upper	Lower	R^2	Perm	Upper	Lower	R^2	Perm	Upper	Lower	R^2
PFA-2_2-1bar 0cycles	1.633E-14	1.901E-14	1.424E-14	0.999	1.646E-14	1.902E-14	1.436E-14	1.000	1.643E-14	1.914E-14	1.433E-14	0.999	1.657E-14	1.915E-14	1.446E-14	1.000
PFA-2_3-1bar 0cycles	1.577E-14	1.839E-14	1.376E-14	0.999	1.604E-14	1.854E-14	1.399E-14	1.000	1.585E-14	1.848E-14	1.382E-14	0.999	1.613E-14	1.863E-14	1.406E-14	1.000
PFA-2_4.1-3.8bar 0cycles	1.078E-14	1.243E-14	9.397E-15	1.000				1.000	1.077E-14	1.243E-14	9.391E-15	1.000				1.000
PFA-2_4.11-5.3bar 0cycles	9.232E-15	1.072E-14	8.052E-15	1.000				1.000	9.257E-15	1.074E-14	8.073E-15	1.000				1.000
PFA-2_4.12-5.3bar 0cycles	9.238E-15	1.072E-14	8.057E-15	1.000				1.000	9.245E-15	1.073E-14	8.063E-15	1.000				1.000
PFA-2_4.13-5.7bar 0cycles	9.196E-15	1.057E-14	8.020E-15	1.000				1.000	9.213E-15	1.059E-14	8.035E-15	1.000				1.000
PFA-2_4.14-5.7bar 0cycles	9.195E-15	1.066E-14	8.019E-15	1.000				1.000	9.213E-15	1.067E-14	8.035E-15	1.000				1.000
PFA-2_4.15-5.7bar 0cycles	8.657E-15	1.059E-14	7.551E-15	0.993				1.000	8.675E-15	1.061E-14	7.566E-15	0.993				1.000
PFA-2_4.2-3.8bar 0cycles	1.076E-14	1.255E-14	9.388E-15	1.000				1.000	1.081E-14	1.260E-14	9.424E-15	1.000				1.000
PFA-2_4.3-3.8bar 0cycles	1.047E-14	1.213E-14	9.131E-15	1.000				1.000	1.048E-14	1.214E-14	9.139E-15	1.000				1.000
PFA-2_4.4-4.3bar 0cycles	9.690E-15	1.118E-14	8.451E-15	1.000				1.000	9.704E-15	1.120E-14	8.463E-15	1.000				1.000
PFA-2_4.6-4.3bar 0cycles	9.369E-15	1.093E-14	8.171E-15	1.000				1.000	9.376E-15	1.094E-14	8.178E-15	1.000				1.000
PFA-2_4.7-4.8bar 0cycles	9.130E-15	1.052E-14	7.963E-15	1.000				1.000	9.137E-15	1.053E-14	7.969E-15	1.000				1.000
PFA-2_4.8-4.8bar 0cycles	9.547E-15	1.106E-14	8.327E-15	1.000				1.000	9.568E-15	1.108E-14	8.345E-15	1.000				1.000
PFA-2_4.9-4.8bar 0cycles	9.410E-15	1.091E-14	8.207E-15	1.000				1.000	9.417E-15	1.092E-14	8.213E-15	1.000				1.000
PFA-3_1-3.8bar 4cycles	1.06E-14	1.24E-14	9.26E-15	1.000				1.000	1.06E-14	1.25E-14	9.28E-15	1.000				1.000
PFA-3_2-3.8bar 4cycles	1.08E-14	1.26E-14	9.46E-15	1.000				1.000	1.09E-14	1.26E-14	9.47E-15	1.000				1.000
PFA-3_3-1bar 0cycles	1.626E-14	1.872E-14	1.418E-14	1.000	1.626E-14	1.871E-14	1.418E-14	1.000	1.632E-14	1.879E-14	1.424E-14	1.000	1.633E-14	1.878E-14	1.424E-14	1.000
PFA-3_3-3.8bar 4cycles	1.039E-14	1.213E-14	9.060E-15	1.000				1.000	1.040E-14	1.214E-14	9.068E-15	1.000				1.000
PFA-3_4-3.8bar 4cycles	1.030E-14	1.193E-14	8.979E-15	1.000				1.000	1.031E-14	1.194E-14	8.995E-15	1.000				1.000
PFA-4_3-1bar 0cycles	1.614E-14	1.860E-14	1.407E-14	1.000	1.620E-14	1.865E-14	1.413E-14	1.000	1.627E-14	1.874E-14	1.419E-14	1.000	1.633E-14	1.880E-14	1.424E-14	1.000
PFA-4_4-1bar 0cycles	1.668E-14	1.935E-14	1.455E-14	1.000	1.663E-14	1.925E-14	1.451E-14	1.000	1.676E-14	1.945E-14	1.462E-14	1.000	1.671E-14	1.933E-14	1.457E-14	1.000
FEP-2_1-3.8bar 4cycles	9.504E-15	1.107E-14	8.289E-15	1.000				1.000	9.495E-15	1.107E-14	8.281E-15	1.000				1.000
FEP-2_2-1bar 0cycles	1.622E-14	1.871E-14	1.415E-14	1.000	1.623E-14	1.872E-14	1.415E-14	1.000	1.637E-14	1.888E-14	1.428E-14	1.000	1.636E-14	1.888E-14	1.427E-14	1.000
FEP-2_2-3.8bar 4cycles	7.812E-15	1.086E-14	6.813E-15	0.948				1.000	7.785E-15	1.084E-14	6.790E-15	0.948				1.000
FEP-2_3-3.8bar 4cycles	9.150E-15	1.067E-14	7.980E-15	1.000				1.000	9.167E-15	1.068E-14	7.995E-15	1.000				1.000
FEP-2_4-3.8bar 4cycles	9.029E-15	1.058E-14	7.875E-15	1.000				1.000	9.043E-15	1.060E-14	7.887E-15	1.000				1.000
FEP-3_2-1bar 0cycles	1.432E-14	1.650E-14	1.249E-14	1.000	1.433E-14	1.648E-14	1.250E-14	1.000	1.445E-14	1.664E-14	1.260E-14	1.000	1.444E-14	1.660E-14	1.259E-14	1.000
FEP-3_3.1-3.8bar 0cycles	9.447E-15	1.106E-14	8.240E-15	0.999	9.447E-15	1.106E-14	8.240E-15	0.999	9.458E-15	1.107E-14	8.249E-15	0.999	9.458E-15	1.107E-14	8.249E-15	0.999
FEP-3_3.10-5.3bar 0cycles	8.745E-15	1.011E-14	7.627E-15	1.000	8.760E-15	1.015E-14	7.641E-15	1.000	8.743E-15	1.011E-14	7.626E-15	1.000	8.757E-15	1.015E-14	7.637E-15	1.000
FEP-3_3.11-5.3bar 0cycles	8.720E-15	1.010E-14	7.605E-15	1.000	8.748E-15	1.012E-14	7.630E-15	1.000	8.721E-15	1.010E-14	7.606E-15	1.000	8.749E-15	1.012E-14	7.631E-15	1.000
FEP-3_3.12-5.3bar 0cycles	8.612E-15	9.968E-15	7.511E-15	1.000	8.590E-15	9.928E-15	7.492E-15	1.000	8.605E-15	9.961E-15	7.505E-15	1.000	8.584E-15	9.919E-15	7.487E-15	1.000
FEP-3_3.13-5.7bar 0cycles	8.496E-15	9.822E-15	7.410E-15	1.000	8.499E-15	9.810E-15	7.412E-15	1.000	8.498E-15	9.826E-15	7.412E-15	1.000	8.501E-15	9.814E-15	7.414E-15	1.000
FEP-3_3.14-5.7bar 0cycles	8.585E-15	9.919E-15	7.488E-15	1.000	8.621E-15	9.919E-15	7.519E-15	1.000	8.591E-15	9.926E-15	7.493E-15	1.000	8.627E-15	9.926E-15	7.524E-15	1.000
FEP-3_3.15-5.7bar 0cycles	8.416E-15	9.715E-15	7.340E-15	1.000	8.415E-15	9.720E-15	7.340E-15	1.000	8.414E-15	9.715E-15	7.338E-15	1.000	8.421E-15	9.727E-15	7.345E-15	1.000
FEP-3_3.2-3.8bar 0cycles	9.835E-15	1.133E-14	8.578E-15	1.000	9.875E-15	1.136E-14	8.613E-15	1.000	9.846E-15	1.134E-14	8.587E-15	1.000	9.886E-15	1.137E-14	8.622E-15	1.000
FEP-3_3.3-3.8bar 0cycles	9.526E-15	1.101E-14	8.309E-15	1.000	9.488E-15	1.094E-14	8.275E-15	1.000	9.523E-15	1.100E-14	8.305E-15	1.000	9.486E-15	1.094E-14	8.273E-15	1.000
FEP-3_3.4-4.3bar 0cycles	8.678E-15	1.003E-14	7.569E-15	1.000	8.643E-15	1.002E-14	7.538E-15	1.000	8.661E-15	1.002E-14	7.554E-15	1.000	8.628E-15	9.998E-15	7.525E-15	1.000
FEP-3_3.5-4.3bar 0cycles	8.783E-15	1.015E-14	7.660E-15	1.000	8.766E-15	1.014E-14	7.645E-15	1.000	8.791E-15	1.016E-14	7.668E-15	1.000	8.775E-15	1.015E-14	7.653E-15	1.000
FEP-3_3.6-4.3bar 0cycles	8.692E-15	1.010E-14	7.581E-15	1.000	8.638E-15	9.982E-15	7.534E-15	1.000	8.701E-15	1.011E-14	7.589E-15	1.000	8.649E-15	9.994E-15	7.544E-15	1.000
FEP-3_3.7-4.8bar 0cycles	8.511E-15	9.814E-15	7.423E-15	1.000	8.499E-15	9.790E-15	7.412E-15	1.000	8.518E-15	9.822E-15	7.429E-15	1.000	8.505E-15	9.798E-15	7.418E-15	1.000
FEP-3_3.8-4.8bar 0cycles	8.658E-15	9.979E-15	7.551E-15	1.000	8.638E-15	9.935E-15	7.534E-15	1.000	8.673E-15	9.993E-15	7.564E-15	1.000	8.657E-15	9.959E-15	7.550E-15	1.000
FEP-3_3.9-4.8bar 0cycles	8.621E-15	9.953E-15	7.519E-15	1.000	8.664E-15	1.002E-14	7.557E-15	1.000	8.620E-15	9.953E-15	7.518E-15	1.000	8.665E-15	1.002E-14	7.558E-15	1.000
FEP-4_1-1bar 0cycles	1.405E-14	1.622E-14	1.225E-14	1.000	1.400E-14	1.614E-14	1.221E-14	1.000	1.418E-14	1.636E-14	1.236E-14	1.000	1.412E-14	1.628E-14	1.232E-14	1.000

	No corrections				No corrections, outliers removed				Corrections applied				Corrections applied, outliers removed			
Sample	Perm	Upper	Lower	R^2	Perm	Upper	Lower	R^2	Perm	Upper	Lower	R^2	Perm	Upper	Lower	R^2
AS4UD-1_1 - 3.8bar 0cycles	4.058E-16	5.186E-16	3.542E-16	0.978	4.171E-16	5.182E-16	3.641E-16	0.991	4.931E-16	6.178E-16	4.304E-16	0.984	4.801E-16	5.899E-16	4.191E-16	0.994
AS4UD-2_1 - 3.8bar 0cycles	1.976E-16	3.227E-16	1.725E-16	0.934	1.879E-16	2.898E-16	1.640E-16	0.992	2.476E-16	3.765E-16	2.161E-16	0.957	2.343E-16	3.467E-16	2.045E-16	0.986
AS4UD-3_1 - 3.8bar 0cycles	7.018E-16	8.446E-16	6.126E-16	0.997	7.026E-16	8.406E-16	6.132E-16	0.999	7.138E-16	8.625E-16	6.230E-16	0.995	7.141E-16	8.594E-16	6.233E-16	0.998
AS4UD-4_1 - 3.8bar 0cycles	7.620E-16	9.074E-16	6.652E-16	0.999	7.655E-16	9.079E-16	6.682E-16	1.000	8.761E-16	1.037E-15	7.647E-16	0.999	8.760E-16	1.031E-15	7.646E-16	1.000
AS4Q-1_1 - 3.8bar 0cycles	5.114E-16	6.391E-16	4.464E-16	0.996	5.087E-16	6.207E-16	4.440E-16	1.000	5.980E-16	7.433E-16	5.220E-16	0.994	5.892E-16	7.187E-16	5.144E-16	0.999
AS4Q-1_2 - 3.8bar 0cycles	2.636E-16	3.701E-16	2.301E-16	0.925	2.466E-16	3.341E-16	2.153E-16	0.972	3.178E-16	4.419E-16	2.774E-16	0.915	3.115E-16	4.200E-16	2.719E-16	0.970
AS4Q-1_3 - 3.8bar 0cycles	5.731E-16	7.296E-16	5.003E-16	0.971	5.836E-16	7.281E-16	5.095E-16	0.992	3.096E-16	4.592E-16	2.702E-16	0.835	3.107E-16	4.307E-16	2.713E-16	0.953
AS4Q-1_4 - 3.8bar 0cycles	7.725E-16	9.256E-16	6.744E-16	0.998	7.714E-16	9.237E-16	6.734E-16	0.999	6.988E-16	8.468E-16	6.101E-16	0.995	7.095E-16	8.532E-16	6.194E-16	0.999
AS4Q-1_5 - 3.8bar 0cycles	7.429E-16	8.864E-16	6.485E-16	0.999	7.403E-16	8.837E-16	6.462E-16	1.000	7.489E-16	8.999E-16	6.537E-16	0.997	7.640E-16	9.115E-16	6.669E-16	0.999
AS4Q-1_6 - 3.8bar 0cycles	7.552E-16	9.217E-16	6.592E-16	0.994	7.867E-16	9.485E-16	6.867E-16	0.999	7.732E-16	9.461E-16	6.750E-16	0.992	8.012E-16	9.684E-16	6.995E-16	0.998
AS4Q-1_7 - 3.8bar 0cycles	6.829E-16	8.206E-16	5.961E-16	0.999	6.818E-16	8.226E-16	5.952E-16	1.000	6.768E-16	8.178E-16	5.908E-16	0.998	6.663E-16	8.070E-16	5.817E-16	1.000
AS4Q-2_1 - 3.8bar 0cycles	3.515E-17	7.270E-17	3.069E-17	0.798	4.517E-17	7.817E-17	3.943E-17	0.938	2.384E-17	6.725E-17	2.081E-17	0.564	4.510E-17	8.122E-17	3.937E-17	0.876
AS4Q-2_2 - 3.8bar 0cycles	2.356E-16	3.165E-16	2.057E-16	0.984	2.497E-16	3.240E-16	2.180E-16	0.996	2.728E-16	3.638E-16	2.382E-16	0.977	2.859E-16	3.669E-16	2.495E-16	0.994
AS4Q-3_1 - 3.8bar 0cycles	9.574E-17	1.487E-16	8.357E-17	0.926	1.060E-16	1.582E-16	9.249E-17	0.987	1.255E-16	1.998E-16	1.096E-16	0.820	1.617E-16	2.275E-16	1.411E-16	0.975
AS4Q-3_2 - 3.8bar 0cycles	1.670E-16	2.387E-16	1.457E-16	0.973	1.705E-16	2.387E-16	1.488E-16	0.997	1.065E-16	1.716E-16	9.293E-17	0.938	1.114E-16	1.711E-16	9.724E-17	0.996
AS4Q-4_1 - 3.8bar 0cycles	1.150E-17	6.444E-17	1.004E-17	0.629	2.671E-17	7.374E-17	2.332E-17	0.957	7.022E-17	1.328E-16	6.130E-17	0.855	8.116E-17	1.387E-16	7.085E-17	0.964
AS4A-1_1 - 3.8bar 0cycles	5.202E-16	6.477E-16	4.541E-16	0.997	5.096E-16	6.218E-16	4.449E-16	1.000	5.495E-16	6.806E-16	4.797E-16	0.997	5.526E-16	6.786E-16	4.824E-16	0.999
AS4A-1_2 - 3.8bar 0cycles	3.472E-16	4.883E-16	3.031E-16	0.906	3.167E-16	4.231E-16	2.765E-16	0.964	3.177E-16	4.590E-16	2.773E-16	0.882	3.036E-16	4.071E-16	2.650E-16	0.969
AS4A-2_1 - 3.8bar 0cycles	4.318E-17	9.754E-17	3.769E-17	0.926	4.962E-17	1.060E-16	4.331E-17	0.986	2.440E-17	8.392E-17	2.130E-17	0.748	2.345E-17	7.686E-17	2.048E-17	0.958
AS4A-3_1 - 3.8bar 0cycles	6.508E-16	7.846E-16	5.681E-16	0.998	6.525E-16	7.802E-16	5.696E-16	0.999	6.892E-16	8.305E-16	6.016E-16	0.997	6.995E-16	8.314E-16	6.107E-16	1.000
AS4A-4_1 - 3.8bar 0cycles	3.626E-16	4.574E-16	3.165E-16	0.995	3.582E-16	4.517E-16	3.127E-16	0.999	3.989E-16	5.087E-16	3.482E-16	0.986	4.182E-16	5.213E-16	3.651E-16	0.997

	No corrections				No corrections, outliers removed				Corrections applied				Corrections applied, outliers removed			
Sample	Perm	Upper	Lower	R^2	Perm	Upper	Lower	R^2	Perm	Upper	Lower	R^2	Perm	Upper	Lower	R^2
A130-1_1 - 3.8bar Ocycles	3.229E-15	4.327E-15	2.815E-15	0.884	3.143E-15	3.962E-15	2.740E-15	0.956	3.290E-15	4.375E-15	2.868E-15	0.893	3.239E-15	4.044E-15	2.824E-15	0.965
A130-1_2 - 3.8bar Ocycles	8.544E-16	1.079E-15	7.449E-16	0.996	8.553E-16	1.071E-15	7.457E-16	0.999	9.743E-16	1.225E-15	8.494E-16	0.994	9.600E-16	1.192E-15	8.369E-16	0.999
A130-2_1 - 3.8bar Ocycles	1.621E-15	2.121E-15	1.413E-15	0.900	1.560E-15	1.970E-15	1.360E-15	0.949	1.745E-15	2.262E-15	1.521E-15	0.911	1.696E-15	2.119E-15	1.478E-15	0.958
A130-3_1 - 3.8bar Ocycles	1.013E-15	1.279E-15	8.833E-16	0.965	9.654E-16	1.180E-15	8.417E-16	0.992	1.094E-15	1.361E-15	9.533E-16	0.975	1.048E-15	1.274E-15	9.139E-16	0.993
A130-4_1 - 3.8bar Ocycles	2.028E-15	2.453E-15	1.768E-15	0.986	2.027E-15	2.428E-15	1.767E-15	0.991	2.141E-15	2.578E-15	1.866E-15	0.988	2.135E-15	2.546E-15	1.861E-15	0.994
A950-1_1 - 3.8bar Ocycles	2.900E-15	3.553E-15	2.528E-15	0.976	2.917E-15	3.524E-15	2.544E-15	0.990	2.953E-15	3.610E-15	2.575E-15	0.977	2.967E-15	3.576E-15	2.587E-15	0.991
A950-1_2 - 3.8bar Ocycles	1.756E-15	2.178E-15	1.531E-15	0.999	1.776E-15	2.191E-15	1.548E-15	1.000	1.753E-15	2.175E-15	1.529E-15	0.999	1.773E-15	2.188E-15	1.546E-15	1.000
PFA-1_1 - 1bar Ocycles	1.589E-14	1.887E-14	1.386E-14	0.994	1.566E-14	1.827E-14	1.366E-14	0.999	1.368E-14	1.625E-14	1.194E-14	0.993	1.348E-14	1.570E-14	1.176E-14	0.999
PFA-1_2 - 1bar Ocycles	1.487E-14	1.735E-14	1.297E-14	0.999	1.495E-14	1.737E-14	1.304E-14	1.000	1.306E-14	1.521E-14	1.140E-14	0.999	1.318E-14	1.528E-14	1.150E-14	1.000
PFA-1_3 - 1bar Ocycles	1.424E-14	1.661E-14	1.242E-14	0.999	1.422E-14	1.654E-14	1.240E-14	1.000	1.267E-14	1.471E-14	1.105E-14	1.000	1.268E-14	1.469E-14	1.106E-14	1.000
PFA-2_1 - 1bar Ocycles	1.618E-14	1.893E-14	1.411E-14	0.998	1.621E-14	1.894E-14	1.413E-14	1.000	1.344E-14	1.577E-14	1.172E-14	0.998	1.330E-14	1.562E-14	1.161E-14	0.999
PFA-3_1 - 1bar Ocycles	1.672E-14	1.955E-14	1.458E-14	0.998	1.674E-14	1.945E-14	1.460E-14	1.000	1.432E-14	1.677E-14	1.249E-14	0.998	1.426E-14	1.659E-14	1.244E-14	1.000
PFA-3_2 - 1bar Ocycles	1.699E-14	1.968E-14	1.481E-14	1.000	1.699E-14	1.968E-14	1.482E-14	1.000	1.489E-14	1.724E-14	1.299E-14	1.000	1.483E-14	1.711E-14	1.294E-14	1.000
PFA-4_1 - 1bar Ocycles	1.509E-14	1.763E-14	1.316E-14	0.999	1.520E-14	1.777E-14	1.325E-14	0.999	1.379E-14	1.610E-14	1.203E-14	0.998	1.397E-14	1.633E-14	1.219E-14	0.999
PFA-4_2 - 1bar Ocycles	1.280E-14	1.485E-14	1.116E-14	0.999	1.279E-14	1.481E-14	1.115E-14	1.000	1.102E-14	1.293E-14	9.614E-15	0.997	1.074E-14	1.247E-14	9.370E-15	1.000
FEP-1_1 - 1bar Ocycles	1.604E-14	1.882E-14	1.399E-14	0.998	1.599E-14	1.854E-14	1.395E-14	1.000	1.235E-14	1.448E-14	1.077E-14	0.998	1.231E-14	1.427E-14	1.074E-14	1.000
FEP-2_1 - 1bar Ocycles	1.543E-14	1.811E-14	1.346E-14	0.998	1.546E-14	1.802E-14	1.348E-14	0.999	1.183E-14	1.391E-14	1.033E-14	0.997	1.183E-14	1.382E-14	1.032E-14	0.999
FEP-3_1 - 1bar Ocycles	1.353E-14	1.600E-14	1.180E-14	0.996	1.346E-14	1.574E-14	1.174E-14	0.999	1.016E-14	1.198E-14	8.862E-15	0.997	1.007E-14	1.176E-14	8.787E-15	0.999
PTFE-1_1 - 1bar Ocycles	1.365E-14	1.644E-14	1.191E-14	0.987	1.371E-14	1.615E-14	1.196E-14	0.998	1.197E-14	1.430E-14	1.044E-14	0.991	1.194E-14	1.400E-14	1.042E-14	0.998
PTFE-2_1 - 1bar Ocycles	1.251E-14	1.505E-14	1.091E-14	0.989	1.255E-14	1.494E-14	1.095E-14	0.994	1.043E-14	1.281E-14	9.100E-15	0.977	9.799E-15	1.200E-14	8.548E-15	0.992
PTFE-3_1 - 1bar Ocycles	7.774E-15	9.076E-15	6.780E-15	0.999	7.810E-15	9.049E-15	6.812E-15	1.000	6.592E-15	7.682E-15	5.750E-15	0.999	6.592E-15	7.675E-15	5.750E-15	1.000

E

Automation of measurements

In case it is desired to improve the current volumetric measurement method, it was advised in section 7.3 to automate the measurements. This will have some advantages with respect to the manual measurement system that was employed in this project:

- More precise capillary readings;
- Time control is better;
- Less time required from the researcher;
- All data stored in one place;
- Inexpensive solution with the Raspberry Pi.

At the end of this project a first attempt was done to achieve this. The aim was to replace the current thermometer and atmospheric pressure sensor by sensors that are able to communicate with the computer and directly store data to it. Secondly, a camera should be connected to the computer, being able to make an accurate photograph of the current position of the liquid slug in the capillary at each time interval. Lastly, the pressure transducer is currently communicating through an expensive NI9219, which acts as a basic analog to digital converter (ADC), to a second computer: this needs to be replaced by an inexpensive one purpose ADC which is able to store data to the single computer.
The proposed solution is build around the inexpensive (35 euro) Raspberry Pi 2 computer, which has many I/O pins for communicating with sensors and is therefore an interesting platform for the goals mentioned earlier. The entire system consists of:

- Raspberry Pi 2 (the computer), with a Linux based operating system;
- A "MCP9808" temperature sensor, with an accuracy of 0.25 $^{\circ}C$ and a precision of 0.0625 $^{\circ}C$;
- A "BMP180" atmospheric pressure sensor, with an accuracy of ± 0.12 hPa and a precision as low as 0.02 hPa;
- An "ADC Pi", a 17 bit ADC with a possible gain amplifier of 8, a reference voltage of 2.048 V and a $\pm 0.05\%$ accuracy;
- A C270 webcam, with a resolution of 800x600.

Of the above items, the ADC and webcam need further explanation how they will be used in the data acquisition system. As the ADC has a reference voltage of 2.048 V and 2^{17} steps, the input Voltage from the pressure transducer is discretised in steps of $1.56E^{-2}$ mV/step. The pressure transducer has a maximum voltage output of 100 mV at 21 bar, which will result in 21000 Pa/mV. As the gain can be amplified, this value can be reduced to 2625 Pa/mV. So the final resolution of the pressure transducer attached to the ADC will be 41 Pa. As for the webcam: as it makes pictures with a height of 800 pixels and because the usable length of the capillary is 80 mm, the maximum achievable precision with a webcam is 0.1 mm, which is much better than the optical measurements as are currently performed.
An overview of the two sensors (not attached to Raspberry Pi) is shown in figure E.1.

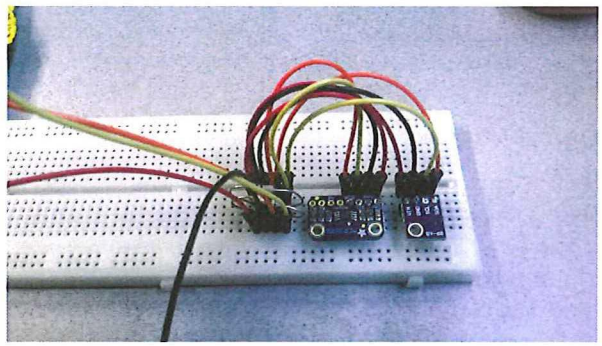

Figure E.1: MCP9808 and BMP180 sensors connected on a breadboard.

F

O-ring seal

It was desired to know if the O-ring was able to completely seal of a (possibly microcracked) composite sample, so no helium would spill into the atmosphere ruining the measurement performed. As this was not possible to check inside the apparatus itself, it was decided to remove the O-ring from the aluminium cell and test its sealing capabilities in a new test setup. To do this, the greased O-ring was placed on a composite sample and together placed on a larger aluminium plate. Just outside of the O-ring a breather (wool) was placed and the outer edge of the aluminium plate was prepared with tacky-tape, so the vacuum bag could be placed. Applying vacuum to the system showed that, on multiple attempts, the O-ring sealed well (see figure F.1) as the atmospheric pressure did not press the foil down in the test area inside the ring.

Figure F.1: First test with regular air.

However, this only proved the O-ring was airtight, not heliumtight. Therefore a second test was conducted, using a helium balloon (Mylar?), instead of the standard vacuum bag foil for resin infusion, to ensure less helium would be lost due to permeation during the test. Apart from this and an additional inlet for the helium the setup remained the same (setup shown in figure F.2). After purging the vacuum bag with helium, the inlet was closed and a block of aluminium was pressed onto the O-ring, taking care the vacuum bag was placed tightly and smoothly around the O-ring. After vacuum was applied however, the area inside of the O-ring was also at vacuum (figure F.3). The cause was discovered to be a couple of wrinkles at the O-ring, hence flow of helium was achieved out of the ring. Despite repeating the test carefully multiple times, the vacuum bag never was wrinkle free. Because of this, the test is regarded inconclusive and a new way should be investigated to gain knowledge how well the O-ring performs with composite materials and helium.

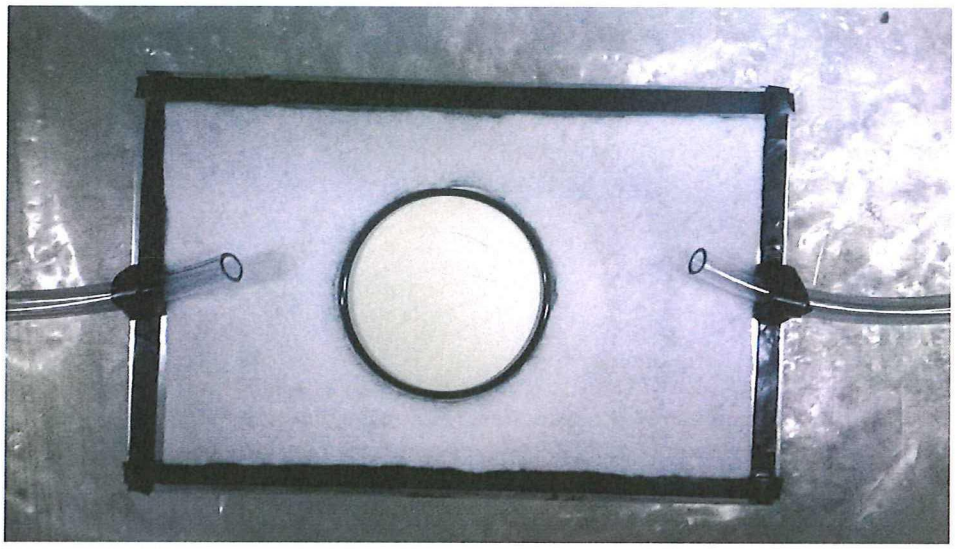

Figure F.2: Second test setup without helium balloon vacuum bag.

Figure F.3: Second test result with helium.

[20] L.W. Mckeen. *Permeability Properties of Plastics and Elastomers*, chapter Fluoropolymers. Elsevier, 2012.

[21] A.T. Nettles. Permeability testing of composite materials and adhesive bonds for the dc-xa composite feedline program. Technical report, NASA, 1995.

[22] A.T. Nettles. Permeability testing of impacted composite laminates for use reusable launch vehicles. Technical report, NASA, 2001.

[23] L. Rafaelli. *Thermomechanics of Fibre Reinforced Epoxies for Cryogenic Pressurized Containment.* PhD thesis, University of Technology Münich, 2006.

[24] Akira Shimamoto, Taku Shimomura, and Jeonghwan Nam. The development of servo dynamic biaxial loading device. *Key Engineering Materials*, 243:99–104, 2003.

[25] A. Smits, D. Van Hemelrijck, T.P. Philippidis, and A. Cardon. Design of a cruciform specimen for biaxial testing of fibre reinforced composite laminates. *Composites science and technology*, 66:964–975, 2006.

[26] Eric H. Stokes. Hydrogen permeability of polymer based composites under bi-axial strain and cryogenic temperatures. In *45th AIAA/ASME/ASCE/AHS/ASC Structures, Structural Dynamics & Materials Conference*, Palm Springs, California, 2004.

[27] P. Sturm et al. Permeation of atmospheric gases through polymer o-rings used in flasks for air sampling. *Journal of Geophysical Research*, 2004.

[28] I.G. Tapeinos and S. Koussios. Experimental study on various liner materials for cryogenic liquid hydrogen storage. *Materials*, 2013.

[29] J.F. Timmerman, M.S. Tillman, B.S. Hayes, and J.C. Seferis. Matrix and fibre influences on the cryogenic microcracking of carbon fibre/epoxy composites. *Composites Part A*, 33:323–329, 2002.

[30] P. Tremblay, M.M. Savard, J. Vermette, and R. Paquin. Gas permeability, diffusivity and solubility of nitrogen, helium, methane, carbon dioxide and formaldehyde in dense polymeric membranes using a new on-line permeation apparatus. *Journal of Membrane Science*, (282):245–256, 2006.

[31] J. VanPelt. Effect of strain on the gas permeability of composite laminates. Technical report, 2006.

[32] Yokozeki et al. Experimental cryogenic gas leakage through damaged composite laminates for propellant tank application. *Journal for spacecraft and rockets*, 42:363–366, 2005.

Bibliography

[1] Final report of the x-33 liquid hydrogen tank test investigation team. Technical report, Huntsville, Alabama, 2000.

[2] D1434-82: Determining gas permeability characteristics of plastic film and sheeting. Technical report, ASTM International, 2009.

[3] V.T. Bechel, M. Negilski, and James. J. Limiting the permeability of composites for cryogenic applications. *Composites Science and Technology*, pages 2284–2295, 2005.

[4] Celia Blum, Dennis Puissegur, Zeb Tidwell, and Carol Webber. Quarter scale rlv multi-lobe lh2 tank test program. Technical report.

[5] S. Choi and B.V. Sankar. Gas permeability of various graphite/epoxy composite laminates for cryogenic storage systems. *Composites Part B: Engineering*, pages 782–791, 2007.

[6] J. Crank. *The mathematics of diffusion.* Oxford University Press, 1975.

[7] J. Crank and G.S. Park. *Diffusion in polymers.* University Press, 1968.

[8] T.J. Dingemans, S. van der Zwaag, A. Knijnenberg, E.S. Weiser, and B.J. Jensen. Novel liquid crystal thermoset resins for cryogenic fuel tank applications. In *24th Congress of International Council of the Aeronautical Sciences*, 2004.

[9] G. Ferron and A. Makinde. Design and development of a biaxial strength testing device. *Journal of Testing and Evaluation*, 16:253–256, 1988.

[10] Thomas S. Gates, Ray W. Grenoble, and Karen S. Whitley. Permeability and life-time durability of polymer matrix composites for cryogenic fuel tanks. In *45th AIAA/ASME/ASCE/AHS/ASC Structures, Structural Dynamics and Materials Conference*, Palm Springs, California, 2004.

[11] Ray W. Grenoble and Thomas S. Gates. Hydrogen permeability of polymer matrix composites at cryogenic temperatures. In *46th AIAA/ASME/ASCE/AHS/ASC Structures, Structural Dynamics & Materials Conference*, Austin, Texas, 2005.

[12] A. Hannon and P. Tiernan. A review of planar biaxial tensile test system for sheet metal. *Journal of materials processing technology*, 198, 2008.

[13] Henaff-Gardin, Lafarie-Frenot, and Gamby. Doubly periodic matrix cracking in composite laminates part 2: thermal biaxial loading. *Composite Structures*, 36:131–140, 1996.

[14] H. Herring. Characterization of thin film polymers through dynamic mechanical analysis and permeation. Technical report, NASA, 2003.

[15] J. Humpenoder. Gas permeation of fiber reinforced plastics. *Cryogenics*, page 143–147, 1998.

[16] P. Ifju, D. Myers, and W. Schultz. Residual stress and thermal expansion of graphite epoxy laminates subjected to cryogenic temperatures. *Composites Science and Technology*, 66(14):2449–2455, 2006.

[17] M. Karimi. *Mass Transfer in Chemical Engineering Processes*, chapter Diffusion in Polymer Solids and Solutions, pages 17–40. InTech, 2011.

[18] S.S. Kessler, T. Matuszeski, and H. McManus. Cryocycling and mechanical testing of cfrp for x-33 liquid h2 fuel tank structure. In *Proceedings of the American Society for Composites*, 2001.

[19] Kumazawa, Hisashi, Susuki, Ippei, Aoki, and Takahira. Gas leakage evaluation of cfrp cross-ply laminates under biaxial loadings. *Journal of Composite Material*, 40:853–871, 2006.